AD NUMBER
AD375897
CLASSIFICATION CHANGES
TO: **UNCLASSIFIED**
FROM: **CONFIDENTIAL**
LIMITATION CHANGES
TO: **Approved for public release; distribution is unlimited.**
FROM: **Distribution authorized to U.S. Gov't. agencies and their contractors; Critical Technology; 27 JUN 1966. Other requests shall be referred to Rocket Propulsion Laboratory, Attn: RPCL, Edwards AFB, CA. This document contains export-controlled technical data.**
AUTHORITY
31 Dec 1972, per document marking; AFRPL ltr, 7 May 1973

GENERAL DECLASSIFICATION SCHEDULE

IN ACCORDANCE WITH
DOD 5200.1-R & EXECUTIVE ORDER 11652

THIS DOCUMENT IS:

Subject to General Declassification Schedule of Executive Order 11652-Automatically Downgraded at 2 Years Intervals- DECLASSIFIED ON DECEMBER 31, 1972

BY

Defense Documentation Center
Defense Supply Agency
Cameron Station
Alexandria, Virginia 22314

SECURITY MARKING

The classified or limited status of this report applies to each page, unless otherwise marked.
Separate page printouts MUST be marked accordingly.

THIS DOCUMENT CONTAINS INFORMATION AFFECTING THE NATIONAL DEFENSE OF THE UNITED STATES WITHIN THE MEANING OF THE ESPIONAGE LAWS, TITLE 18, U.S.C., SECTIONS 793 AND 794. THE TRANSMISSION OR THE REVELATION OF ITS CONTENTS IN ANY MANNER TO AN UNAUTHORIZED PERSON IS PROHIBITED BY LAW.

NOTICE: When government or other drawings, specifications or other data are used for any purpose other than in connection with a definitely related government procurement operation, the U. S. Government thereby incurs no responsibility, nor any obligation whatsoever; and the fact that the Government may have formulated, furnished, or in any way supplied the said drawings, specifications, or other data is not to be regarded by implication or otherwise as in any manner licensing the holder or any other person or corporation, or conveying any rights or permission to manufacture, use or sell any patented invention that may in any way be related thereto.

FINAL REPORT AFRPL-TR-66-203

FLAME TEMPERATURE MEASUREMENT OF METALIZED PROPELLANT (u)

S. E. COLUCCI
and
J. M. ADAMS

Prepared for

ROCKET PROPULSION LABORATORY
Air Force Systems Command
Edwards, California

"When U.S. Government drawings, specifications or other data are used for any purpose other than a definitely related Government procurement operation, the government thereby incurs no responsibility or any obligation whatsoever, and the fact that the government may have formulated, furnished, or in any way supplied the said drawing, specification, or other data, to be regarded by implication or otherwise, or in any matter licensing the holder or any other person or corporation, or convey any rights or permission to manufacture, use, or sell any patented invention that may in any way be related thereto."

Scr - - 1506

FINAL REPORT AFRPL-TR-66-203

FLAME TEMPERATURE MEASUREMENT OF METALIZED PROPELLANT (u)

S. E. COLUCCI
and
J. M. ADAMS

In addition to security requirements which must be met, this document is subject to special export controls and each transmittal to foreign governments or foreign nationals may be made only with prior approval of AFRPL (RPPR-STIN-FO), Edwards, California 93523.

Prepared for

ROCKET PROPULSION LABORATORY
Air Force Systems Command
Edwards, California

9196T

AEROJET-GENERAL CORPORATION
A SUBSIDIARY OF THE GENERAL TIRE & RUBBER COMPANY

FOREWORD

This is the final report of work performed on Contract AF 04(611)-10545, Project No. 3148, BPSN 314803, and program structure No. 750G, covering the period from 1 May 1965 through 27 June 1966. Mr. Curtiss Selph is project engineer at the Rocket Propulsion Laboratory at Edwards, California. Mr. S. E. Colucci is project manager and Dr. J. M. Adams is principal investigator at Aerojet-General Corporation, Sacramento, California.

This report has been reviewed and is approved.

Curtis E. Lundblad
Acting Chief, Propellant Division

UNCLASSIFIED ABSTRACT

The spectral comparison method has been developed for the measurement of temperatures of both the gas and condensed phase in a flame. This method utilizes measurements of spectrum line emission from the gas and continuum emission from the particle cloud to allow determination of the temperature of both phases. The method accounts for the effect of scattering by the particle cloud through measurements of effective particle size and number density used in conjuction with the Mie theory.

The measurement precision for this method for a clean gas was determined from measurements on a H_2/O_2 flame; the resulting standard deviation in gas temperature was 16°K. With particles of alumina introduced into the flame, the standard deviation in gas temperature was increased to 40.8°K. For the particle temperature the standard deviation was 140°K, a relatively high value because of the uncertainty in the refractive index of molten alumina.

The first spectral line of the sodium doublet (0.589μ) was assessed to be a good indicator of the gas temperature in flames. This was determined by a comparison to the lithium line at 0.6708μ which is associated with an electron transition of longer radiative lifetime.

Measurements of particle cloud emittance in small flames were obtained under controlled conditions from which the imaginary part of the refractive index for molten alumina could be determined. These measurements and emittance data of other investigators were used to determine an approximate average value of 0.005 for the imaginary part for alumina above its melting temperature. Light scattering measurements were also performed using small flames with entrained alumina particles. Particle number density determined from the scattering measurements gave striking agreement with the quantity derived from a material balance.

Measurements were taken of light extinction and emission in the plumes of small rocket motors having propellants which contained aluminum, LM-2, or LMH-2. These measurements indicated a mean particle diameter in the plume of 0.6 to 1.0 and thermal lag as high as 700°K. Gas and particle temperatures were measured in the chamber of an LM-2-type motor, which indicated that significant combustion is occurring downstream of the propellant grain. The measurements definitely help to clarify the combustion-expansion phenomena and demonstrate the valuable utility of the measurement technique in this type of investigation.

TABLE OF CONTENTS

		Page
I.	Introduction	1
	A. Objectives	1
	B. Summary	1
	C. Technical Approach	3
II.	Technical Discussion	5
	A. Description of Apparatus	5
	1. Spectral Comparison Pyrometer	5
	2. Flame and Motors	7
	3. Apparatus for Light Scattering Studies	8
	B. Experimental Studies of Small Flames	8
	1. Calibration of SCP	8
	2. Determination of Measurement Precision	9
	3. Thermodynamic Equilibrium Studies	12
	4. Light Scattering Studies	13
	5. Determination of Imaginary Part of Refractive Index for Alumina	16
	6. Conclusions	19
	C. Experimental Studies of Small Rocket Motors	20
	1. Summary of Test Program	20
	2. Motor Test Results	22
	3. Conclusions	34
III.	Proposed Future Effort	36
IV.	Proposed Applications of the Measurement Techniques	37
V.	Nomenclature	39
VI.	References	42

APPENDIXES

	Appendix
The Determination of Emissive Properties of Scattering Media	A
Mie Theory of Scattering by Spherical Particles	B
Properties of Propellants	C
Description of Rocket Motor, Test Hardware	D

LIST OF TABLES

Table		Page
I.	Precision of Flame Temperature Measurements at 2600°K	11
II.	Measured and Calculated Variables in Scattering Experimer	15
III.	Measured Particle Temperature - Dependence on n'	17
IV.	Determination of n' for Molten Alumina, Obtained from Experiments on Flames Containing Particles	18
V.	Particle Size Distribution Used in Determining γ_a, Table IV	18
VI.	Determination of n' for Molten Alumina, Obtained from Measurements of Carlson (Ref. 15)	19
VII.	Summary of 1KS-250 Motor Test Conditions and Results	23
VIII.	Summation of 1KS-250 Motor Performance Test Results	24
IX.	Measured Temperatures on 1KS-250 Motor No. 3, Exhaust Plume	26
X.	Theoretical Temperature for 1KS-250 Motor No. 4, at Measurement Station	28
XI.	Measured Temperatures on 1KS-250 Motor No. 6, Chamber Plenum	29
XII.	Particle Sizes Observed in Exhaust Plume of 1 KS-250 Motor No. 4	32

LIST OF FIGURES

	Figure
Optics and Electromechanical Schematic of Spectral Comparison Pyrometer	1
Internal Optics of 0.5 Meter Jarrell-Ash Spectrometer	2
Laboratory Apparatus, Spectral Comparison Pyrometer	3
Optical Sampling Equipment Used on Motor Tests 1 and 2	4
Test Motor Assembly	5
Scattering Detector Assembly, Exploded View	6
Optics for Light Scattering Measurement	7
Temperature Measurements Using Spectrum Line Intensities of Sodium, Lithium, and Cesium	8
Scattering Detector Schematic Showing Planes of Polarization	9
Light Scattering Diagrams i_1 for Various Particle Size Distribution, Normalized to $i_1(30°)$	10
Light Scattering Diagrams i_2 for Various Particle Size Distribution, Normalized to $i_2(30°)$	11
Particle Size Distributions, Measured and Hypothetical, Used to Generate Scattering Diagrams	12
Apparatus Used for Flame Temperature Measurements on Small Motors	13
Close-up View of Apparatus	14
Spectrometer and Optical Sampling Switch Assembly	15
Carbon Arc and Optical Sampling Switch Assembly	16
Apparatus Used for Flame Temperature Measurement on Small Motors	17
Close-up View of Apparatus	18
Nozzle Postfiring View Looking Aft from Plenum to Throat (Test 2)	19
Optical Viewport Components--Postfiring Test 2	20
Nozzle Postfiring Views (LM-2 Propellant)	21
Nozzle Postfiring Views (LMH-2 Propellant)	22
Motor Performance (Test Series FT-ZX-01S-BH-1)	23
Motor Performance (Test Series FT-ZX-01S-BH-2)	24

LIST OF FIGURES (cont.)

	Figure
Motor Performance (Test Series FT-ZX-01S-BH-5)	26
Motor Performance (Test Series FT-ZX-01S-BH-6)	27
Motor Performance (Test Series FT-ZX-01S-BH-7)	28
Motor Performance (Test Series FT-ZX-01S-BH-8)	29
Motor Performance (Test Series FT-ZX-01S-BH-9)	30
Measured Gas and Particle Temperatures, Exhaust Plume of 1KS-250 Motor, Aluminized Propellant	31
Measured Gas and Particle Temperatures, Exhaust Plume of 1KS-250 Motor, LM-2 Propellant	32
Measured Gas and Particle Temperatures, Exhaust Plume of 1KS-250 Motor, LMH-2 Propellant	33
Light Scattering Diagram, i_2, Normalized to $i_2(0°)$, Motor Tests No. 3 and 4	34
Particle Size Distribution Measured in Electrostatic Particle Precipitation, Motor Test 4	35
Extinction Parameter, Determined from Light Extinction Measurements in Exhaust Plume of 1KS-250 Motor (Tests 3 and 4) at λ = 0.589μ	36
Particle Size Distributions Used in Generating Curves of Extinction Parameter Versus Mean Particle Diameter	37
Extinction Parameter, Determined from Light Extinction Measurements in Exhaust Plume of 1KS-250 Motor (Tests 3 and 4 at λ = 0.436μ	38
Extinction Parameter, Determined from Light Extinction Measurements in Exhaust Plume of 1KS-250 Motor (Tests 7 and 8) at λ = 0.589μ	39
Extinction Parameter, Determined from Light Extinction Measurements in Exhaust Plume of 1KS-250 Motor (Test 6) at λ = 0.436μ	40

I.

INTRODUCTION

A. OBJECTIVES

The immediate objective of this program is to develop a method for measuring chamber and exhaust temperatures of metalized propellants and to distinguish between the temperatures of both the gaseous and condensed species in a rocket motor exhaust.

The specific objective is to utilize the measurement techniques developed in this program for those propellants specified in Exhibit A of this contract to gain insight into the actual performance potential of such systems and into methods of improving their performance.

A secondary objective is to obtain thrust and chamber pressure measurements on small motor tests to correlate measured thrust and specific impulse with the measurements of temperature.

B. SUMMARY

The program was initiated on 19 May 1965. The first half of the program was devoted to (1) initial analysis, (2) checkout and calibration of spectroscopy equipment and optics, (3) determination of measurement precision, and (4) spectroscopic and light scattering measurements using small H_2/O_2 flames with entrained alumina particles (0.1 to 1.0 μ dia).

The second half of the program was devoted to (1) development of equipment ancillary to that used in the laboratory so that the motor test measurements could be taken and (2) testing of 1KS-250 motors.

Measurement precision was determined by measuring small H_2/O_2 flames that contained Al_2O_3 particles. Briefly, the results of the random error determination indicated a confidence interval about temperature typified by the following:

With no particles in the flame:

$$T_g = 2600 \pm 17°K \text{ (25 degrees of freedom)}^{(1)}$$

With particles in the flame:

$$T_g = 2600 \pm 41°K \text{ (50 degrees of freedom)}$$

$$T_p = 2600 \pm 75°K \text{ (50 degrees of freedom)}$$

(1) For the case where one mean of a set has been determined, the number of degrees of freedom is one less than the number of measurements. In the usual case throughout this report, the number is only approximate, and is stated in this manner to allow the reader to draw his own statistical inference from the set.

I, B, Summary (cont.)

The confidence interval about particle temperature does not include the uncertainty in Al_2O_3 refractive index or particle size which causes a larger interval. Data from the laboratory and elsewhere (Ref 1) bear on this problem and will be discussed below. These uncertainties do not affect the gas temperature variance but the present uncertainty in alumina refractive index broadens the standard deviation in particle temperature to 140°K.

The results from the experiments on thermodynamic equilibrium in hydrogen-oxygen flames were obtained by studying emission from the spectral lines of barium, cesium, lithium, and sodium. It was found that barium and cesium were poor trace elements to be used for flame temperature measurement, but that sodium and lithium appeared to be satisfactory (Ref 2). Subsequent measurements on small rocket motors have been performed on the first line of the sodium doublet (0.588995μ). The results of the motor tests are described herein.

Light scattering measurements on a particle-laden flame were related to effective particle size and number concentration through Mie scattering theory. Particle size distribution determined from microscopic examination of a sample collected from the flame was in striking agreement with that determined from the optical measurements. A further check on number concentration was possible because the mass flow rate of particles was monitored. Again, the agreement with that value of number concentration obtained from the optical measurements was very good, and good confidence in the light scattering measurement technique was established.

Motor firings were then conducted with measurements of spectral emission and scattered light intensity being recorded in the exhaust plume just past the exit plane of the motor. Initially, ancillary equipment was fabricated and installed to allow three sequential spectroscopic measurements to be taken at different axial locations during the firing (Ref 3). It was learned from the first two motor firings that the reference light source when coupled to the ancillary equipment was of insufficient intensity to allow determination of the plume extinction coefficient. Upon eliminating a portion of the ancillary equipment, successful measurements of gas and particle temperatures were obtained at one station in the exhaust plume during three small-motor tests. Successful measurements were also obtained in the chamber region during one test.

The light-scattering measurements in the rocket motor exhaust plumes, which were conducted to isolate cloud scattering properties, were not completely successful because the intense emission of light from the plume obscured the scattered radiance. However, good light extinction measurements resulted from these studies, which allowed delineation of cloud scattering and absorption characteristics in a manner shown in the text.

I, B, Summary (cont.)

The exhaust plume measurements indicated that a large amount of thermal energy was lost from the system in the form of molten oxide particles, particularly during the last portion of the motor firing. It was observed in the LM-2 and LMH-2 firings that the "freezing front" (i.e., that region where the particles reach their freezing temperature) passed downstream of the exit plane at some time approximately halfway through the firing. Hence the heat of fusion of the particles made essentially no contribution to the motor specific impulse. The chamber measurements further indicated that considerable combustion has occurred downstream of the grain surface, somewhere between the plenum (where the measurements were made) and the exit plane. This is corroborated by the particle temperature measurements. Although the measurements should be considered as preliminary until verified by further tests, they definitely help clarify the combustion-expansion phenomena. Further, they clearly demonstrate the valuable utility of this measurement technique in investigating propellant combustion.

From the knowledge gained during the present effort, earlier measurement techniques which were applicable only to optically thin regions have been improved to allow treatment of the optically thick case which is normally encountered in the chambers and plumes of large motors. It is now evident that the incorporation of this more general technique into the present system will permit meaningful and precise measurements leading to a more complete understanding of the combustion and expansion phenomena of metalized propellant systems. No other technique has demonstrated meaningful temperature measurements under these conditions.

C. TECHNICAL APPROACH

The method used for the measurement of both gas and particle temperature is the spectral comparison method(1), which has been used in various forms by other investigators (Ref 4 through 8). This method uses spectrometric measurements of radiation intensity from the flame and particles to determine the electronic temperature of the gas and the thermal lag between the gas and molten particles.

The components of the spectral comparison pyrometer (SCP) consists of a carbon-arc lamp, calibrated against a tungsten ribbon lamp (a secondary standard), associated optics, motorized light choppers, a spectral dispersion element, and a detection scheme arranged in a manner shown in Figure 1. A high-speed scanning spectrometer is used to provide spectral dispersion and detection.

(1) Also referred to as the "brightness-emissivity method."

I, C, Technical Approach (cont.)

A beam of light from the carbon-arc reference light source is passed through the rocket motor flame, yielding a continuum of light which is focused on the dispersion element of the spectrometer. This continuum contains light from the carbon-arc lamp and the condensed species in the flame and the gas. This light is resolved into its separate wavelength constituents by the dispersion element. At a particular wavelength isolated from all possible spectrum lines, a spectral radiance[1] from the continuum is determined with the reference light source both on and off. The first reading is, of course, greater because of the light from the lamp being transmitted through the flame. The difference between these two readings is indicative of the radiation absorbed and scattered from the reference source beam by the particles, from which the absorptivity and, hence, emissivity of the particle cloud are obtained. With the light source off, the measurement of radiance from the particle cloud together with the value for emissivity is used in Planck's radiation law to determine particle temperature.

Additional measurements like those above are made at a spectrum line of a trace element in the gas, such as sodium, barium, or lithium. With the lamp off, the recorded radiance is that of both the particles and the gas, but that contribution from the particles, having already been measured, allows isolation of the radiance from the gas. The light from the lamp transmitted through the gas and particle cloud at the trace element spectrum line is attenuated by absorption by both the gas and particles. The attenuation due to the particles can be established with the previously determined values of particle cloud absorptivity and reflectivity, thus allowing the calculation of gas emissivity. The gas temperature can then be determined from the values of gas radiance and emissivity, again using Planck's law. A detailed treatment of this method is shown in Ref 3.

In order to separate the effects of scattering and absorption by the particle cloud, either a knowledge of condensed species size distribution and refractive index is necessary or further measurements on the cloud are required. These considerations are discussed further in this report.

(1) Radiance or radiancy is the radiant flux emitted in a given direction per unit solid angle per unit projected area of the emitting surface. In this case the "surface" is at the plane of the reference source image, within the flame.

II.

TECHNICAL DISCUSSION

A. DESCRIPTION OF APPARATUS

The design features of the apparatus used in this program are presented in the following paragraphs.

1. Spectral Comparison Pyrometer

The spectral comparison pyrometer is built around a Jarrell Ash Model 82-010, manual-drive scanning spectrometer. The instrument has been modified to scan a 200A°(1) range at a frequency of at least 100 cps, allowing a measurement of both particle and gas temperature to be made every 0.020 sec.

The internal optical system of the spectrometer is shown in Figure 2. The concave mirror has a 500-mm focal length and a diameter of 150 mm. Light enters the entrance slit and passes to the 150-mm concave mirror where it is collimated and reflected to a 58-mm-square planar reflection grating. The diffracted light is reflected back to the mirror where it is again reflected and focused on the exit slit. The wavelength of the light brought to the exit slit is changed simply by rotating the grating about its center. The grating used for the measurements on rocket motors and flames has 30,000 grooves/in., and is blazed for 5000 A°. This grating allows dispersion of light in the 3000 to 8000A° range with 0.05A° resolution.

The scanning arm of the spectrometer was modified to achieve the high scanning frequency by replacing the original rigid scanning arm with an articulated assembly. Movement of the articulated assembly is induced by two electromagnetic coils that are excited by a push-pull amplifier. The coils alternately attract and repel the movable arm. The arm can be driven as much as 0.050 in. at its tip, which produces a spectral scan of approximately 200A° near the sodium doublet 5839A°. A manual adjustment is used to set the wavelength around which the scan is centered. For most of the measurements the scan width was 15A° with the scan centered at 5890A°, the first line of the sodium doublet.

The detector used in the spectrometer is an RCA 1P21 multiplier phototube located at the 40 micron exit slit of the spectrometer. This phototube has a broad spectral sensitivity curve and an excellent time response. Radiation with wavelengths from 3000 to 7000A° can be detected with this tube, which has maximum sensitivity at 4000A°. The signal from the tube is amplified with a Dana amplifier, having variable gain from 2 to 1000. Output from the amplifier is used to drive a 2500-cps galvanometer and is monitored on an oscilloscope.

The primary comparison source used in the experimentation is a tungsten ribbon lamp, which also serves as a secondary standard. This lamp has a

---

(1) 10^4 angstroms (A°) = 1 micron (μ).

II, A. Description of Apparatus (cont.)

horizontal tungsten-ribbon filament, 1/8 in. high by 1/2 in. wide. The tungsten-ribbon lamp can be used without damage at temperatures to 2870°K (4700°F). However, if the lamp is operated at this temperature for extended periods, the glass envelope will cloud because of tungsten vapor deposition on the inside. A regulated dc power supply provides power to the lamp circuit with less than 0.2% ripple. It is necessary to keep the ripple at this low value so that fluctuations in temperature do not confound the results.

The lamps were first calibrated by measuring brightness temperature at a wavelength of 0.65 μ with a hand-balanced optical pyrometer. Having this brightness temperature, the true lamp temperature was calculated and used with tabulated emissivity values to generate the entire radiance curve for various current settings.

For the measurement of temperature in gases containing large particle concentrations where scattering is extreme, a comparison source of high intensity is required. For such cases, a carbon arc is used because it provides a radiance approximately 15 times that of the tungsten ribbon lamp. Intended as a microscope illuminator, the machine used in the experimentation uses a carbon feeding system that automatically strikes and feeds the arc.

Typically, the emissivity of the carbon arc is very high (Ref 9), having a value of 0.97 from 4200 to 6300A° at a temperature of 3900°K (6550°F). The image of the crater in the horizontal electrode (for dc operation, the positive electrode) is projected in the flame and used for comparison. A brightness temperature of 3700°K at 0.65 μ was measured at the electrode image, with the equipment set up as shown in Figure 1.

As was mentioned previously, four measurements are necessary to ascertain the temperature of both the gas and the particles. Two measurements are made at a spectral line (arising from the trace element in equilibrium with the gas) with and without the comparison source radiation, and two are made at a neighboring wavelength to determine the liquid- or solid-phase temperature.

The scanning arm is synchronized with the interruption of the source light by using a proximity pickup device mounted on the beam chopping assembly of the reference light source. This synchronization scheme is shown in Figure 1. The reference source beam is chopped for 1/2 cycle, i.e., 1/2 of the complete back-and-forth sweep of the grating. The phase-angle between the scanning signal and the chopping frequency can be altered by means of an assembly which rotates the proximity pickup about the axis of the chopper blade.

For laboratory measurement, the flame is placed in the object position and the lenses arranged in a manner such that the image of the comparison source is focused at a point in the flame. The laboratory apparatus consisting of the carbon arc, choppers, lenses, and spectrometer is shown in Figure 3.

II, A, Description of Apparatus (cont.)

Since the combustion time of the test rocket motors was limited to about 1 sec or less, automated techniques for high-speed spectral measurement of the three locations and one reference position were provided. The basic apparatus is the same as that used for the laboratory measurements but high-speed optical switching between the three selected measurement locations was included as shown in Figure 4. This system was revamped after the first two motor tests, when it was learned that the carbon arc source beam was being excessively attenuated by the optical switching components, resulting in insufficient precision in the measurement of cloud emissivity.

2. Flames and Motors

The flame source used in the laboratory studies consists of a small hydrogen/oxygen torch into which alumina particles (about 0.1 μ dia) are injected from a fluidized bed underneath. Hydrogen gas passes from a small rotameter (9000 ml/min max., STP) directly to the gas mixing chamber below the exit nozzle. Oxygen gas, after passing through an identical flowmeter, is split into two streams, one of which passes to the mixing chamber. The other stream enters at the bottom of the Al_2O_3 particle injector, well below the level of the particle bed. To inject particles into the flame, a mechanical vibrator is energized, causing vigorous stirring of the particle bed. Gas is then introduced through the inlet tube, causing partial fluidization of the bed. The fluidized particles enter the plenum and thence flow through the mixing chamber into the flame. Particle number density in the flame is simply controlled by changing the ratio of flow rates of the two oxygen streams. The system was used successfully, with the particle concentration remaining quite steady during the run. Particle mass fraction in the flame of up to 0.4 could be obtained without difficulty.

To determine gas temperature, a trace element such as calcium, sodium, barium or lithium in the form of a salt is injected into the flame where it is ionized. The intensity of the spectral line emitted by the ions is measured. For the motor tests, only sodium was used as a trace element, and because this element exists as an impurity in most propellant raw material, no external injection system was necessary. A wicking arrangement was used to inject the trace elements into the small flame employed in the laboratory tests. The wick, fabricated from rolled asbestos cloth, was soaked in a saturated solution of the trace element halide, and then was dried. The wick was placed around the gas exit of the hydrogen/oxygen mixing chamber, and was exposed to the flame to cause evaporation of the salt. To gain the maximum concentration of trace element in the flame, the iodide of the cation was used, since this group of the halides normally has the highest vapor pressure.

The motors used in the experiments were of the configuration shown in Figure 5, which also shows the design of the viewport used in the chamber measurements. The motors were filled with approximately 1 lb of propellant, and developed a thrust of about 350 lb_f at a chamber pressure of 700 psia. Because of the cylindrical grain configuration, the chamber pressure increased monotonically during a firing, from approximately 400 to 700 psia.

II, A, Description of Apparatus (cont.)

3. Apparatus for Light Scattering Studies

Light scattering measurements were made both on the small flames with entrained particles and on the motor exhaust plumes so that the cloud reflectivity could be determined. The detector used in the laboratory experiments, shown in Figure 6, consists of the collimating tube, filter holder, image elements, and detector. The detector assembly is supported from the framework above the flame and can be rotated around the flame in the so-called observation plane. The scattering volume, subtended by the detectors, can be properly defined through the appropriate location of the lenses in relation to the image elements (Figure 7). A polarizing filter in the detector was positioned to intercept light in either the I_1 or I_2 position as explained in the section on "Experimental Studies." For the motor tests, the detectors were fixed in position about 7 in. from the plume center line at angles of 0°, 57.5°, and 120.5° to the incident light beam.

The light source used for these measurements was a high-intensity water-cooled BH-6 mercury arc lamp, the beam from which was focused at the center of the flame or plume at the position of the scattering volume.

Light striking the phototube detectors was filtered by means of a narrow-band interference filter centered at 0.436 μ. The emf recorded from the detectors was coupled through an RC network to an amplifier and galvanometer. Because the reflected light from the mercury arc was of lower intensity than emission fluctuations from the plume, the recorded emf was basically of an erratic, random character, with a superimposed 120-cps wave representing the light reflected from the mercury arc lamp.

B. EXPERIMENTAL STUDIES ON SMALL FLAMES

Spectroscopic and light scattering measurements were first conducted on small H_2/O_2 flames with injected alumina particles. These measurements were conducted to develop the various techniques of photometric measurement; the apparatus which evolved from these studies has been described. The experiments included measurements of temperature measurement precision (random error), determination of the emission properties of various trace elements, and determination of the emission and scattering properties of alumina particles. These studies were followed by experiments on the small motors, where emission and light scattering measurements were made simultaneously.

1. Calibration of SCP

The primary standards used to establish temperature were a carbon arc standard[1] for one temperature point at 3803.1°K and an NBS tungsten ribbon lamp standard for all temperatures below 2800°K. These standards were employed to calibrate a portable optical pyrometer[2] which was used, in turn, to measure the birghtness

(1) Mole-Richardson Type 2371 enclosed air arc. The temperature was determined by an NBS-certified standard optical pyrometer at 0.653 μ wavelength.

(2) Leeds and Northrup model 8622, Serial No. 1625126 (AGC).

II, B, Experimental Studies on Small Flames (cont.)

temperature of the reference light source image formed by the lens "2" (see Figure 1). This measurement was performed repeatedly during the detector-recorder calibration and again just before a run.

To accomplish the calibration, the optical scheme is arranged as shown in Figure 1, with the tungsten ribbon lamp serving as a reference source. With the reference source as its highest practicable temperature (≈ 4200°F) and a voltage of 900 v across the phototube,(1) the adjustable horizontal entrance slit of the spectrometer was opened until an output current from the phototube of 9 microamp was measured. (This was determined previously to the maximum allowable anode current at which the phototube is within the range of "linear" operation, i.e., where

$$\frac{\text{anode current/voltage divider current}}{\text{light intensity}} = \text{constant (Ref 10).}$$

With the tube voltage held constant at 900 v, the reference source temperature was varied from approximately 2700 to 4100°F with the spectrometer set at wavelength values of 0.4, 0.5, 0.6, and 0.7 μ. The emf output was monitored and recorded on oscillograph traces, and the ratio of emf to incident radiancy was generated as a function of signal level and wavelength. The data indicated that the "tube constant" is not a function of radiancy, but is of course, quite strongly dependent on the wavelength region. It was found that a rather large variance in tube constant resulted because of small changes in line voltage. This condition was rectified by installing a voltage regulator to supply power to the reference light source and phototube high-voltage source.

2. Determination of Measurement Precision

The precision of the temperature measurements is determined from the source variance, i.e., that variance from a large set of recorded measurements of radiance from the tungsten ribbon lamp. With the hydrogen/oxygen flame operating, a measured variance in flame temperature larger than the aforementioned source variance must be due to fluctuations in the flame temperature and emissivity during the run. This variance is termed the temperature variance. When particles are added to the stream, still more uncertainty results due to the fluctuations in particle feed rate and particle temperature; the resulting variance calculated from the latter measurements is termed the gross temperature variance. The last two variances are not necessarily indicative of precision, but only represent the temperature and emissivity fluctuations during a measurement.

(1) For most of the experimentation, an RCA 1P21 phototube was used at the exit slit of the spectrometer. It is a nine-stage type, having a radiant sensitivity at 4000°A of 78,000 amp/w of incident radiation.

II, B, Experimental Studies on Small Flames (cont.)

From Appendix B of Ref 3, the relationship between phototube constant, output emf (inches of galvanometer deflection in this case) and source temperature is given by

$$K_{ij} = K(\lambda_i, E_{ij}) = \frac{\varepsilon(\lambda_i, T_s)\, \tau_w^2(\lambda_i)}{E_{ij}\, \lambda_i^5 \left[\exp\left(\frac{C_2}{\lambda_i T_s}\right) - 1\right]} \qquad \text{(Eq 1)}$$

From Eq 1, the source temperature is given by

$$T_s = \frac{C_2}{\lambda_i \left\{\ln\left[1 + \frac{\varepsilon(\lambda_i, T_s)\, \tau_w^2(\lambda_i)}{E_{ij}\, K_{ij}\, \lambda_i^5}\right]\right\}} \qquad \text{(Eq 2)}$$

Random error in the measurement of any temperature will be no smaller than that associated with the reference source. It is possible to assess the magnitude of this error in temperature measurement through the following approximation:

$$\sigma_{T_s}^2 = \left(\frac{\partial T_s}{\partial K_{ij}}\right)^2 \sigma_{K_{ij}}^2 + \left(\frac{\partial T_s}{\partial \varepsilon}\right)^2 \sigma_\varepsilon^2 \qquad \text{(Eq 3)}$$

$$+ \left(\frac{\partial T_s}{\partial \lambda_i}\right)^2 \sigma_{\lambda_i}^2 + \left(\frac{\partial T_s}{\partial E_{ij}}\right) \sigma_{E_{ij}}^2$$

The partial derivatives were determined from Eq 2 with measured values of ε, K_{ij}, and E_{ij}. The variance in phototube multiplication factor, σK_{ij}, was determined from a set of several hundred oscillogram galvanometer deflections at various tungsten ribbon lamp brightness temperatures. The standard deviation, σ_ε, was estimated from Ref 11; σ_{λ_i} was considered to be negligible compared to the others; and E_{ij} was determined from the variation in galvanometer deflection when a constant signal was introduced to the recording amplifier. The resulting source variance was determined to be $\sigma_{T_s}^2 = 49\ (^\circ K)^2$ with 120 degrees of freedom.(1) This represents the best possible precision in the measured temperature.

(1) See footnote, p. 1

II, B, Experimental Studies on Small Flames (cont.)

An estimate of the temperature variance was obtained by examining data from measurements on H_2/O_2 flames containing Al_2O_3 particles. From Appendix A, the particle and gas temperature are represented by the following:

$$T_p = f_1 (\hat{N}, \gamma_{a1}, \gamma_{s1}, E_{12}, E_{11}, K_{ij}, T_s, \epsilon_s, \lambda_1, t) \qquad \text{(Eq 4)}$$

$$T_g = f_2 (\hat{N}, \gamma_{a2}, \gamma_{s2}, E_{21}, E_{22}, K_{ij}, T_s, \epsilon_s, \lambda_2, t) \qquad \text{(Eq 5)}$$

The measurements of T_p and T_g taken in the laboratory were reduced using a computer program. The temperature variance and gross temperature variance were cast into the form of Eq 3 in terms of the variables of Eq 4 and 5. Partial derivatives were evaluated simply by using the approximation

$$\frac{\partial T_i}{\partial x_j} = \left(\frac{\Delta T_i}{\Delta x_j}\right)_{n, n \neq j} \qquad \text{(Eq 6)}$$

where small changes in x_j were accomplished by change in input to the computer program. Table I presents some typical results of this investigation.

TABLE I

PRECISION OF FLAME TEMPERATURE MEASUREMENTS
AT TEMPERATURE = 2600°K

Std Dev σ, °K	Degrees of Freedom	Remarks
16.5	25	Gas temperature, clean gas
40.8	50	Gas temperature with particles
140	50	Particle cloud

From many separate experiments on flames during this program, it appears that the first value in the table is very close to the minimum value which can be obtained in a measurement of this type. The second figure is larger because it reflects the uncertainty in the change of radiance of the particle cloud from

II, B, Experimental Studies on Small Flames (cont.)

λ_1 (where it is measured) to λ_2. This uncertainty is much less than the uncertainty in cloud emissivity[1] which causes the larger standard deviation in particle temperature.

3. Thermodynamic Equilibrium Studies

These experiments were conducted to explore and assess the presence of thermodynamic disequilibrium in a flame. Such disequilibrium can cause extraneous emission, not indicative of temperature, caused by nonequipartition of energy among the translational, vibrational, rotational, and electronic degrees of freedom. Since the spectral comparison method uses the measurement of electronic temperature to determine translational temperature, it is necessary that the two temperatures be equal, and hence, that equilibrium be achieved.

While simultaneously injecting the halides of barium (spectrum line - 0.553555 μ), cesium (0.455535 μ), lithium (0.610364 μ, 0.670784 μ), and sodium (0.588995 μ, 0.589592 μ, doublet), and with the O_2/H_2 flame burning at several constant mixture ratios, measurements of intensities of the several spectrum lines were made.

Figure 8 presents results for one particular mixture ratio, reduced from the gas temperature measurements at the spectral lines which were studied. The results are presented in such a manner that thermodynamic equilibrium (i.e., the equipartition of energy among the various energy modes) is indicated by a straight line passing from the origin through all the points. The best estimate of flame temperature from the slope is 2535°K. Scatter in the measurements is indicated at both lines of the sodium doublet and the lithium line at 0.6707μ. This scatter is predominantly a result of the temperature fluctuations of the flame during the run, but is not extensive; most of the data falls on the straight line. It was concluded from the approximately 500 measurements at six mixture ratios that the "D" lines of sodium and the line of lithium at 0.6708μ are indicative of equilibrium temperature in a gas at a pressure of one atmosphere and above. The departure of the cesium data from the line could be an indication of disequilibrium, since the radiative lifetime of cesium is extremely short ($< 10^{-8}$ sec).

Measurements made on the 0.61μ line of lithium and the 0.535μ line of barium indicated extremely low spectral radiance from these transitions and resulted in a prohibitively low signal-to-noise ratio. Potassium (0.776491μ) was also examined, but a low signal-to-noise ratio resulted because of the low sensitivity of the RCA 1P21 in this spectral region.

(1) For an optically thin cloud, the emissivity of the particles is given by the term $(1.-\exp(-\tilde{N}\,\gamma_a t))$, where γ_a, the particle absorption cross section, is nearly proportional to n', the imaginary part of the refractive index of alumina. The relatively large standard deviation in particle temperature is principally due to uncertainty in n'. The measurement of n' and its uncertainty are discussed below in a separate section.

II, B, Experimental Studies on Small Flames (cont.)

Self-absorption of the lithium line at 0.6708μ was observed during some of the experiments, which renders lithium undesirable as a trace element under certain circumstances.

4. Light Scattering Studies

The radiation scattered from particles in two-phase flow must be treated in the determination of gas and particle temperature. This is done by making optical measurements of scattered light intensities simultaneously with the spectroscopic measurements. These scattering measurements are used to determine the effective particle size distribution and number density(1) from the Mie scattering theory,(2) which together with a knowledge of the particle refractive index, allows calculation of particle cloud emissivity.

The following experiments were conducted to refine the experimental technique for the optical determination of particle size distribution and number density so that the method could be used with confidence on the motor tests. The apparatus consisted of the scattering detector, mounted to swivel in a vertical plane through the flame, a carbon arc lamp, a mercury arc lamp, the O_2/H_2 flame, and an Al_2O_3 particle injector. A commercial grade of Al_2O_3 powder was purchased for these runs with particle sizes close to that encountered in a rocket motor exhaust plume. The particle diameters in a sample of this powder ranged from 0.05μ to 15μ, with the peak concentration at approximately 0.1μ.

Meaningful measurements were obtained by using a mercury arc lamp and a monochromatic filter on the scattering detectors of 0.436μ, the wavelength at which the intensity of the mercury arc lamp is a maximum. Measurements made under these conditions gave excellent differentiation of the scattered light from that due to radiant emission of the particles. Since the mercury arc lamp operates on ac current, the reflected light pulse is a 120 cps sine wave, impressed upon a randomly fluctuating dc level from the particle emission. The resulting signal from the phototube was amplified and displayed on an oscillograph recording. The amplified signal also passed through a capacitive-coupled network to a thermocouple-type detector, the output of which was recorded on a strip chart. The two outputs represented peak-to-peak ac values and an integrated rms value, respectively, which together facilitated highly accurate data reduction.

(1) In the motor tests, a precise determination of particle number density was not possible because of imprecision in the light-scattering measurements. As is shown in Appendix A, light-extinction measurements at two wavelengths can serve just as well, provided that particle mass fraction is known. Where this is unknown, additional light-extinction measurements can be used.

(2) This theory, attributed to G. Mie, first appeared in 1908 (Ref: Ann. Physik 25, (1908) 377), and presents the solution to the generalized Maxwell equations for the propagation of electromagnetic waves from a spherical boundary between two regions having different refractive index. The determination of scattering properties is described in Appendix B

II, B, Experimental Studies on Small Flames (cont.)

Measurements of reflected radiance were made at angles to the incident beam of 10° to 65°, 110° to 170° in increments of 5°, with the reflected light polarized parallel (I_1) and perpendicular (I_2) to the plane of observation (Figure 9). Runs were made at two O_2/H_2 mixture ratios and at different particle concentrations.

The results of the scattering measurements are plotted in Figures 10 and 11, where the measured and predicted values of the intensity functions i_1 and i_2 have been normalized to the values at 30°, for easy reference to the incident light intensity which was measured at this angle.(1) The measurement of incident light intensity was accomplished before a run with a black glass plate(2) which was inserted at the position of the flame and rotated to reflect the incident light beam directly into the collimating tube of the scattering detector.

Predicted values of i_1 and i_2 are given in Figures 10 and 11 for the size distribution of particles collected during a run (distribution b) and examined with an electron microscope. The other curves (distributions a, c, and d) are hypothetical, having the same shape but different median particle size (see Figure 12). These curves show systematically the differences which appear on the generated scattering curves of $i_1(\theta)$, and $i_2(\theta)$. Clearly, the differences in the shape of the generated curves of i_1 and i_2 between the four distributions are not great enough to allow determination of the correct size distribution from these measurements alone.

The measured and calculated variables for the experimental scattering data presented in Figures 10 and 11 are tabulated in Table II. The striking agreement between the values for particle number density that were calculated using the light scattering measurements and the mass flow rates is a strong indication that Distribution b is indeed the correct distribution for the particles in the flame. It was concluded from these measurements that the light scattering technique

(1) The intensity functions $i_1(\theta)$ are related to the measured polarized lights intensities $I_1(\theta)$, $I_2(\theta)$ and the incident light intensities I_{01}, I_{02} through a relation of the form

$$I_1(\theta) = \frac{\hat{N} V_s \lambda^2 i_1(\theta) I_{01}}{4\pi^2 r^2}, \quad \left(\text{and: } \frac{i_1(\theta)}{i_1(30°)} = \frac{I_1(\theta)}{I_1(30°)}\right)$$

where r is the distance from the scattering volume to the detector and V_s is the scattering volume (see Figure 7). For a through explanation of i_1, i_2, see Erickson (Ref 12).

(2) Pittsburgh Plate Glass Co., "Carrara" black glass. This method was originally used by Erickson (Ref 12).

II, B, Experimental Studies on Small Flames (cont.)

could be used to make meaningful measurements of particle number density in the motor tests but some other means would have to be found to determine mean particle diameter. As is shown later, light extinction measurements were used to allow determination of mean particle diameter. Because of the optical depth of the particle cloud in the motor tests, the scattering measurements were not successful, and particle number density was calculated from the metal oxide mass fraction.

TABLE II

MEASURED AND CALCULATED VARIABLES IN SCATTERING EXPERIMENT

Flow rates during Run 2

Oxygen	0.0375 gm/sec
Hydrogen	0.0336 gm/sec
Al_2O_3	0.00308 gm/sec (avg over run)

Sizes and distances

V_s (scattering volume) at 90°	6.58×10^{-3} cm^3
r (distance from S.V. to detector)	16 cm
λ (wavelength)	0.436μ
A_o (area of incident beam)	0.046 cm^2
A_s (area of beam at detector)	6.57 cm^2

Other pertinent data

$i_1(135°)$	0.035	
$i_1(150°)$	0.064	Distribution b, Figure 12
ρ_{pl} (reference black glass, 15°)	0.0519	
ρ_{pl} (reference black glass, 22.5°)	0.0568	

Calculated number density of particles

$\hat{N}$ (from scattering data)	1.005×10^9 cm^{-3}
$\hat{N}$ (from mass flow rates)	0.964×10^9 cm^{-3}

II, B, Experimental Studies on Small Flames (cont.)

5. Determination of Refractive Index of Alumina

To relate particle temperature to the continuum emission of the particle cloud and to determine the effect on these measurements of scattering by the particles, a knowledge of the refractive index of the condensed phase is required. The refractive index is a complex number, i.e.,

$$m = n - n'i$$

where n is a measure of the change in the speed of light in the medium (in this case, $Al_2O_{3(l)}$) relative to the value in the surrounding medium, and n' is related to the absorption or attenuation of the light beam in the medium. Absorption in the medium can be described through the relation

$$I = I_o e^{-\gamma t}$$

where γ is the usual absorption coefficient and t is the thickness of the medium. It can be readily shown that n' is related to the absorption coefficient in the medium by the following:

$$\gamma = 2n'k = \frac{4\pi n'}{\lambda} \qquad \text{(Eq 7)}$$

For a system of scatterers it can be shown (although not so readily) that the absorption cross section, γ_a, used to determine the emissivity of the particle cloud by

$$\epsilon_p = 1 - e^{-\bar{N}\gamma_a t} \qquad \text{(Eq 8)}$$

is approximately directly proportional to n', i.e.,

$$\gamma_a \propto n' \qquad \text{(Eq 9)}$$

From the above it is obvious that in order to obtain accuracy in the determination of particle emissivity (and hence temperature), n' must be known to within reasonable limits.

Data obtained from Gryvnak and Burch (Ref 13) indicate that a value of $\gamma = 1\ mm^{-1}$ is likely at the melting temperature, where they observed a sharp increase in the alumina emittance. Unfortunately they could not measure the thickness of the molten sample, and hence, could not determine γ to a reasonable precision. However, using the value of $\gamma = 1\ mm^{-1}$

$$n' = \frac{\lambda \gamma}{4\pi} = 0.00008 \text{ at } 1\mu$$

II, B, Experimental Studies on Small Flames (cont.)

Table III indicates the dependence of T_p on n', using the data from a motor firing. This table was generated by calculating an absorption cross section, γ_a, for each given value of n'. The corresponding cloud emissivity was then obtained from Eq 8, and the calculation of particle temperature followed as shown in Appendix A for the optically thin case.

TABLE III

PARTICLE TEMPERATURE, DETERMINED FROM SPECTROSCOPIC MEASUREMENTS--DEPENDENCE ON n'

$m = 1.799 - n'i$ (Ref 14)

T_p(1 sec)[1] °K	T_p(.7 sec)[1] °K	n'
3662	3805	0.0005
3332	3453	0.001
2804	2899	0.005

If the values presented in Table III were the only measurements of temperature available to us, we would suspect that n' $\geq$0.001, since for values of n' less than 0.001, the temperatures determined from the spectral measurements are much higher than the theoretical values for an isentropic expansion.

Fortunately there are other measurements on Al_2O_3 particle cloud emission which can be used. These were obtained on a H_2/O_2 flame into which Al_2O_3 particles were injected at temperatures from 2600 to 3000°K. Particle absorption cross sections were determined from emissivity measurements, and are presented in Table IV, together with cross sections calculated from the Mie theory for various values of n'. The same treatment was given to the data of Carlson and DuPuis (Ref 15); these values are shown in Table VI.

The results of Carlson and DuPuis agree with those of this report to within the uncertainty in all the measurements of both studies. From the data of both Tables IV and VI the best value of n' appears to be $\sim$0.005 for the range of variables used in this study. The recommended complex refractive index of alumina is therefore given by

$$m = 1.799 - 0.005i \quad (T > \text{melting point of } Al_2O_3,\ \lambda \approx 0.6\ \mu)$$

(1) Time refers to elapsed time from start of firing. Measurements were made at the exit plane of the rocket motor nozzle.

II, B, Experimental Studies on Small Flames (cont.)

TABLE IV

DETERMINATION OF n' FOR MOLTEN ALUMINA, OBTAINED FROM EXPERIMENTS ON FLAMES CONTAINING PARTICLES

Calculated γ_a, Mie Scattering Theory(1)

n'	$\gamma_a(\lambda = .588\mu)$
0.0001	1.1508×10^{-13} cm^2
0.0005	5.7435×10^{-13}
0.001	1.146×10^{-12}
0.005	5.623×10^{-12}
0.01	1.099×10^{-11}

Measured γ_a, Experiments on H_2/O_2 Flames(2)

Run	$\gamma_a(\lambda = 0.558\mu)$	T_g(°K)(3)	n' (by interpolation)
1	7.2×10^{-12} cm^2	2685	0.0079
2	3.9×10^{-12}	2466	0.0043
3	6.5×10^{-12}	2750	0.0072
4	8.5×10^{-12}	2885	0.0094
5	7.6×10^{-12}	2700	0.0084

avg n' = 0.0074 $\pm$ 0.0019 (2500-2900°K)(4)

TABLE V

PARTICLE SIZE DISTRIBUTION USED IN DETERMINING γ_a, TABLE IV

D(micron)	f(D)(unnormalized)
0.0950	0.5440
0.1900	0.1270
0.2850	0.0288
0.3800	0.0200
0.4750	0.0144

(1) Conditions on particle size distribution shown in Table V.

(2) γ_a determined from measured emittance by using Eq 1 of the appendix, which is true for optically thin regions. The value of N used in the computation was determined as shown in Table V.

(3) Measured during run with Spectral Comparison Method.

(4) Standard deviation on measured $\gamma_a = 0.5 \times 10^{-12}$ for 25 to 30 degrees of freedom.

II, B, Experimental Studies on Small Flames (cont.)

Number density of particles used in Table IV computed from

$$\hat{N} = \frac{\rho_g \chi}{[\rho_g \chi + \rho_L(1-\chi)]\,\bar{V}}$$

with $\bar{V} = 2.901 \times 10^{-15}$ cm^3/particle, ρ_g is determined from computer routine at mixture ratio used in run and from measured temperature; χ is determined from weight balance on particles before and after run, measured flow rates of gas; ρ_L is determined from data of Kirshenbaum (Ref 16).

TABLE VI

DETERMINATION OF n' MOLTEN ALUMINA, OBTAINED FROM MEASUREMENTS OF CARLSON (Ref 15)

Calculated γ_a, Mie Scattering Theory(1)

n'	$\lambda = 1.3\mu$ γ_a	$\lambda = 1.7\mu$
0.00005	7.4×10^{-11} cm^2	4.7×10^{-11} cm^2
0.0001	1.475×10^{-10}	8.336×10^{-11}
0.0005	7.19×10^{-10}	4.15×10^{-10}
0.001	1.43×10^{-9}	8.32×10^{-10}
0.005	6.95×10^{-9}	4.01×10^{-9}

Measured γ_a, determined from emittance measurements(2)

γ_a(all λ)	T(°K)	n' (by interpolation)
1.94×10^{-10} cm^2	2320	0.000181
2.74×10^{-10}	2400	0.000258
6.3×10^{-10}	2600	0.000595
1.65×10^{-9}	2800	0.00155
3.33×10^{-9}	3000	0.00326

6. Conclusions

The following conclusions could be drawn from the laboratory experiments reported herein:

(1) The temperature of the H_2/O_2 flame at various mixture ratios can be measured in the presence of particles with a precision characterized at 3000°K

(1) Conditions on particle size distribution from Figure 3 (Ref 15).

(2) Calculations shown in (Ref 17). Emittance values obtained by averaging points above 2320° in Figure 12 (Ref 15).

II, B, Experimental Studies on Small Flames (cont.)

by a standard deviation of approximately 40°K with about 15 degrees of freedom. This is better precision than was originally anticipated for the spectral comparison method. It represents considerably better precision than any results previously reported in the available literature using similar methods for temperature measurement.

(2) Temperature measurements using various trace elements in a H_2/O_2 flame indicate that, at pressures of one atmosphere and higher in regions not far removed from a combustion zone, the element sodium is in thermodynamic equilibrium with the gas. Furthermore, for various other reasons which were previously presented, sodium is the most desirable trace element for use in this program.

(3) Scattered light intensity measurements were made in a H_2/O_2 flame seeded with Al_2O_3 particles, and were described. A sample of Al_2O_3 particles was analyzed by photomicrography, and the measured distribution was used to generate a series of scattering diagrams, i_1 (m, θ, α) and i_2 (m, θ, α). The light scattering measurements on this same sample, seeded in the flame, showed good agreement with the predicted diagrams. Furthermore, the particle number density determined from the scattering measurements agreed very closely with that which was calculated from a mass balance on the injected particles. These two checks seemed to verify the accuracy of the method and indicated that no large biases were present in the light-scattering measurements.

(4) The refractive index of alumina above the melting temperature was determined from measurements taken in this investigation and others (Ref 15). The recommended value for refractive index is $m = 1.799 - 0.500i$ at $2320°K < T < 2800°K$, $0.5\mu < \lambda < 1.5\mu$.

C. EXPERIMENTAL STUDIES ON SMALL ROCKET MOTORS

1. Summary of Test Program

To accomplish the stated objectives, nine motor tests were planned. The motor testing program was conducted in three separate phases, distinguished by the type of metalized solid propellant. The properties of the solid propellants used in all tests are presented in Appendix C.

Initially, it was planned that the first phase would consist of three 1KS-250 motor tests with an aluminized propellant (ANP 2969, Appendix C), with temperatures measured both in the chamber and at two stations in the exhaust plume. The required ancillary equipment to accomplish the simultaneous measurements was developed concurrent with the laboratory development of the temperature measurement technique, and utilized in the first two motor tests conducted. From the data of these two tests, it became obvious that the intensity of the carbon arc light source was being attenuated to a value which resulted in insufficient precision in the measurement of particle cloud emissivity. Hence, the third test was conducted, with RPL concurrence, by eliminating a portion of the ancillary equipment and moving the carbon arc to a position approximately 12 in. from the

II, C, Experimental Studies on Small Rocket Motors (cont.)

plume center line. The reference light source beam penetrated the plume, and radiance measurements were obtained. However, because of a malfunction of an electrical component in the spectrometer, poor precision was realized, and a fourth test using the aluminized propellant was conducted before moving into the LM-2 propellant (ANP 2991 Mod 1A, Appendix C) motor tests. This fourth test was completely successful. Motor thrust, chamber pressure, exhaust gas temperature, exhaust particle temperature, and light scattering measurements were obtained.

In the second phase of this program, three tests of an LM-2 propellant were planned, followed by three tests with LMH-2 type propellants (ANP 3130, Appendix C) in Phase III. However, when it became necessary to conduct a fourth aluminized propellant test, the scope of Phase II was reduced to two tests. In addition, it was felt most desirable to obtain early knowledge of the problems to be faced with the LMH-2 type propellants; hence, the fifth test was conducted with this propellant instead of the Phase II propellant, LM-2.

In addition to the normal measurements of chamber pressure and motor thrust which were obtained on the fifth test, measurements of spectral radiance, light extinction,and optical scattering were attempted in the chamber of this motor to allow determination of gas and particle temperatures in that region. These optical measurements were unsuccessful because of the extreme optical depth within the chamber and what appeared to be extreme viewport erosion. The high mass fraction of particles which results from this propellant (LMH-2) prevented successful light-scattering measurements in the exhaust plume during this test.

Following the fifth test on the LMH-2 propellant, and with RPL concurrence, some effort was expended in the development of a more intense reference light source, utilizing a xenon flash lamp and power supply furnished by RPL. It was decided that the available power supply and triggering system was not adequate and would require extensive modification in order to serve as a repetitive flash lamp system. The flash lamp studies were substituted for one motor test to prevent an extension of the program scope.

The sixth test was conducted using an LM-2 type propellant, and spectroscopic measurements of continuum emission from the particle cloud and spectrum line emission from the gas were made in the motor chamber region, again using optical viewports installed in a plenum just downstream of the end of the grain. Erosion of the viewports was not a problem as it had been with the LMH-2 propellant. Light scattering measurements were made in the exhaust plume as in test number five. Particle and gas temperatures were determined successfully from the chamber measurements, using the "optically thick" analysis described in Appendix A.

The last two tests of the program were conducted with each of the two propellants, LM-2 and LMH-2. Spectroscopic measurements were taken in the exhaust plume and scattering measurements were attempted in the chamber using the viewport arrangement previously described. A successful determination of gas and particle temperatures in the plume resulted. The light scattering studies in the

chamber were inconclusive, again because of extreme optical depth. A detailed description of the results and method follows. A summary of motor test conditions and results is given in Table VII.

2. Motor Test Results

a. Component Evaluation

A detailed description of the ancillary equipment is presented in Appendix D. This Appendix also contains a complete description of the optical viewport construction, test fixture, and motor construction. Compositions for the three propellants used (Aluminum, LM-2, LMH-2) are shown in Appendix C. Figures 13 through 18 show the test hardware used in the eight motor tests.

Postfiring inspection of the motor hardware from the first two tests revealed that the ATJ graphite throat inserts were slightly eroded in the throat vicinity. Further, a thin film of aluminum oxide was observed on the nozzle exit cone. The complete aft-closure assembly, which includes insulators, graphite throat inserts and steel closures, was in excellent condition after firing. It was decided to reuse the complete assembly from the second test on the third and again on the fourth motor test with the aluminized propellant. A view of the assembly looking aft from the chamber plenum is shown in Figure 19 with optical viewports installed. The picture was taken after the first test with this assembly (motor test No. 2).

It can be seen from Figures 19 and 20 that the optical viewport assembly tips (adjusting seat) were slightly melted. This problem was solved by flame-spraying the AISI 1010 steel adjusting-seats with Rokide Z (zirconium oxide) for the third motor test. A postfiring inspection showed that the flame-sprayed probe tips did not melt or erode. Hence, all the probe tips for the remaining motor tests were flame-sprayed with Rokide Z. Soot observed on the transparent windows after firing was attributed to the propellant liner charring due to residual heat in the chamber after the propellant had been consumed.

To verify this thesis, window transmissivity measurements were taken on the fourth motor test, which showed that the windows remained reasonably clear throughout the firing. A reliable measurement of the time change of window transmissivity, varying from 0.3 to 0.4, was obtained.

The aft closures used on motor tests with the LM-2 and LMH-2 also performed satisfactorily, although it was found that in Motor Test 5 (BH-006), the probe tips were severely attacked with an extensive loss in transmissivity. Figures 21 and 22 show the post-fire views of these aft closures. Table VIII presents the prefiring and postfiring throat areas for all nozzles tested.

TABLE VII

SUMMARY TABLE OF 1KS-250 MOTOR TEST CONDITIONS AND RESULTS

Motor Test No.	1	2	3	4	5	6	7	8
Test Series: PT-ZI-015-BH	001	002	003	005	006	007	008	009
Propellant No.	AEP 2969	AEP 2969	AEP 2969	AEP 2969	AEP 3130	AEP 2991	AEP 3130	AEP 2991
Metal Ingredient	Al	Al	Al	Al	LMH2	LM2	LMH2	LM2
Temp. Meas. Position	4 Stations	4 Stations	A/A* = 9.74	A/A* = 9.74	Chamber	Chamber	A/A* = 8.6-10.5	A/A* = 11-12.5
Temp. Meas. Results	none(1)	none(1)	Table IX	Figure 31	none(2)	Table XI	Figure 33	Figure 32
Scattering Meas. Position	A/A* = 6.4-113	A/A* = 6.4-11.3	A/A* = 6.4-11.3	A/A* = 6.4-11.3	A/A* = 7.9-8.9	A/A* = 10.5-13.6	Chamber	Chamber
Scattering Meas. Results	none(3)	none(3)	Figure 34 Figure 38	Figure 34 Figure 38	none(4)	Figure 40	none(4)	none(4)
Number Mean(5)	-	-	0.75μ	0.60μ	-	-	0.96μ	0.80
Particle Size(6)	-	-	0.65μ	0.56μ	-	0.71μ	-	-
Meas. Specific	233	234	235	234.5	264.5	244	265	248
Impulse Efficiency	88.8	89.1	89.6	89.5	84.3	86.16	84.38	87.76

Notes: (1) Source brightness insufficient.
(2) Excessive viewport erosion.
(3) Recording equipment failure.
(4) Excessive optical depth.
(5) Extinction measurement at 0.589μ.
(6) Extinction measurement at 0.436μ.

TABLE VIII

SUMMATION OF 1KS-250 MOTOR PERFORMANCE TEST RESULTS

Test Series: FT-ZX-01S-BH	1	2	3	5	6	7	8	9
Propellant No.	ANP 2969	ANP 2969	ANP 2969	ANP 2969	ANP 3130	ANP 2991	ANP 3130	ANP 2991
Test Date	12-7-65	12-10-65	1-7-66	1-25-66	2-18-66	4-26-66	4-29-66	4-2-66
Nozzle Flow Rate, lb/sec	0.775	0.733	0.723	0.735	1.54	0.645	1.645	0.650
$\int F d\theta$, lb-sec	258.8	239.5	259.2	258.0	228.8	239.5	249.1	244.0
I_s, sec	221.4	221.2	221.3	221.3	253.9	224.3	253.4	230.2
I_s, (std), sec	232.6	233.8	235.0	234.9	264.8	243.6	265.0	248.1
$\int P_c d\theta$, psia-sec	899	909	880	820	398.0	866.8	395.0	857.0
C_w, sec	0.00657	0.00652	0.00656	0.0066	0.00589	0.00622	0.00586	0.00625
θ, sec	1.509	1.600	1.620	1.584	0.585	1.651	0.596	1.625
P_c(avg), psia	596	568	543	541	681	525	662	526
r_b, in./sec	0.283	0.268	0.271	0.264	0.963	0.269	0.962	0.282
C_f	1.46	1.44	1.45	1.46	1.50	1.39	1.49	1.44
A/A*	7.290	7.290	7.076	6.952	7.111	7.261	7.130	7.300
A* prefire, in.	0.196	0.196	0.201	0.205	0.407	0.197	0.441	0.196
A* postfire, in.	0.200	0.201	0.205	0.207	0.362	0.199	0.409	0.199
c*, ft/sec	4900	4940	4920	4872	5470	5180	5480	5150
c* efficiency, %	94.7	95.5	95.0	94.5	91.0	95.5	91.4	94.8
I_s theo (shifting equil with solidif.)	262.2	262.2	262.6	262.6	314.1	282.7	314.1	282.7
I_s efficiency, %	88.8	89.1	89.6	89.5	84.3	86.16	84.38	87.76
Thermal efficiency, %						95.0		

II, C. Experimental Studies on Small Rocket Motors (cont.)

b. Performance Measurements

In addition to the development of techniques for temperature measurement the secondary objective of this program was to obtain thrust and chamber pressure measurements in order to correlate with the measured temperatures to obtain insight into the actual performance potential of the LM-2 propellant systems.

These measurements were obtained on each of the motor firings, and are shown in Figures 23 through 30. The pressure- and thrust-time curves are integrated to obtain specific impulse and characteristic exhaust velocity data. These then, together with the theoretical values, are used to obtain specific impulse efficiency, E_{I_s}, and characteristic exhaust velocity efficiency, E_{c^*}. The motor performance data are summarized in Table VIII (cf. Table VII).

The specific impulse measured at motor condictions is corrected to a standard condition (optimum expansion for 15° conical nozzle from 1000 psia to 14.7 psia) for the aluminized propellant only. This is divided by the theoretical specific impulse using the shifting-equilibrium-with-solidification option of Ref 18. This does not require a special computer run for each separate test condition.

Data reduction for the LM-2 and LMH-2 propellants, however, requires a calculation of the theoretical specific impulses at exact motor conditions (average chamber pressure, ambient pressure, and nozzle expansion ratio) and at standard conditions (optimum expansion from 1000-psia chamber pressure to sea-level ambient pressure, and nozzle expansion ratio). The efficiency at motor conditions, i.e.,

$$\text{Efficiency} = \frac{I_s \text{ measured at motor conditions}}{I_s \text{ theoretical at motor conditions}}$$

is multiplied by the theoretical I_s computed at standard conditions to calculate an extrapolated I_s at standard conditions. In essence, the motor efficiency is assumed to remain constant over the range of conditions spanning actual motor conditions and standard conditions.

Briefly, the Aerojet computer program (Ref 18) involves an iterative solution of simultaneous equilibrium constants with adiabatic combustion at fixed chamber pressure, followed by isentropic flow through the nozzle. The theoretical specific impulse is then calculated from the difference in enthalpy between the chamber and the nozzle exit plane.

The necessary input data required by the computer program includes the heats of formation of the propellant ingredients plus the heats of formation, entropies, and heat capacities as a function of temperature for all

II, C, Experimental Studies on Small Rocket Motors (cont.)

conceivable combustion products. The latest JANAF data (Ref 19) are used where available, and all thermodynamic data for propellant ingredients and combustion products are periodically revised as new data become available.

c. Temperature Measurements

After the first two motor tests,[1] the carbon arc reference source was placed close to the exhaust plume and measurements were taken at a point approximately 0.5 in. downstream from the exit plane (see Table VII). The fiber bundles and rotating sampling scanners had been eliminated in order to increase the radiance of the reference source approximately 15 times. Satisfactory determinations of temperature were then obtained from the light extinction and emission measurements; the results of Motor Test 3 are presented in Table IX.

TABLE IX

MEASURED TEMPERATURES ON 1KS-250 MOTOR NO. 3

Time, sec	Temp, °K	Particle Cloud	
		Emissivity	Reflectivity
0.1	2804	0.2421	0.9907
0.2	2822	0.2575	0.9909
0.3	2845	0.2615	0.9925
0.4	2856	0.2679	0.9942
0.7	2899	0.2991	0.9975

(1) No temperatures could be determined from the data of Tests 1 and 2 within reasonable limits because of lack of detectable penetration of the reference source beam through the plume or chamber precluded a determination of plume emissivity. As is shown later, for optically thick regions, reasonable limits on emissivity can be established even in the absence of a good light extinction measurement. However, in motor tests 1 and 2, the plume was not optically thick, and hence, the minimum limit for emissivity is extremely low (0.2). The measurements taken in the chamber (which is optically thick) were obscured because of melting of the viewport probe tips, which was mentioned above. The firings did serve the useful function of delineating unforeseen difficulties in measurement techniques on motors.

II. C. Experimental Studies on Small Rocket Motors (cont.)

The measurements, which show that the particles are still in the molten state, are an indication of conditions at the center of the plume. This is true because of the narrow "depth of field" of the receptor optical system; i.e., more light from the center of the plume strikes the detector than that from any other region.

Successful measurements of both gas and particle temperatures were made on the fourth motor test, with the apparatus positioned as in the third test (see Table VII). These results, which are presented in Figure 31, indicate that the thermal lag between particles and gas reached a value greater than 700°K. These measurements can be compared to theoretical temperatures presented in Table X, which were calculated for the cases of frozen (at both chamber and throat) and shifting equilibrium, where the particles are either solidified or supercooled. The temperatures presented in Figure 31 differ from those values for this test previously reported in Ref 17 because an error was present in the previous analysis of emissivity at this optical depth. The analysis, originally presented by Kuby, et al. (Ref 20), incorrectly accounted for the effect of increased optical depth, thereby resulting in an erroneously large emissivity. This error was later pointed out to the authors by Carlson (Ref 21).

The particle temperatures determined from measurements on Firing 3 are higher than those for Firing 4, a difference which cannot be due to random fluctuations. The measurements made on Firing 3 were of much less precision, as previously mentioned, because there was insufficient gain on the recording channel to obtain a reasonable galvanometer deflection. This condition was corrected on Firing 4.

It can be seen from Figure 31 that the measured gas temperature, although initially at a relatively low value (1902°K) rises during the firing to a level above that predicted for the shifting equilibrium case No. 6 (Table X). The particle temperatures are also seen to rise, always remaining far above the melting temperature. The excessive particle temperature suggests that combustion is occurring at this point in the exhaust plume, resulting in an "effective" particle temperature. If either active combustion is occurring at this station or if appreciable molten aluminum exists here, the measured particle temperature will be higher than expected. In the former case, i.e., where active combustion is occurring near the droplet surface, the measurement will indicate a temperature somewhere between the freshly condensed liquid alumina temperature (near the reaction zone) and the surface temperature of the parent drop. If molten aluminum metal exists here, the emissivity based on the refractive index of the oxide is incorrect and a higher temperature results.

Gas and particle temperatures were also measured successfully in the exhaust plumes of two 1KS-250 motors having propellants with the ingredients LM-2 and LMH-2. These measurements are presented in Figures 32 and 33, where the chamber pressure trace is also indicated for comparison.

II, C, Experimental Studies on Small Rocket Motors (cont.)

TABLE X

THEORETICAL TEMPERATURE FOR 1KS-250 MOTORS AT MEASUREMENT STATION

One-dimensional case, P_c: 400 to 1000 psia Expansion ratio: 9.74

Conditions in one-dimensional computation	Temperature, °K (Assuming no thermal lag)
1-Frozen equilibrium at chamber with supercooling of particles	1810
2-Frozen equilibrium at throat with supercooling of particles	1880
3-Frozen equilibrium at chamber with solidification of particles	2020
4-Frozen equilibrium at throat with solidification of particles	2100
5-Shifting equilibrium with supercooling of particles	2160
6-Shifting equilibrium with solidification of particles	2277

Axisymmetric case,(1) determination of radial temperature profile at A/A* of 9.74:

P_c, psia	Temperature, °K		
	Center	Minimum Temp.	Edge
700	2000	1970	2319
400	2130	2090	2460

(1) Estimate for shifting equilibrium with supercooling. These numbers serve only to indicate the radial temperature profile across the plume.

II. C. Experimental Studies on Small Rocket Motors (cont.)

Figure 32 indicates that little thermal lag occurred in the LM-2 propellant test. The gas and particle temperatures appear to follow each other rather closely, but since they are both above the theoretical temperature at this station, some combustion must have occurred during the expansion process. This conclusion is strengthened by the chamber temperature measurements which were made in this propellant system; they are shown below.

An interesting but unexplained phenomenon occurred approximately 0.1 sec before the end of the test on the LM-2 propellant. At this time (see Figure 32), the transmissivity and radiance of the plume dropped suddenly, both coming to levels of about one-half their previous level. This phenomenon occurred momentarily after a pressure "blip" in the chamber. This could be explained as a sudden opening of the nozzle throat due to sudden release of an oxide film from the throat. The pressure "blip" was reproduced exactly in Motor Test 8 (cf. Figures 28 and 30), but since no plume temperatures were measured in Test 8, no confirmation of these conclusions is immediately forthcoming.

Greater thermal lag is apparent from Figure 33 for the LMH-2 propellant test. It can be seen from the figure that the LM oxide "freezing front" passed the measurement station at t = 0.3 sec. As in the case of aluminum, the measurements indicate continuing combustion for the reasons previously given.

Some additional insight into LM-2 propellant combustion was gained from measurements of gas and particle temperature in a plenum located just aft of a burning grain of LM-2 propellant. These measurements are shown in Table XI. The results are extremely interesting because they seem to indicate incomplete combustion in the chamber region. More measurements are definitely required, particularly with the well-characterized aluminum propellant which would serve as a good standard of comparison.

TABLE XI

MEASURED TEMPERATURES, LM-2 PROPELLANT
CHAMBER PLENUM REGION, 1KS-250 MOTOR

	T_g, °K	T_p, °K	P_c
Upper Limit[1]	3430	3035	As shown in Figure 28.
Lower Limit	3340	2880	

Theoretical Temperature: 3570°K

(1) This uncertainty is due to the combined uncertainties in particle cloud emissivity and window transmissivity. The limits of emissivity are discussed under "Analysis for Optically Thick Clouds," presented in Appendix A.

II, C, Experimental Studies on Small Rocket Motors (cont.)

A calculation of particle temperature assuming convection to be the important heat transfer mechanism to LM drops of one-micron diameter indicates that the droplet temperature in the chamber could lag the gas temperature by only 10°K, a conservative result which is not borne out by the measurements. Instead, the measurements indicate that the phase change from $LM_{(l)}$ to $LM_{(g)}$ is occuring at temperatures lower than the saturation temperature (corresponding to the chamber pressure) and that this vaporization/$LM_{(g)}$-diffusion process is the rate-controlling process which prevents sufficient combustion of LM in the chamber. The model for the combustion of LM is similar to that used in the studies of aluminum combustion, i.e., an evaporating droplet within a spherical laminar diffusion flame. An analytical study using this model should be very enlightening, resulting in a good prediction of particle temperatures and fraction of metal burned at various axial stations.

A comparison of the results of Table XI to the other measured performance parameters can be obtained from Table VIII, which gives further evidence that combustion is occurring downstream of the plenum where the chamber temperatures were measured. Other comparison is difficult because of the limited quantity of data present.

More tests are required with similar motors to increase the statistical confidence in the measurements and eliminate the possibility of some heretofore unknown systematic bias which could cause erroneous measurements. However, there is no reason to doubt the validity of the measurements, and there are several possibilities which can account for the difference between the calculated and theoretical temperatures (in addition to the considerations already mentioned):

1. Air is diffusing into and reacting with the gases in the exhaust plume. This phenomenon was observed to occur during radar attenuation studies (Ref 22) on exhaust plumes, where it accounted for appreciable increase in plume temperature. The effect can be minimized through the use of a nitrogen "blanket" in subsequent exhaust plume studies. Because of the close proximity of the measurement station to the nozzle exit, this effect cannot be very important.

2. The uncertainty in the thermodynamic data which must be used to establish the composition of the gas and the relationship between the internal energy of the gas and its temperature, could alone account for more than half the observed difference between the theoretical and measured temperatures.

3. Disequilibrium between the sodium and the surrounding gas could account for a higher observed temperature; however, a conservative estimate of the extent of this effect could account for an increase of less than 10°K.

II, C, Experimental Studies on Small Rocket Motors (cont.)

d. Light Scattering and Extinction Measurements

A determination of effective particle size and number density was also accomplished on these motor tests so that particle cloud reflectivity and emissivity could be evaluated. These measured effective particle sizes at various times during the firing are shown in Table XII. The measurements were conducted with apparatus very similar to that used in the laboratory experiments on light scattering; it was set up around the exhaust plume at a station approximately 0.75 in. downstream from the temperature-measurement stations.

Figure 34 presents the measurements of light scattering during Motor Tests 3 and 4, together with the curve calculated for the particle size distribution shown in Figure 35. This latter curve was obtained from a photomicroscopic examination of a sample of particles taken during Test No. 4 with a high-voltage particle precipitator stationed about 4 ft downstream of the motor exit plane.

The particle size and number density used in the determination of emissivity could not be obtained from the light scattering measurements with much confidence. Instead, they were determined from the extinction parameter $\gamma_t/\overline{V}$ at $\gamma = 0.588\mu$, obtained by measurements of extinction of the reference light source beam together with data on plume thickness, alumina mass fraction and gas density. A curve of extinction parameter versus particle diameter was generated from the Mie theory, and is presented in Figure 36, where the measured coefficients are also shown.(1) There are two values of (number) mean particle diameter corresponding to the measured values of extinction parameter. The larger of the two possible diameters is the most probable, judging from the particle sample taken during the firing. Also, since the extinction parameter decreased (as the pressure increased) during the firing, it seems more likely that this is attributed to an increasing particle size (associated with the larger values of diameter on the curve (Figure 36)) since agglomeration of the particles should be proportional to pressure. As shown in Appendix A, the determination of mean particle diameter during the test is only incidental to the analysis and is not necessary to the computation of particle temperature. Instead, once $\gamma_t/\overline{V}$ is determined from the extinction measurements, the parameter γ_a/γ_t can be found from which emissivity and then temperatures are computed. As shown in Appendix A, the functional relationship of γ_a/γ_t to $\gamma_t/\overline{V}$ depends on refractive index and the particle size distribution function; fortunately, the latter variable is relatively unimportant to this relationship.

(1) The relationship between extinction parameter and the measured transmitted light intensity from the reference light source is presented in Appendix A. Figure 37 shows the particle size distribution (typical unimodal) used to generate the broken curve in Figure 36.

TABLE XII

PARTICLE SIZE OBSERVED IN EXHAUST PLUME

Experiment No. 660125

Throat diameter: 0.512 in.

Aluminum loading: 0.738 moles Al/100 g

Measurement location: 12 mm downstream of exit plane

Expansion ratio at measurement location: 9.74

Plume thickness at measurement location: 4.43 cm

Time, sec	P_c, psia	D*, Micron
0.05	415	0.435
0.10	420	0.550
0.15	455	0.600
0.20	460	0.620
0.25	465	0.630
0.30	475	0.640
0.40	500	0.650
0.50	520	0.675
0.60	550	0.685
0.70	570	0.700
0.80	590	0.765
0.90	610	0.800
1.00	640	0.820
1.20	690	0.830

*Effective mean diameter, determined from measurements of extinction parameter, $\gamma_t/\overline{V}$, shown in Figure 36.

II, C, Experimental Studies on Small Rocket Motors (cont.)

Good agreement was achieved between the measured value of extinction parameter at 0.588μ and that value predicted from the measured particle size distribution shown in Figure 35. It can be seen in Figure 36 that the effective particle diameter changed during Motor Test 4.(1) The resulting particle sizes used in the calculation of cloud emissivity are given in Table XII.

A regression analysis was performed on the recorded phototube emf which allowed discrimination between the reflected radiance from the mercury arc lamp (a 120 cps ac signal) and the radiance emitted by the particle cloud (an erratic dc signal). This was discussed previously on Pages 8 and 13.

The four data points presented in Figure 34 for the angles 57.5° and 120.5° are of very low precision because of the relatively low intensity of the scattered light at these angles. In fact, from the regression analysis there is less than 5% confidence that the 120-cps signal actually accounts for the reported data points. That is, it could be stated that the measured signal is completely random with greater than 95% confidence.

This is not the case with the measurement at 0°, however; there the difference between a completely random signal and the observed signal is due to the superimposed 120 cps with a confidence level greater than 99% for both firings.(2) For this reason, the extinction coefficient at $\lambda = 0.436\mu$ was determined from the measurement at 0° and is presented in Figure 38, together with values calculated for a typical unimodal distribution (see Figure 37). The data presented in Figure 38 serves to strengthen the conclusion that the effective particle diameter is in the range 0.5 to 0.7μ.

Extinction parameters were also measured at 0.589μ on Motor Tests 7 and 8, again using the measured transmission of the reference light source in the exhaust plume. These measurements are shown in Figure 39, where the extinction parameter is related to mean particle size for a unimodal distribution. As in the cases of Motor Tests 3 and 4, the smaller of the two possible particle sizes was eliminated. The measurements of Sehgal (Ref 23) indicated a number mean for an LM propellant of less than 0.1μ, which would seem to indicate that the smaller of the two sizes was the correct choice. However, examination of the photomicrographs of Sehgal show large spherical particles (~1μ) surrounded by small single crystals of mean diameter less than 0.1μ. These small crystals which greatly contribute to the reported size distribution are believed to have come from fracture of the large particles after the LM oxide had frozen. This fracture can occur from at least two causes: (1) from the thermal stresses at freezing which occur either during freezing because the solid phase has a higher density than the liquid or after complete freezing due to intercrystalline shear, and (2) from impingement upon the walls of the tank in which Sehgal collected his sample.

(1) A time-resolution of extinction parameter was not obtained for Motor Test 3' only the time-average value is presented in Figure 36.
(2) The additional contribution to the signal from forward-scattered light was considered to be negligible.

II, C, Experimental Studies on Small Rocket Motors (cont.)

From the above arguments together with the measurements at $\lambda = 0.588\mu$, it is concluded that the mean particle diameter for the LM-2 propellant is in the range 0.7 to 0.8μ. This conclusion is further strengthened by the measurements taken farther down the exit plume at $\lambda = 0.436\mu$ (again using the mercury arc lamp) during Motor Test 6, which are shown in Figure 40. For the motor tests with the LMH-2 propellant, the particle size (from Figure 39) appears to be 0.9 to 1.0μ.

In an attempt to obtain particle sizes in the chamber region during Motor Tests 7 and 8, the mercury arc light source and scattering detectors were installed at the optical viewports installed at the chamber plenum region. The results of these tests indicated that no radiance from the mercury arc lamp could be detected at the three angles at which detectors were placed (0°, 63°, and 117°). Calculations of the extinction parameter for the chamber region indicate that the transmitted beam intensity would be less than 10^{-70} of the incident intensity if all the expected metal or metal oxide were present in the condensed phase. This was essentially verified by the several experiments in the chamber region.

3. Conclusions

This report has described work on the spectroscopic measurement of gas and particle temperature in small flames and rocket motor exhaust plumes. The following conclusions are drawn:

1. The spectral comparison method is readily applicable to optically thin regions where the emission characteristics of the condensed phase present are well known. For optically thick regions, a slight revision to the technique is necessary. Successful measurements of gas and particle temperatures were obtained in both the optically thin case (rocket motor exhaust plume) and the optically thick region associated with a small motor chamber with a high condensed phase mass fraction. These measurements are reported herein.

2. The precision of the measurement is extremely good for the optically thin case with a standard deviation for a clean gas of less than 20°K. In the presence of particles, the standard deviation for the gas temperature is about 40°K, with the refractive index of alumina accounting for a larger uncertainty in particle temperature.

3. Sodium appears to be desirable for use as a trace element, since it has been shown to be in equilibrium with the gas for pressures at 1 atm and above. Calculations indicate that no appreciable disequilibrium between sodium atoms and their neighbors could occur in the expansion of an exhaust plume. Lithium, on the other hand, is undesirable because of its observed tendency for self-absorption.

II, C, Experimental Studies on Small Rocket Motors (cont.)

4. Light scattering and extinction measurements appear to offer promise as a method for defining effective particle size in a cloud of particles, such that the cloud reflectivity can be determined. However, light scattering measurements of good precision in an optically thick plume do not appear to be possible with a conventional light source. The applicability of a Q-switched laser for this purpose is described in Appendix A.

5. Measurments of gas and particle temperature in the exhaust plume of a small motor are presented together with a discussion of differences between the measured and theoretical temperatures. It is concluded from these measurements that a more intense continuum reference source will be required for greater optical depths (larger motors).

III. PROPOSED FUTURE EFFORT

A future program would involve measurements of particle and gas temperature on "3KS" size motors containing approximately 10-lb propellant grains and of 3-sec duration. A Q-switched laser having a 200 MW power capability (20 Joules for a 100 nanosecond pulse) will be used to give narrow limits on cloud emissivity and hence good accuracy on both the gas and particle temperature either in the chamber or exhaust plume. These measurements would be made for an aluminized propellant as well as LM-2 and LMH-2 propellants in order to utilize the relatively well established behavior of the aluminized propellants as a reference for comparison.

The area obviously requiring the greatest effort in the near future is that of gas and particle temperature measurement in optically thick regions. Results of the present program have indicated that the chamber region of a typical solid rocket motor represents a cloud of "infinite" optical depth, which, because of the presence of certain particle sizes, prevents the penetration of the reference light beam. This precludes the direct measurement of cloud emissivity. However, computational techniques developed during this program allow limits to be placed on the magnitude of cloud emissivity, resulting in narrow limits on temperature. It has been shown that, with the use of a Q-switched optical maser, even if no light penetration of the cloud occurs, because of the high intensity of the source, very narrow limits can be placed on emissivity, and hence temperature (e.g., with a 200 MW laser system, the limits on temperature at 2500°K would be $\pm$ 50°K).

The gas emissivity in the optically thick region will be determined with the technique used in the sixth motor test. The method depends on a measurement of gas emissivity (sodium D line emissivity in the previous case) in an optically thin region of the motor under test. The emissivity of the optically thick region in the same motor can then be determined because the trace element mass concentration does not change from the one station to the other. Actually (although some sodium reaction, for example, may occur) the effect on line strength is slight. Most of the emissivity change results from a change in the gas density. The effect of temperature on the population of upper and lower states connected with the spectrum line used is easily determined from the Maxwell-Boltzmann distribution.

IV. PROPOSED APPLICATIONS OF FLAME TEMPERATURE MEASUREMENT

The equipment and techniques for flame temperature measurement may be used in various solid, liquid, or hybrid propulsion systems both to further an understanding of the combustion process and as a means of measuring performance (I_s), where conventional measurement methods cannot be used. Three major areas of applications for this technique come to mind:

1. IM-2 Propellant Improvement Program

The ultimate objective of Contract AF 04(611)-10545 is to obtain an understanding of the factors contributing to the lower than expected specific impulse efficiencies of these metalized propellant systems. Measurements obtained on 1KS-250 size motors, both in the chamber and in the exhaust, with IM-2 propellants have strongly suggested that a sizeable quantity of unreacted metal is leaving the combustion chamber. Additional chemical reaction is occurring between the chamber and the exhaust plume resulting in both particle and gas temperatures approximately 200°C above the theoretical temperature. Further, measured particle temperatures in the exhaust are well above (50°C) their melting point for the bulk of the motor firing duration. Hence, the heat of fusion of the particles made essentially no contribution to the motor specific impulse.

The same measurement equipment and techniques can be adapted for use in any metalized propellant improvement program such as the liquid beryllazine or beranizine propellants. In addition, metalized propellants are contemplated for future air augmented propulsion systems. Measurements of particle temperatures will yield important insight into ignition and combustion time delay which in turn will dictate the length of the after-burning section.

2. Advanced NERVA with Elevated Temperature

Present NERVA engine designs utilize tungsten/26% rhenium thermocouples to monitor thrust chamber temperature and use this value through suitable control systems to control the criticality of the atomic reactor. This thermocouple, although highly reliable, is limited to measurements at a fixed immersion depth and position in the thrust chamber. An optical system coupled with suitably located fiber bundles and transparent windows would be capable of scanning both axially and radially across the thrust chambers. This would allow pinpointing trouble spots such as hot channels of gas leaving the reactor, and in turn, supplement the measured thermocouple temperatures.

Future gas core reactors are expected to operate at temperatures beyond the scope of any existing thermocouple material system. Here an optical means for control will be a necessity.

3. Small Liquid Attitude Control Motors

Small liquid attitude control motors, with impulse bits lasting approximately 30 millisec, will use immeasurably small flow rates for both the oxidizer and fuel. Hence, the most important measured performance parameter,

IV, Proposed Applications of Flame Temperature Measurement (cont.)

specific impulse, is missing. Specific impulse determinations, then, must rely on a calculated mass flow rate which is not reliable, particularly during the transient period. By measurement of chamber temperature along with the normal measurement of chamber pressure, the flow rate through the critical section of the nozzle is obtained. This together with measured thrust gives the specific impulse. The required time for measurements with the spectral comparison technique has already been demonstrated to be well within the 30-millisec pulse duration. Further, by measurement of temperature in the chamber and in the exhaust plume the enthalpy change and hence the specific impulse is obtained directly (with knowledge of the gas specific heat.) Thus, impulse measurements need not depend on pressure and thrust measurements alone. Temperature measurements can be used to supplement existing impulse measurement techniques.

NOMENCLATURE

A/A^* = expansion ratio

A^* = area of nozzle throat

c^* = characteristic exhaust velocity, $I_s g/C_f$

C_f = $F/P_c A^*$

C_2 = constant in Planck's equation, 1.4388×10^4 micron °K

C_w = g/c^*

D = diameter

E_{ij} = Emf generated from radiance detected by phototube

i - refers to wave length λ_i

j = 0 - refers to reference source alone

j = 1 - refers to radiance from both flame + reference source

j = 2 - refers to radiance from flame alone

F = thrust, lbf

$f(d)$ = frequency function of D, normalized such that $\int_0^\infty f(D)\, dD = 1$

I = intensity of light

I_o = incident light intensity

I_l = plane-polarized component of light intensity perpendicular to plane of observation

I_s = specific impulse

I_i = intensity function, see footnote, p. 14.

i = 1 plane polarized in direction perpendicular to observation plane

i = 2 plane polarized in observation plane

k = $2\pi/\lambda$

K_{ij} = phototube multiplication constant at E_{ij}

NOMENCLATURE (cont.)

m = refractive index

N = particle number density, cm^{-3}

n = real part of refractive index

n' = imaginary part of refractive index

R_{io} = radiance from Planck's law, defined in Appendix A, Equation 7

r = distance from light stop of scattering detector to scattering volume

r_b = burning rate

T = temperature, °K

T_b = brightness temperature,

T_s = source temperature, °K

t = thickness, cm

$\bar{V}$ = mean particle volume

V = volume

$\dot{w}$ = mass flow rate, lbm/sec

Greek Symbols

α = $\pi D/\lambda$, particle size function, dimensionless

γ_a = absorption cross section, spectral absorption coefficient

γ_s = scattering cross section, spectral scattering coefficient

γ_t = $\gamma_a + \gamma_s$

ϵ = emissivity

μ = micron, 10^{-6} meter

λ_i = wavelength, micron

i = 1 refers to wavelength removed from a spectrum line

i = 2 refers to spectrum line

NOMENCLATURE (cont.)

θ	=	angle between center line of detector and center line of incident light beam as shown in Figure 9.
ρ	=	reflectivity of particles, mirrors, etc. or density
σ_X	=	standard deviation of the variable X, $\equiv \sqrt{\text{variance about } X}$
τ	=	transmissivity
χ	=	mass fraction of particles
ξ	=	function of propellant properties

Subscripts

ai	=	absorption, at γ_i
b	=	brightness
L	=	liquid
g	=	gas
o	=	comparison source
p	=	particles
si	=	scattering, at γ_i
wi	=	window, at γ_i

REFERENCES

1. Adams, J. M. and S. E. Colucci, "The Spectroscopic Measurement of Gas and Particle Temperatures in Metallized Propellant Combustion". Paper S66-175 ICRPG/AIAA Conference to be presented July 18-21, 1966 Washington, D. C.

2. Colucci, S. E. and J. M. Adams "Flame Temperature Measurements in Metallized Propellant", 2nd Qtrly. Technical Report to AFRPL, Project 3148, Aerojet-General Corp., Report SPO 20, Nov. 1965.

3. Colucci, S. E. and J. M. Adams "Flame Temperature Measurement of Metallized Propellant", First Quarterly Tech. Report to AFRPL, Project 3148, Aerojet-General Corporation, August 1965.

4. Hett, J. H. and J. B. Gilstein, "Pyrometer for Measuring of Instantaneous Temperatures in Flames", J. Opt. Soc. of America, 30, 11(1949) 909.

5. Sutherland, G. S. "The Mechanism of Combustion of an Ammonium Perchlorate-Polyester Resin Composite Solid Propellant", Ph.D. Thesis in Aeronautical Engineering, Princeton University, 1956.

6. Bundy, F. P. and H. M. Strong, "Measurement of Flame Temperature, Pressure, and Velocity", Phys. Meas. in Gas Dynamics and Combustion, Princeton Series Vol. IX, 1954.

7. Carlson, D. J., Temp., Its Meas. and Cont. in Sci and Ind. 3, Part 2. Reinhold, New York, (1962) 535.

8. Tourin, R. H. et. al., "Measurement of Temperatures in Ionized Gases by Means of Infrared Radiation", ARL 62-314, Office of Aerospace Research (1962).

9. Null, M. R. and W. W. Lozier, "The Carbon Arc as a Radiation Standard", Temp. Its Meas. and Cont. in Science and Ind. 3, Part 1, Reinhold, New York (1962) 551.

10. RCA Electron Tube Division 1P21-10-58 "1P21 Multiplier Ohototube". n.d.

11 DeVos, J. C. "A New Determination of the Emissivity of Tungsten Ribbon", Physica 20 (1954) 690-714.

12. Erickson, W. D. "Light Scattering, a Technique for Studying Soot in Flames" Ph.D. Thesis in Chemical Engineering, MIT, Dec. 1961.

13. Gryvnak, D. A. and D. E. Burch, "Optical and Infrared Properties of Alumina at Elevated Temperatures", Philco Publ. U-2623 (AD 606 793), 1964.

REFERENCES (cont.)

14. Maltison, I. H. et. al., "Refractive Index of Synthetic Sapphire", J. Opt. Soc America 48, 1 Jan 1958.

15. Carlson, D. J. and R. A. Dupuis, "Alumina Absorption and Emittance", Philco Publ. No. 2627 (1964).

16. Kirshenbaum, A. D. and J. A. Cahill, "The Density of Liquid Aluminum Oxide", J. Inorg. Nucl. Chem. 14, (1960) 283-287.

17. Colucci, S. E. and J. M. Adams "Flame Temperature Measurement of Metallized Propellant", Third Quarterly Techn Report, Project 3148, Aerojet-General Corporation Report SRO 20, November, 1965.

18. Couglin, J. P. and Smith. R. M., "A description of the Aerojet-General Corporation Computer Program for Calculation of Specific Impulse." n.d.

19. JANAF Thermochemical Data, the DOW Company Thermal Laboratory, Midland, Michigan, 31 December 1960, and subsequent revisions.

20. Kuby, W., et al., "An Investigation of Recombination and Particle Lags Effects in Rocket Nozzles," (U) Aeronutronic Report C-1938, CONFIDENTIAL, December 1962.

21. Carlson, D. J., Personal Communication with J. M. Adams, April, 1966.

22. Coughlin, J. P. and Hollingsworth, S. W. "A Correlation between Measured and Computed Values of Microwave Attenuation for Solid Propellant Exhausts Part II: Theoretical Calculations and Correlations", Special Session, 20th Interagency Solid Propellant Meeting, Philoadelphia, Penn., July 1964 (Volume IV, Bulletin).

23. Sehgal, R. JPL Space Programs Summary 37-22(B) "The Collection and Evaluation of Particulate Matter" CONFIDENTIAL, No date.

FIGURES

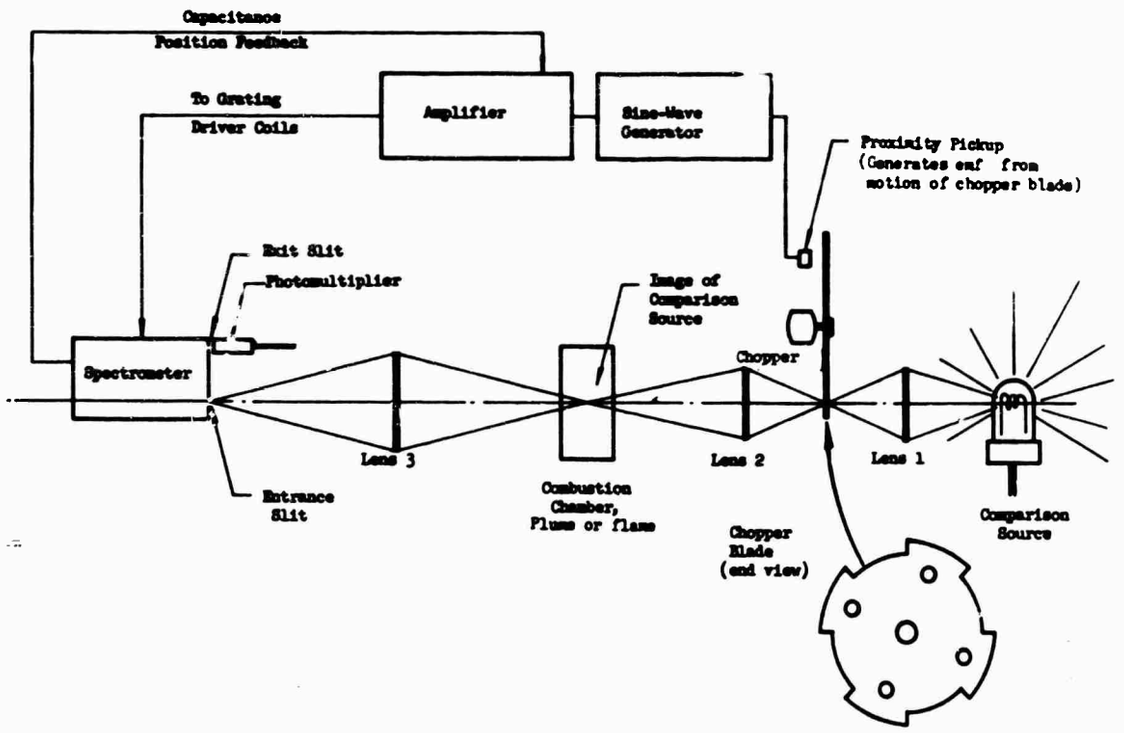

Optics and Electromechanical Schematic of Spectral Comparison Pyrometer

Figure 1

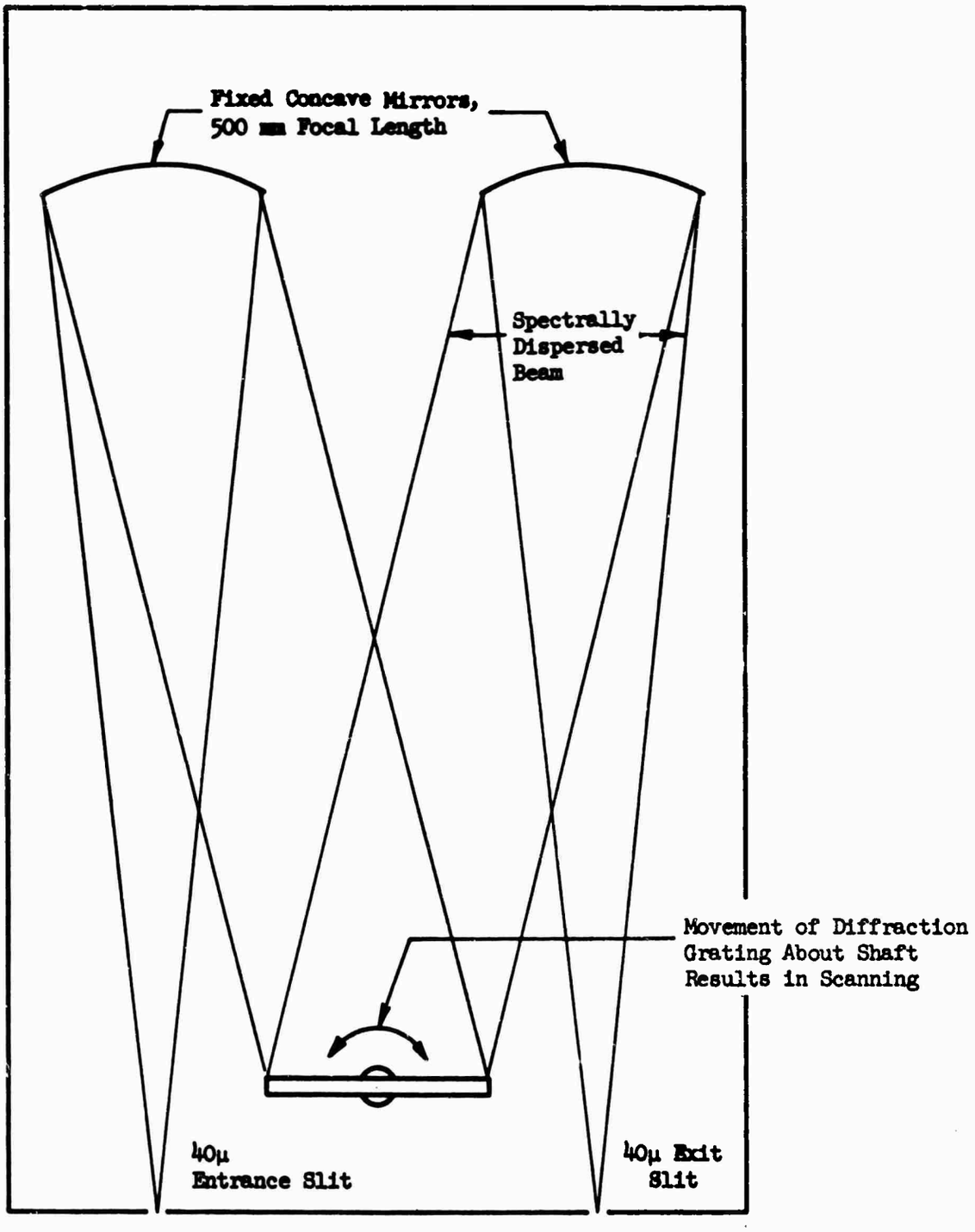

Internal Optics of 0.5 Meter Jarrell-Ash Spectrometer

Figure 2

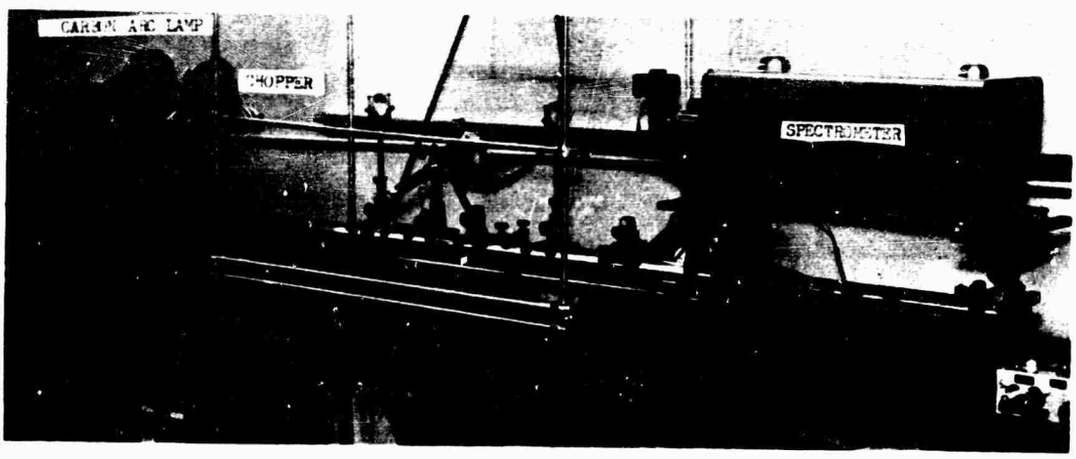

Laboratory Apparatus, Spectral Comparison Pyrometer

Figure 3

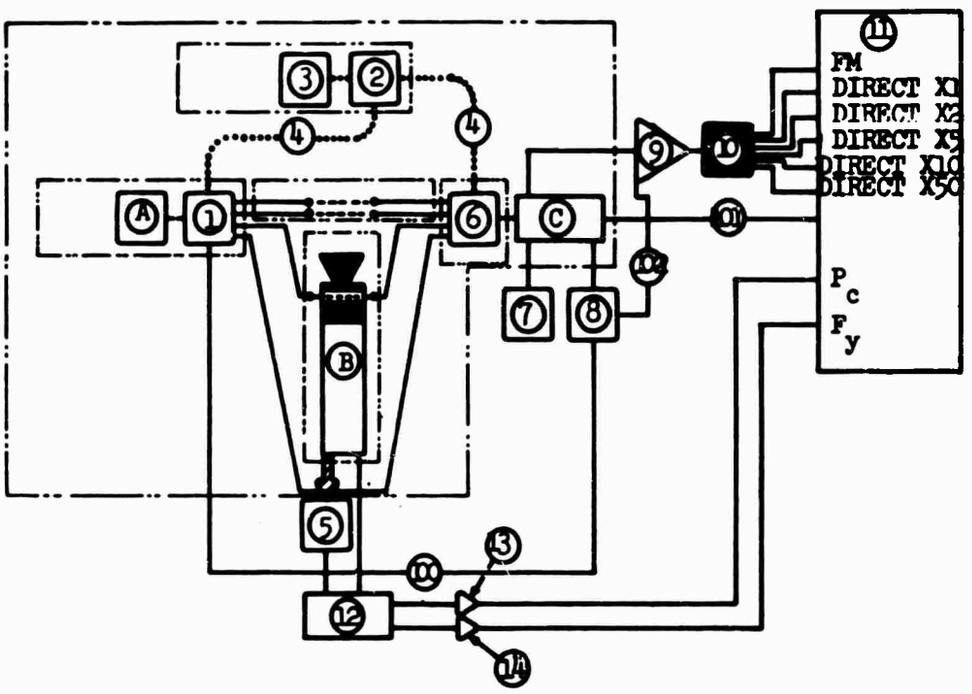

No.	DESCRIPTION
A	CARBON ARC OR OPTICAL MASER
B	MOTOR
C	SPECTROMETER
1	OPTICAL SAMPLING SWITCH
2	MITER GEAR COUPLING
3	D.C. SHUNT WOUND MOTOR
4	FLEXIBLE SHAFT
5	LOAD CELL
6	OPTICAL SAMPLING SWITCH
7	POWER SUPPLY (PHOTO TUBE)
8	POWER SUPPLY (SCANNING EXCITER COIL)
9	AMPLIFIER
10	DATA RANGING
11	RECORDING EQUIP.
12	ATTENUATOR CIRCUIT
13	AMPLIFIER
14	AMPLIFIER
100	TIMING SIGNAL FOR SCANNER
101	OUTPUT FROM SCANNING EXCITER COIL
102	POWER FOR AMP

Optical Sampling Equipment Used on Motor Tests 1 and 2

Figure 4

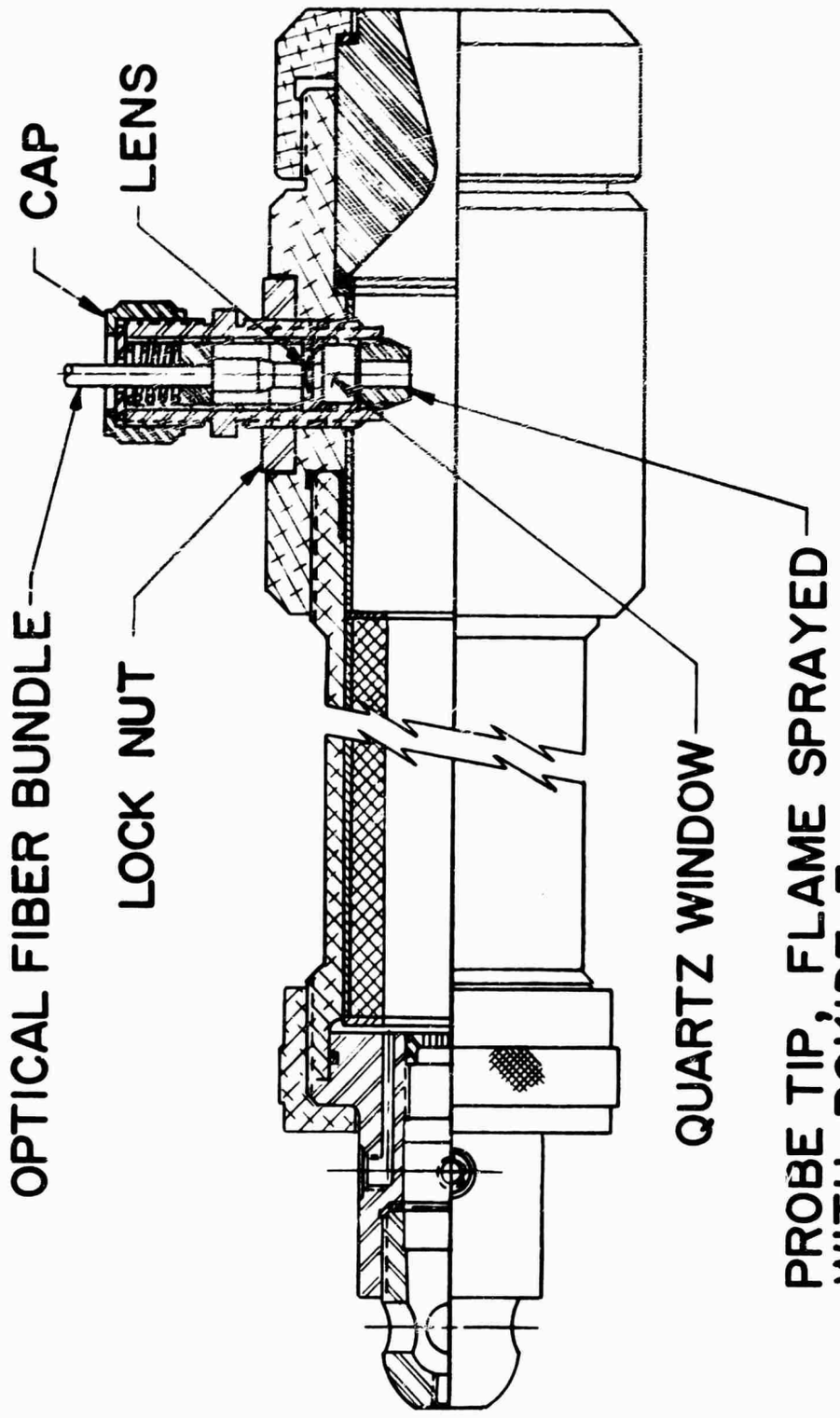

Test Motor Assembly

Figure 5

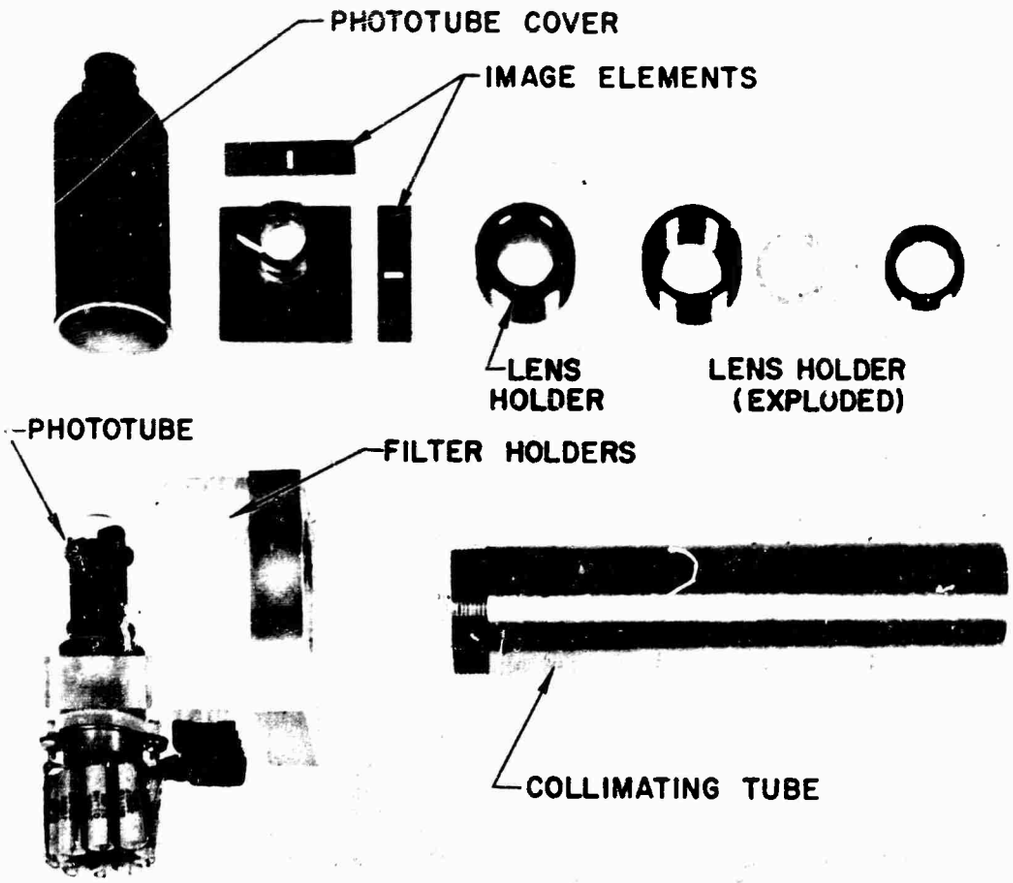

Scattering Detector Assembly, Exploded View

Figure 6

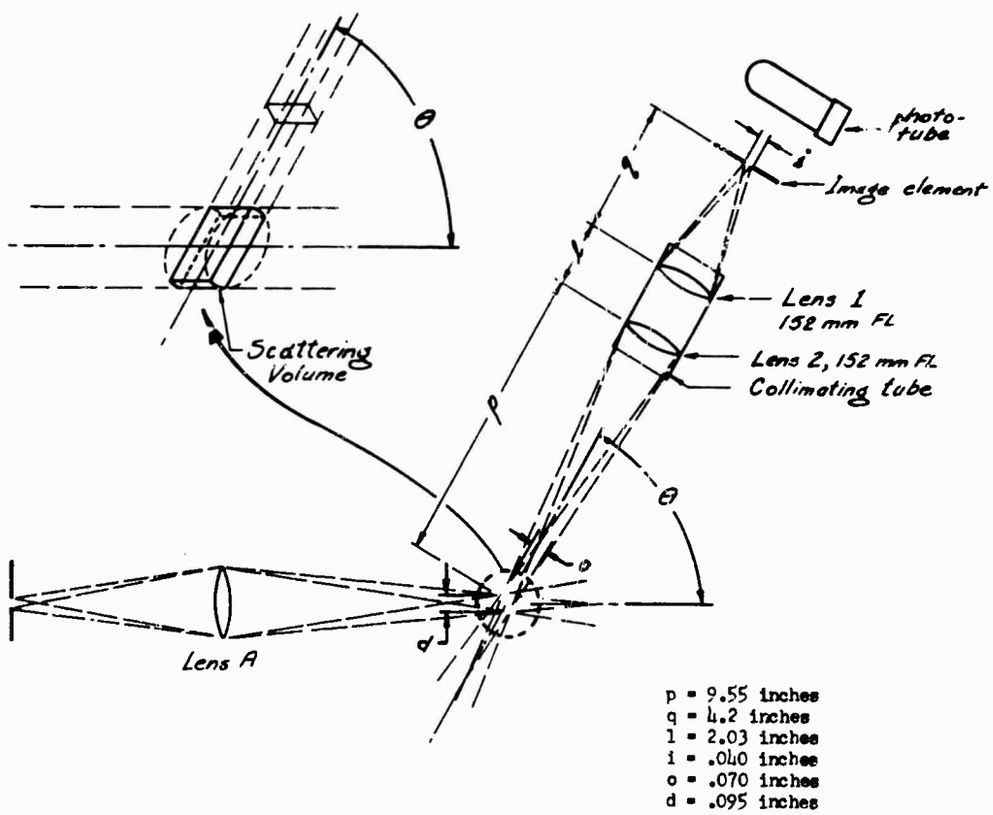

Optics for Light Scattering Measurement

Figure 7

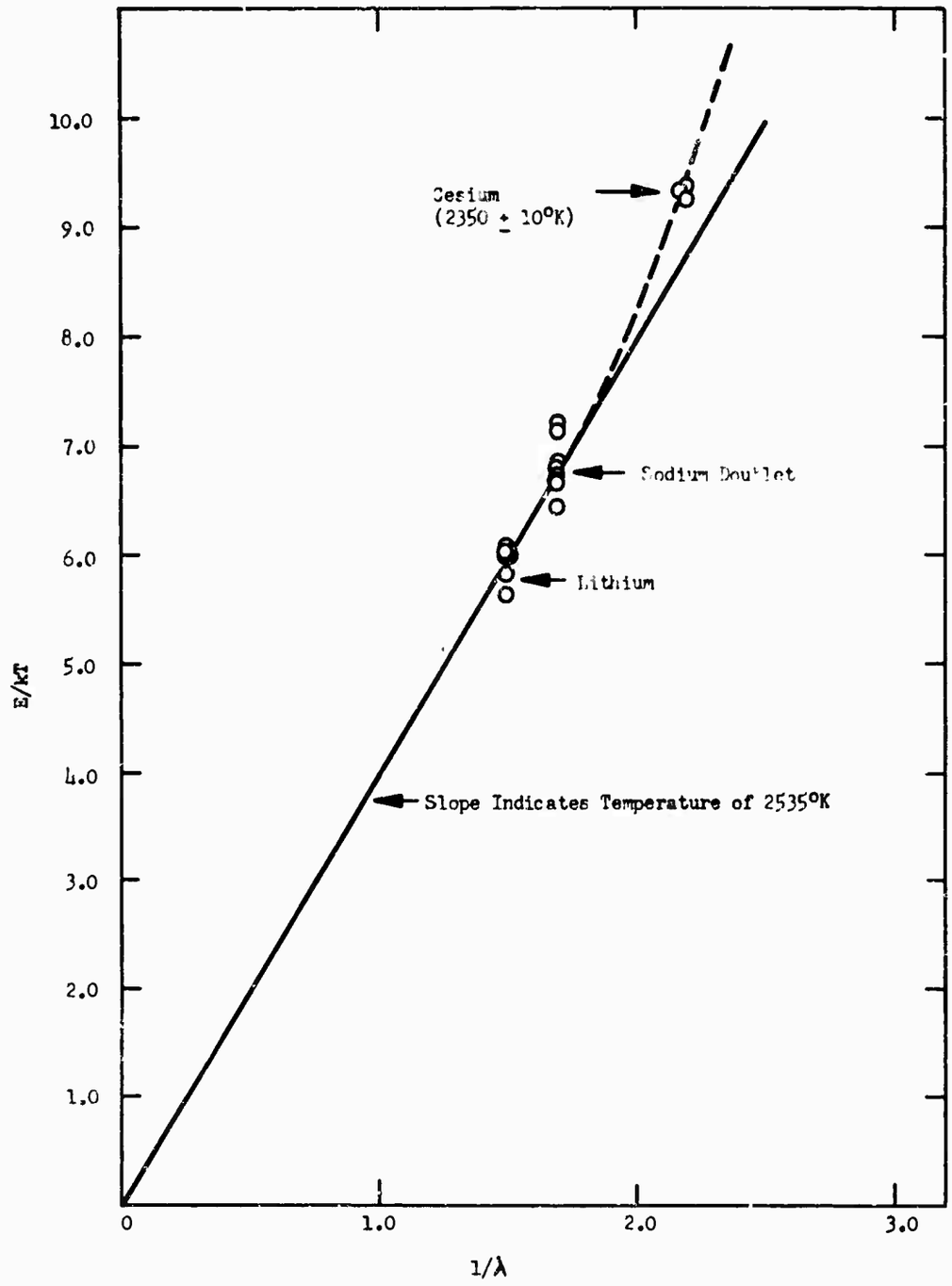

Temperature Measurements Using Spectrum Line Intensities of Sodium, Lithium, and Cesium

Figure 8

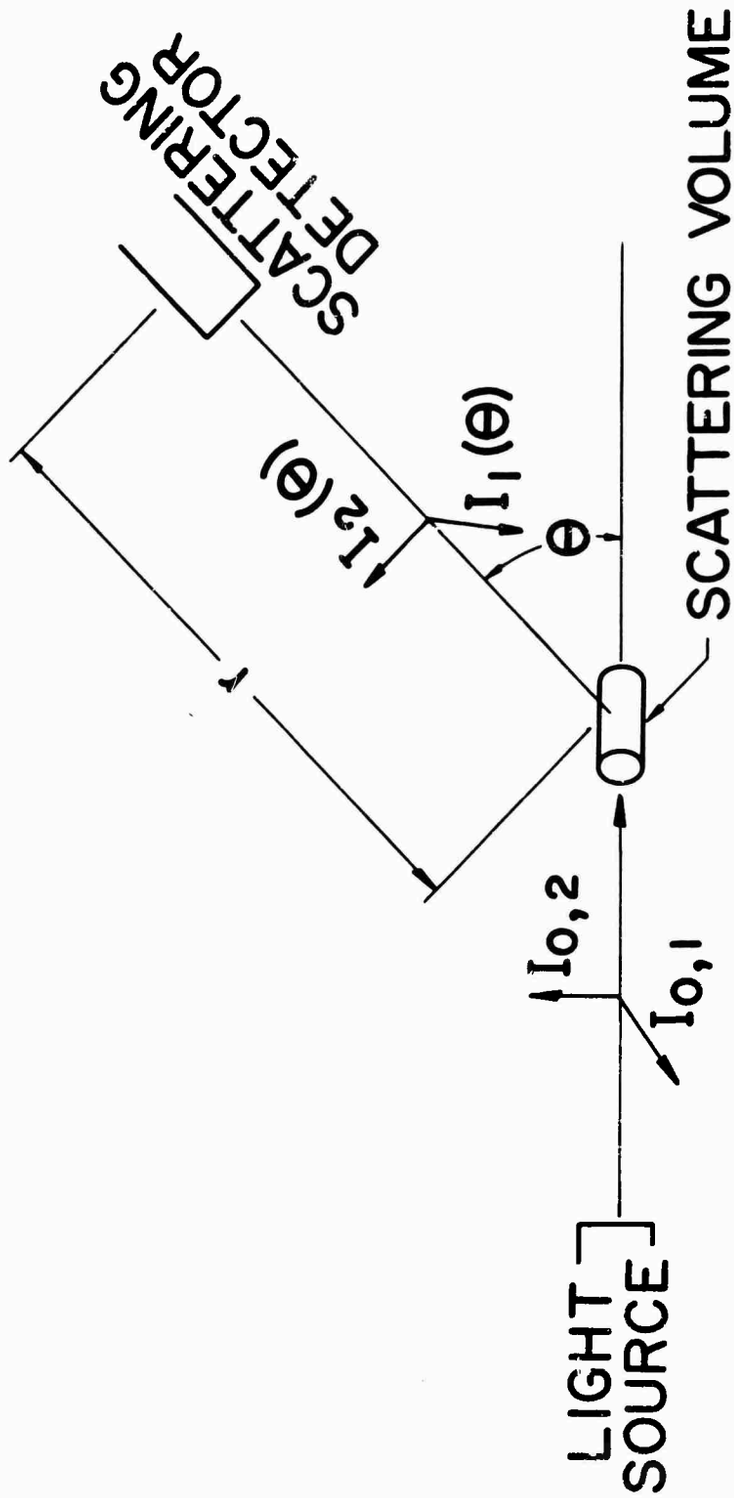

Scattering Detector Schematic Showing Planes of Polarization

Figure 9

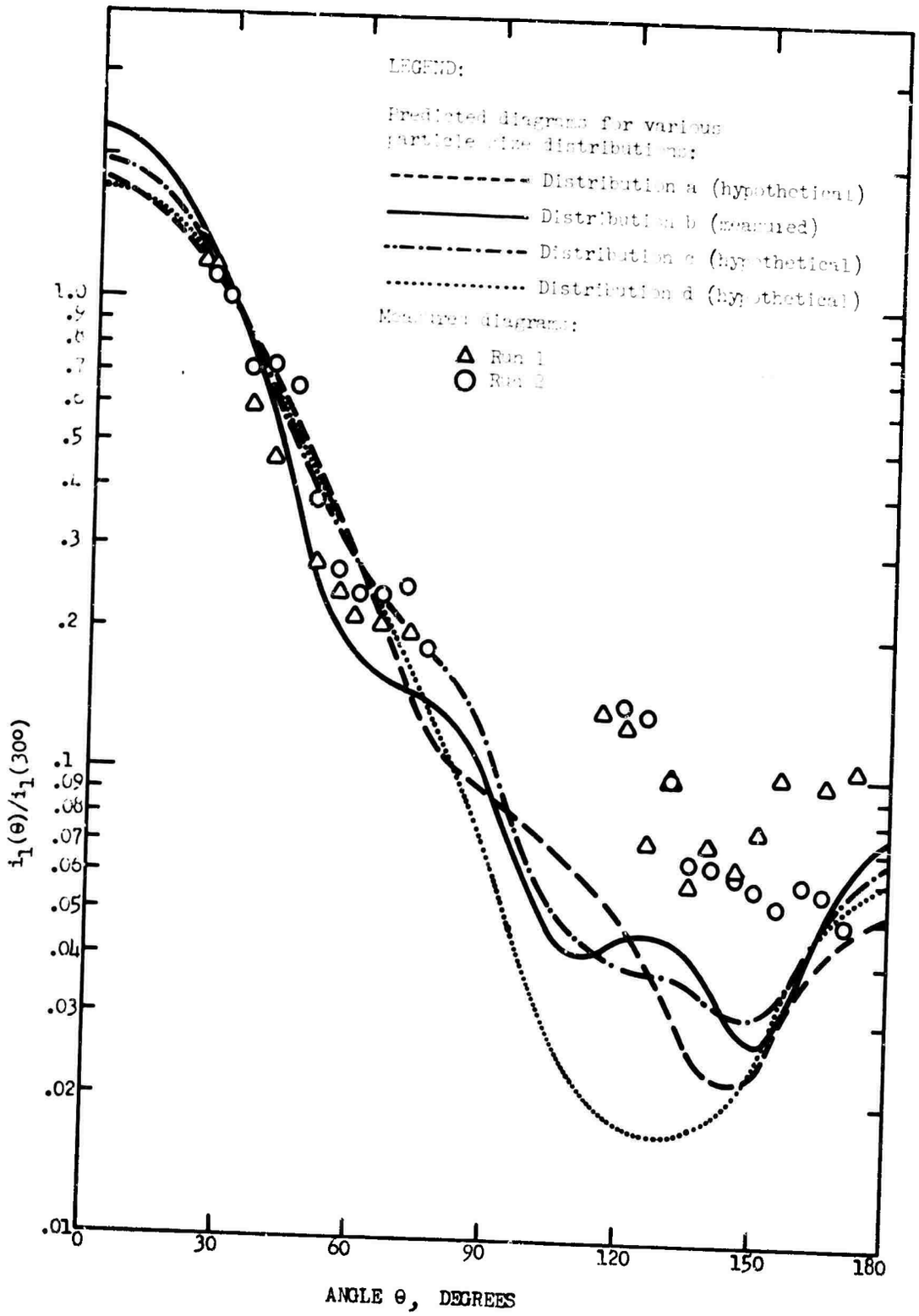

Light Scattering Diagrams i_1 for Various Particle Size Distribution, Normalized to i_1 (30°)

Figure 10

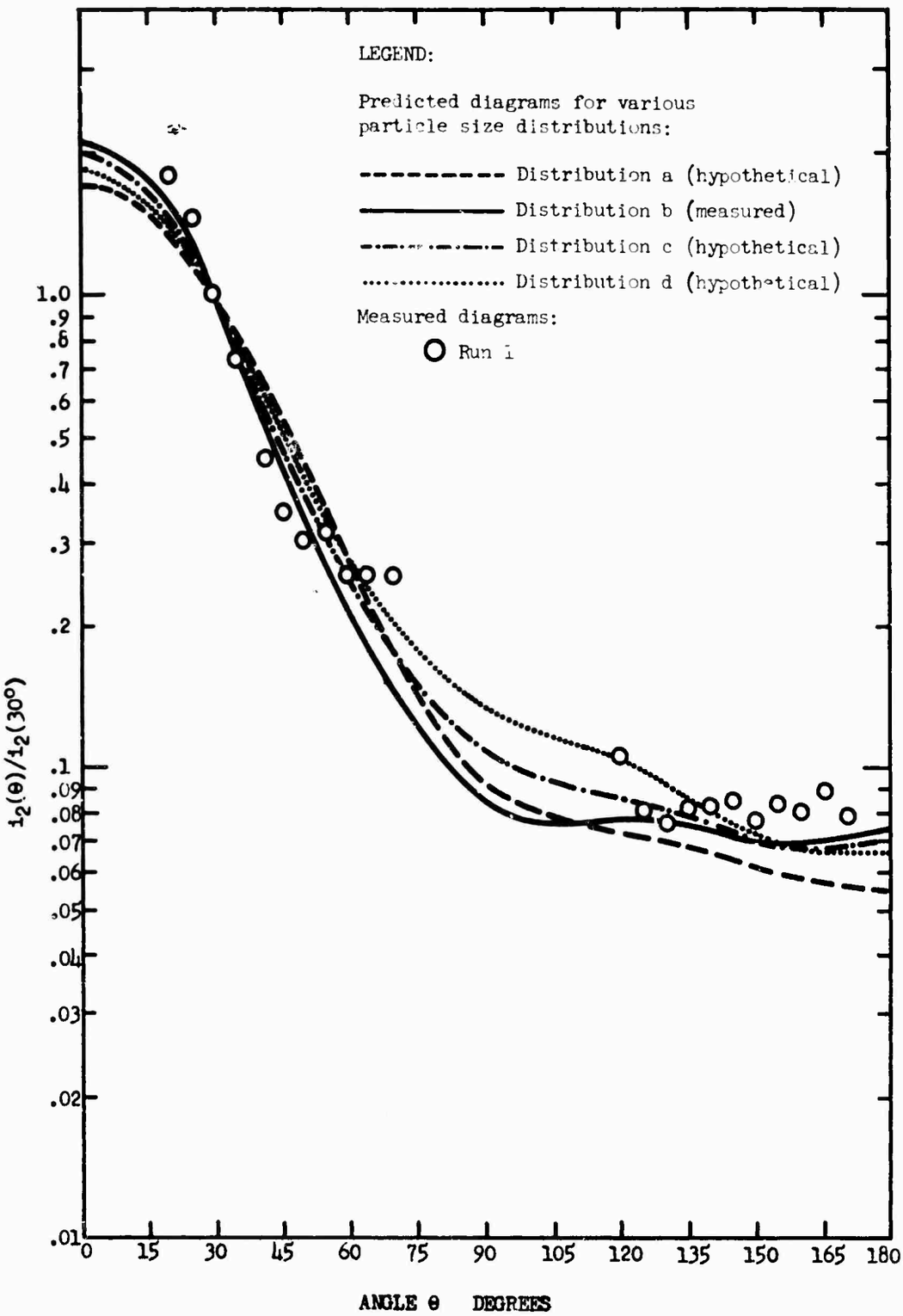

Light Scattering Diagrams i_2 for Various Particle Size Distribution, Normalized to i_2 (30°)

Figure 11

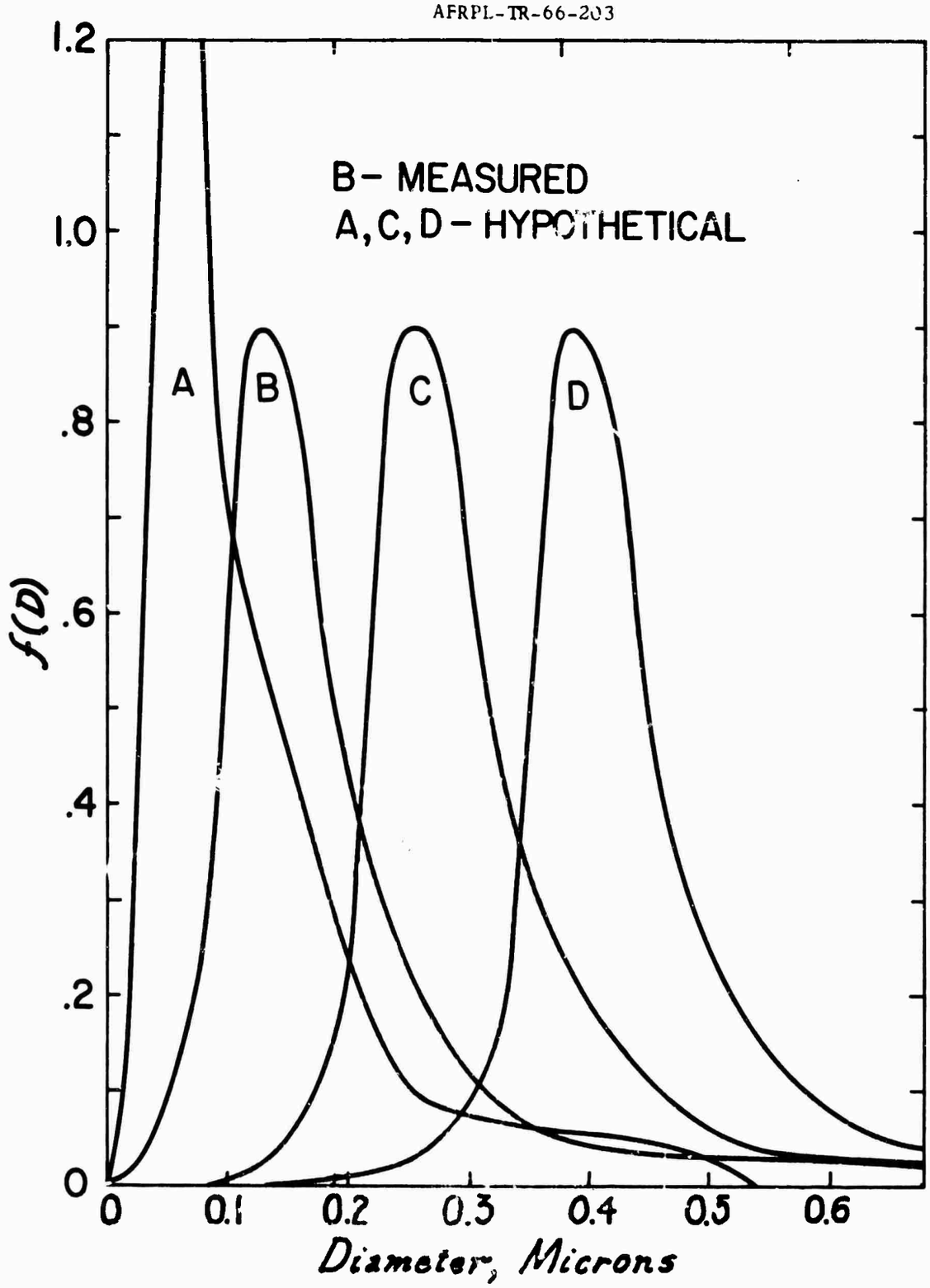

Particle Size Distributions, Measured and Hypothetical, Used to Generate Scattering Diagrams in Figures 10 and 11

Figure 12

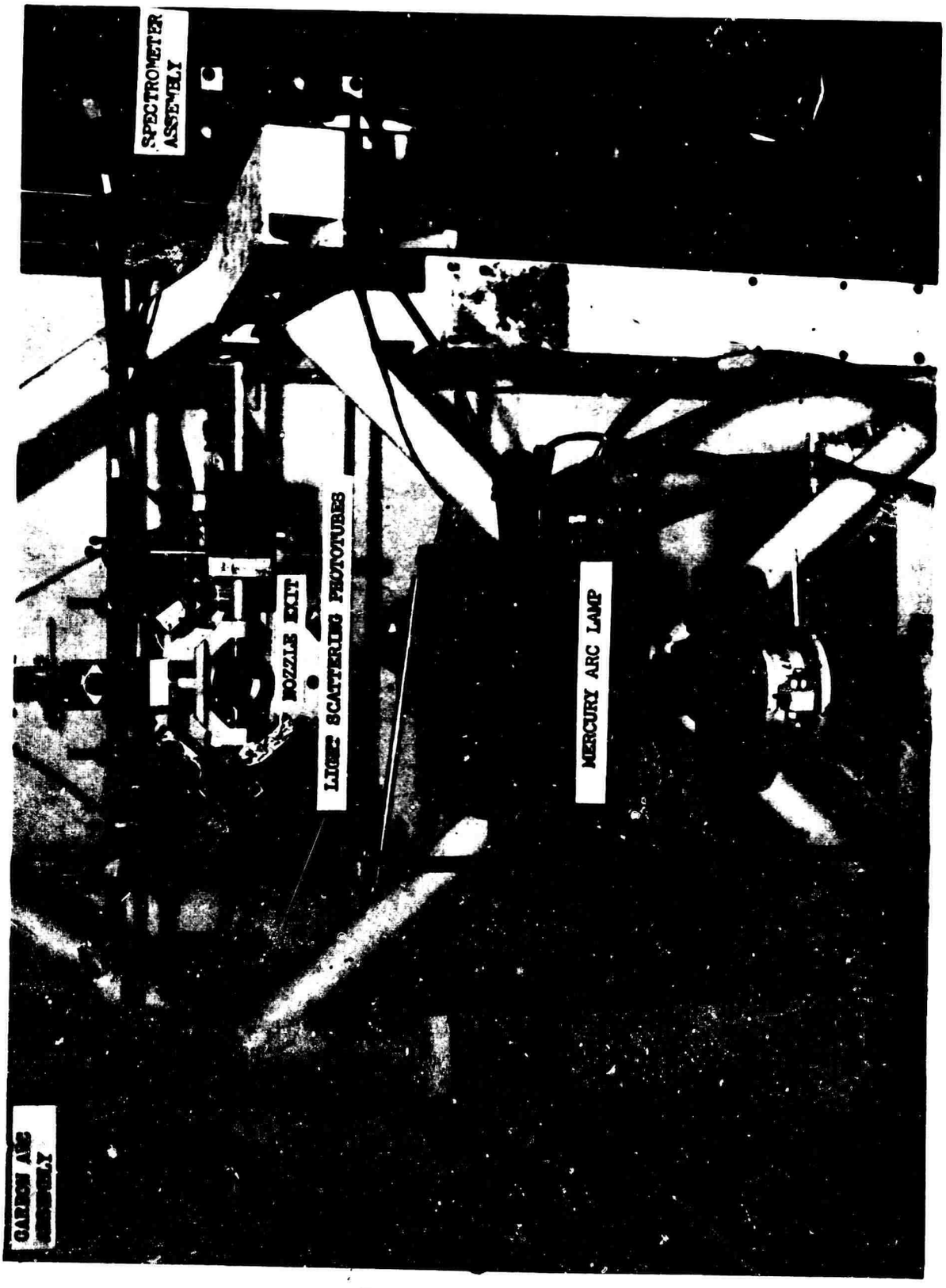

Apparatus Used for Flame Temperature Measurements on Small Motors

Figure 13

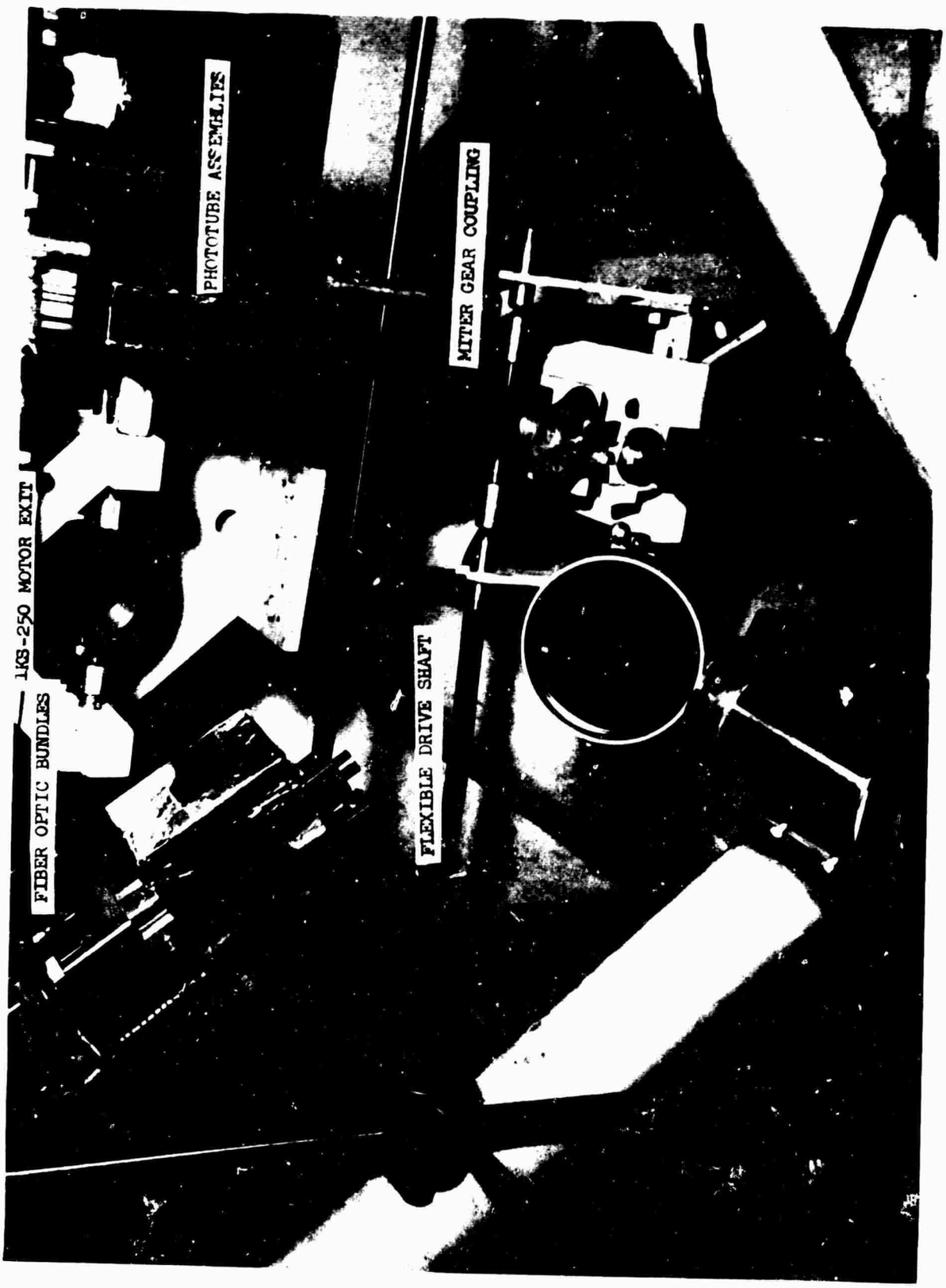

Close-up View of Apparatus

Figure 14

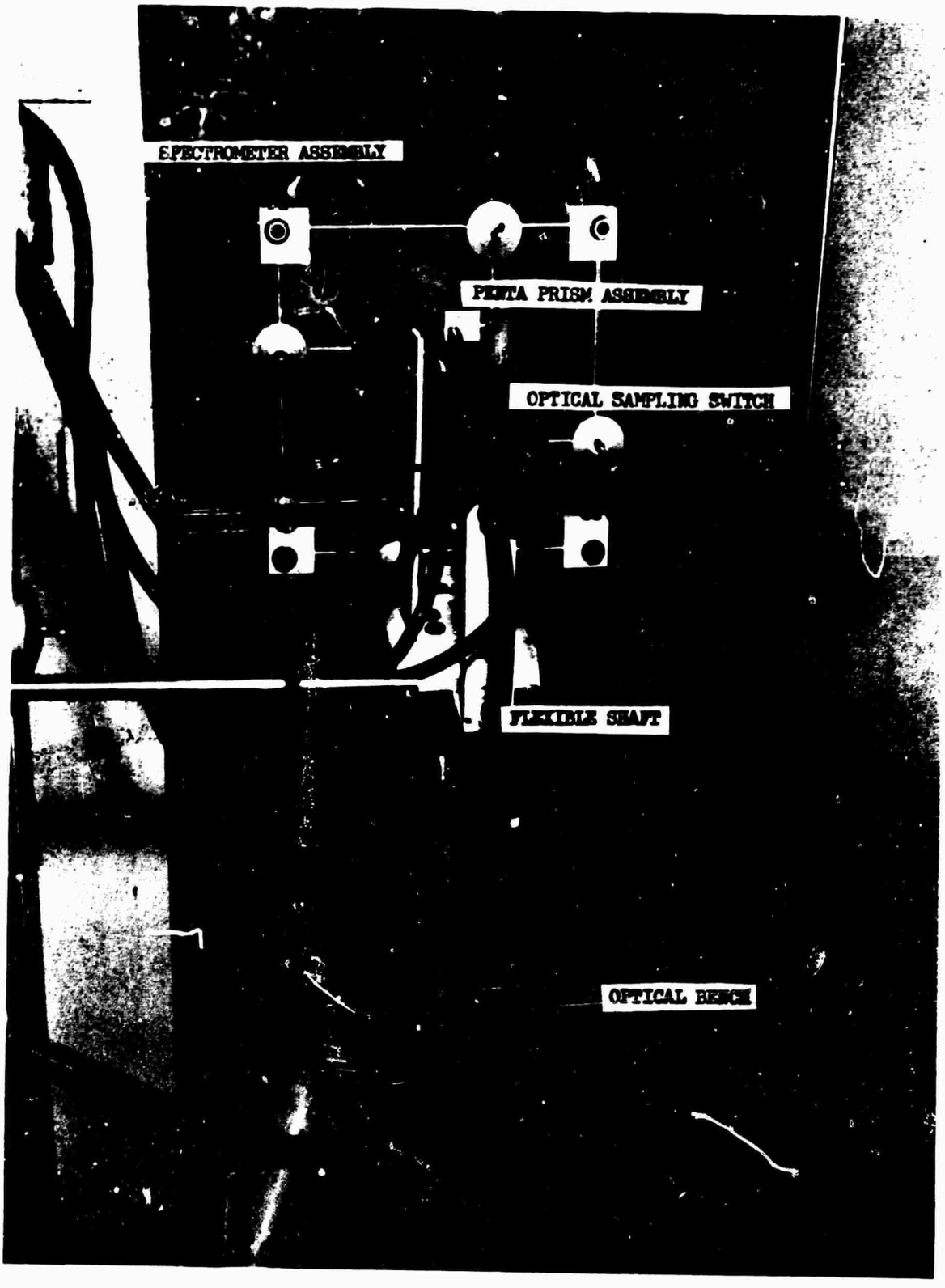

Spectrometer and Optical Sampling Switch Assembly

Figure 15

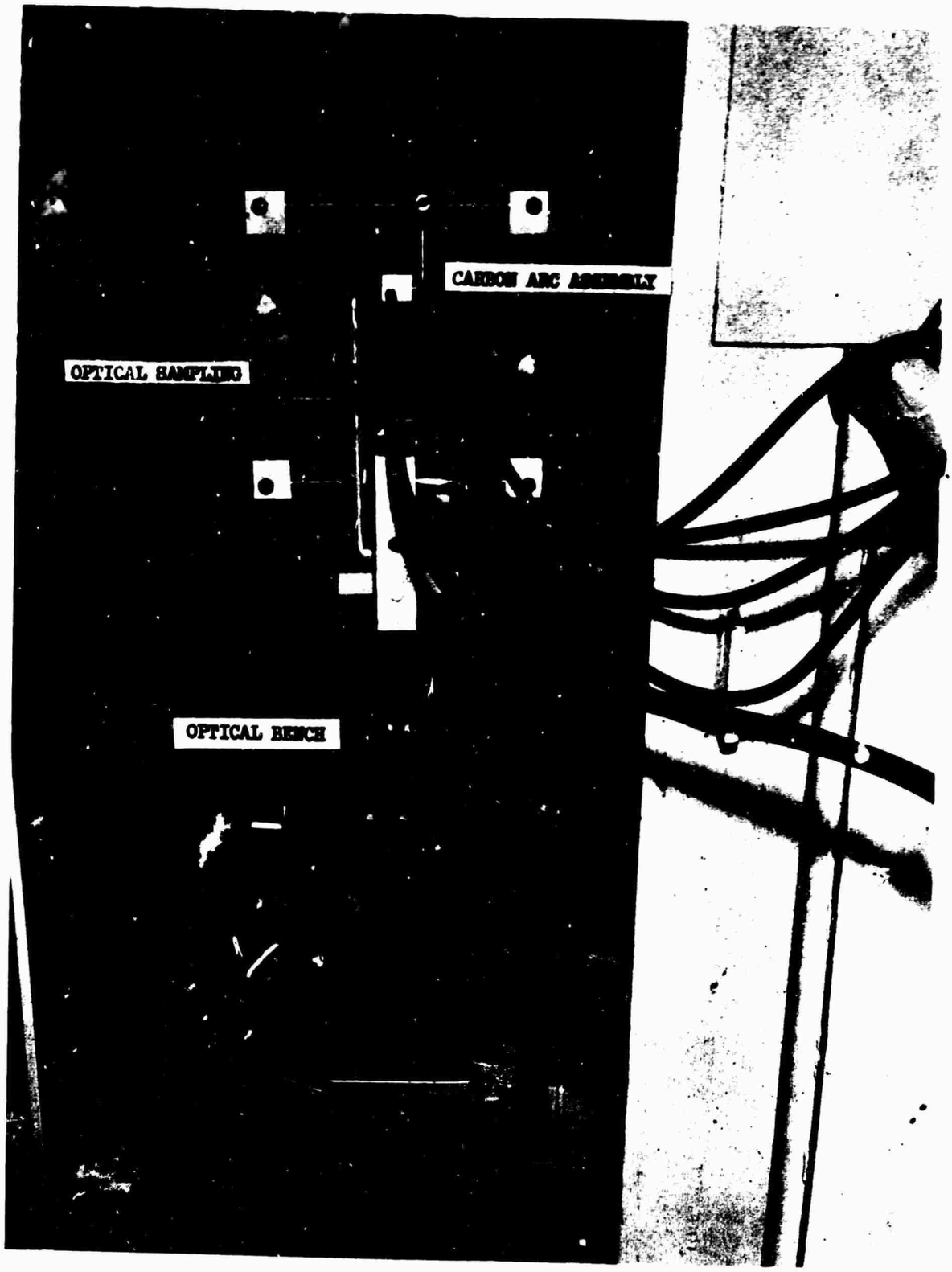

Carbon Arc and Optical Sampling Switch Assembly

Figure 16

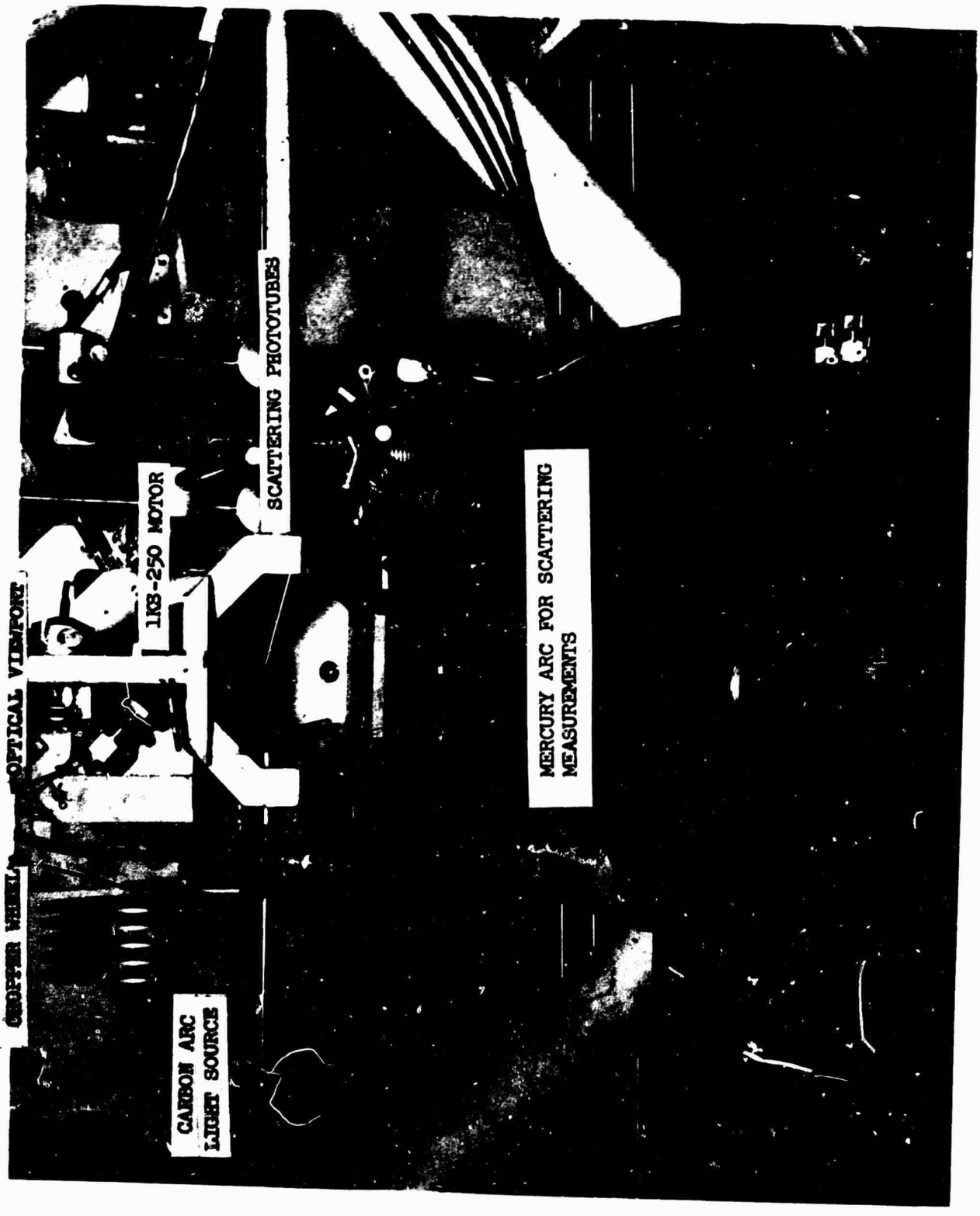

Apparatus Used for Flame Temperature Measurement on Small Motors

Figure 17

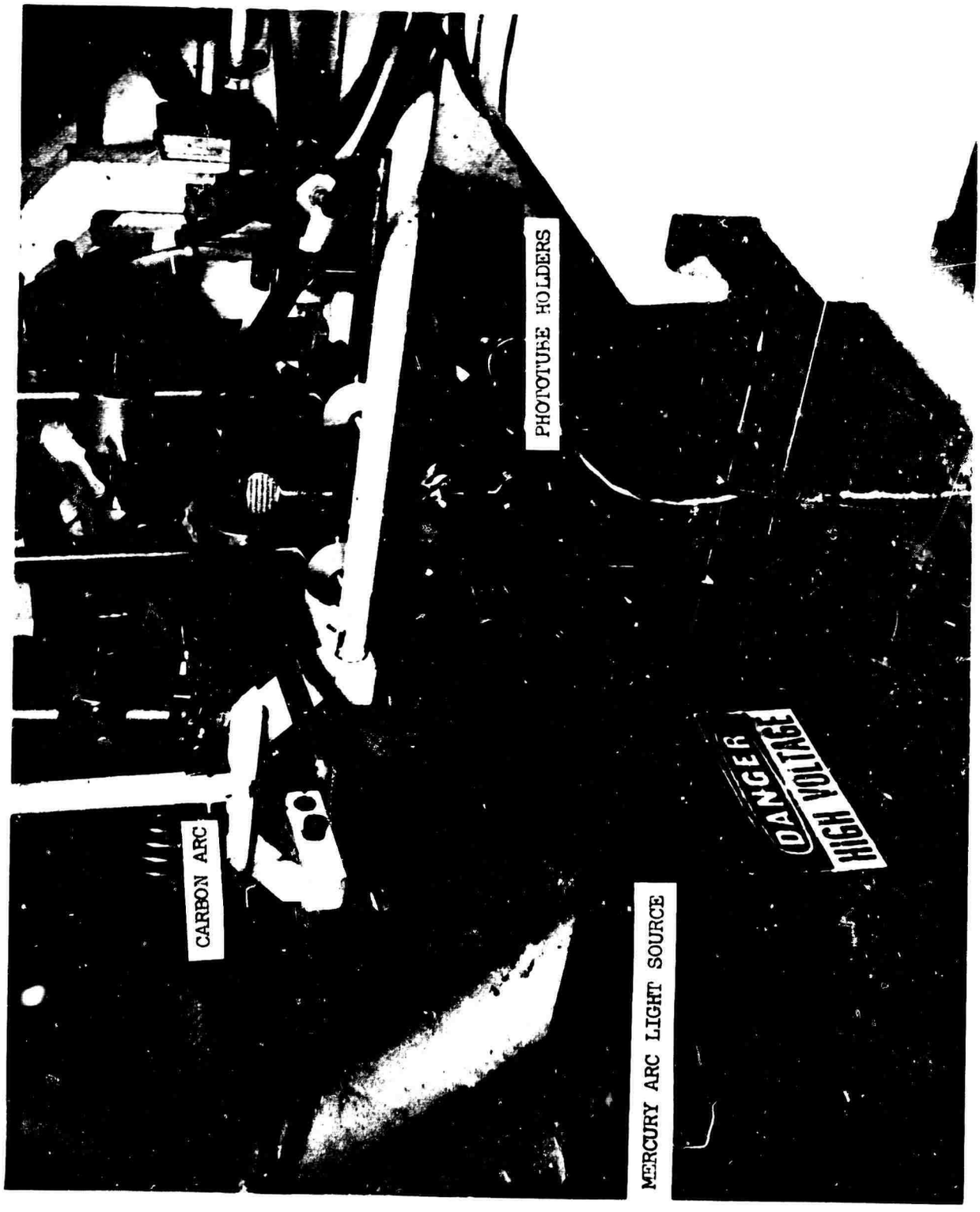

Close-up View of Apparatus

Figure 18

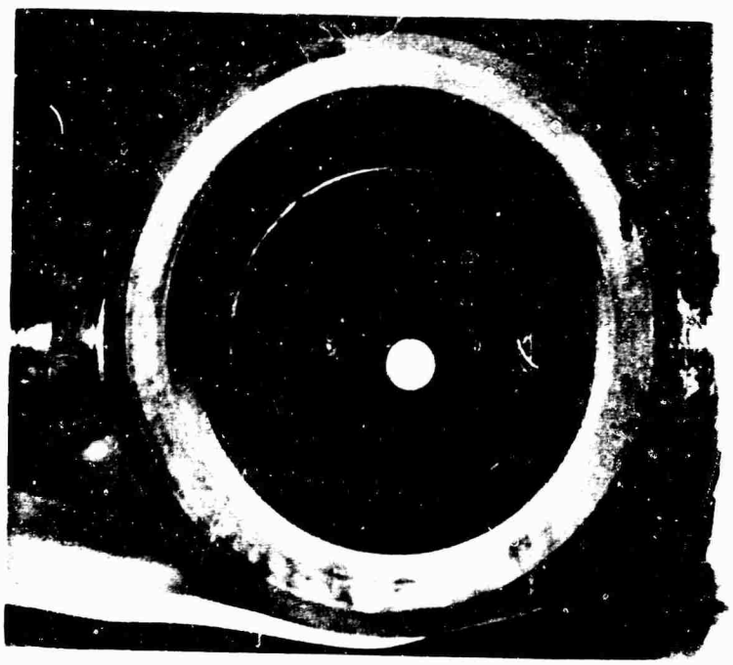

Nozzle Postfiring View Looking Aft from Plenum to Throat (Test 2)

Figure 19

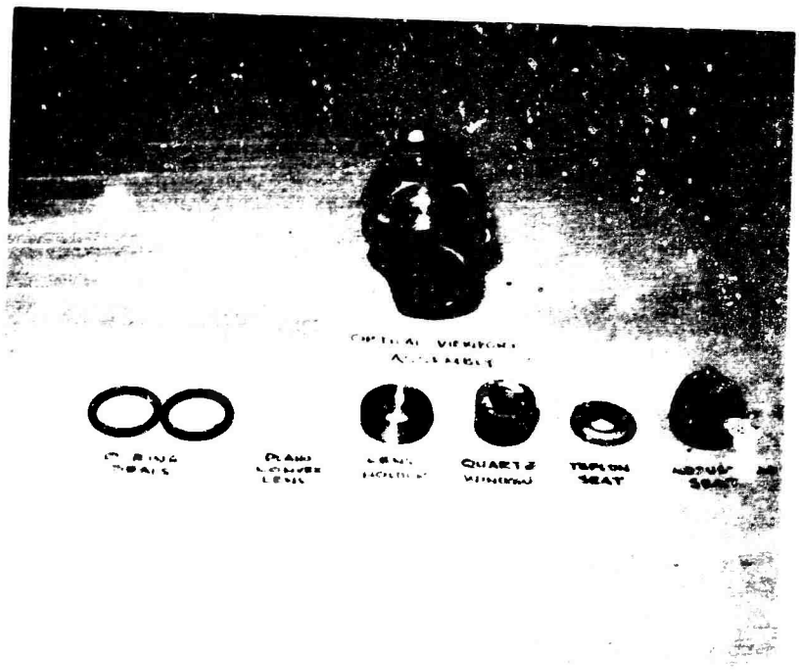

Optical Viewport Components - Postfiring Test No. 2

Figure 20

Series FT-ZX-01S-BH-006 (LMH-2)

(Taken after Test 5)

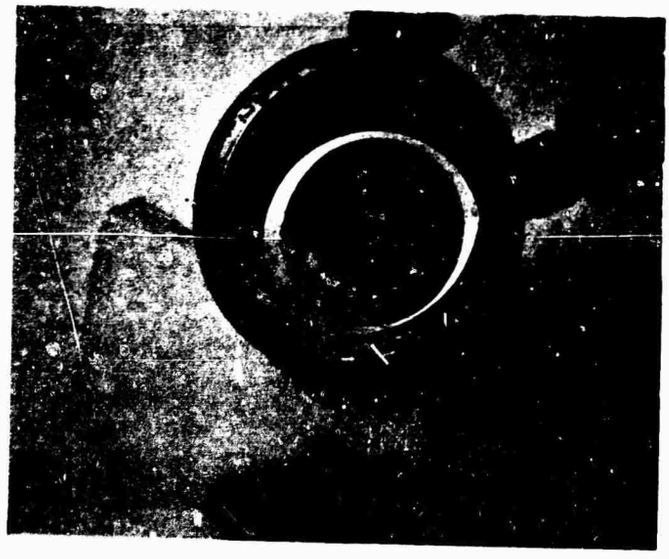

(Taken after Test 7)

Series FT-ZX-01S-BH-008 (LMH-2)

Nozzle Postfiring Views (LMH-2 Propellant)

Figure 21

Series FT-ZX-01S-BH-007 (LM-2)

(Taken after Test 6)

Series FT-ZX-01S-BH-009 (LM-2)

(Taken after Test 8)

Nozzle Postfiring Views (LM-2 Propellant)

Figure 22

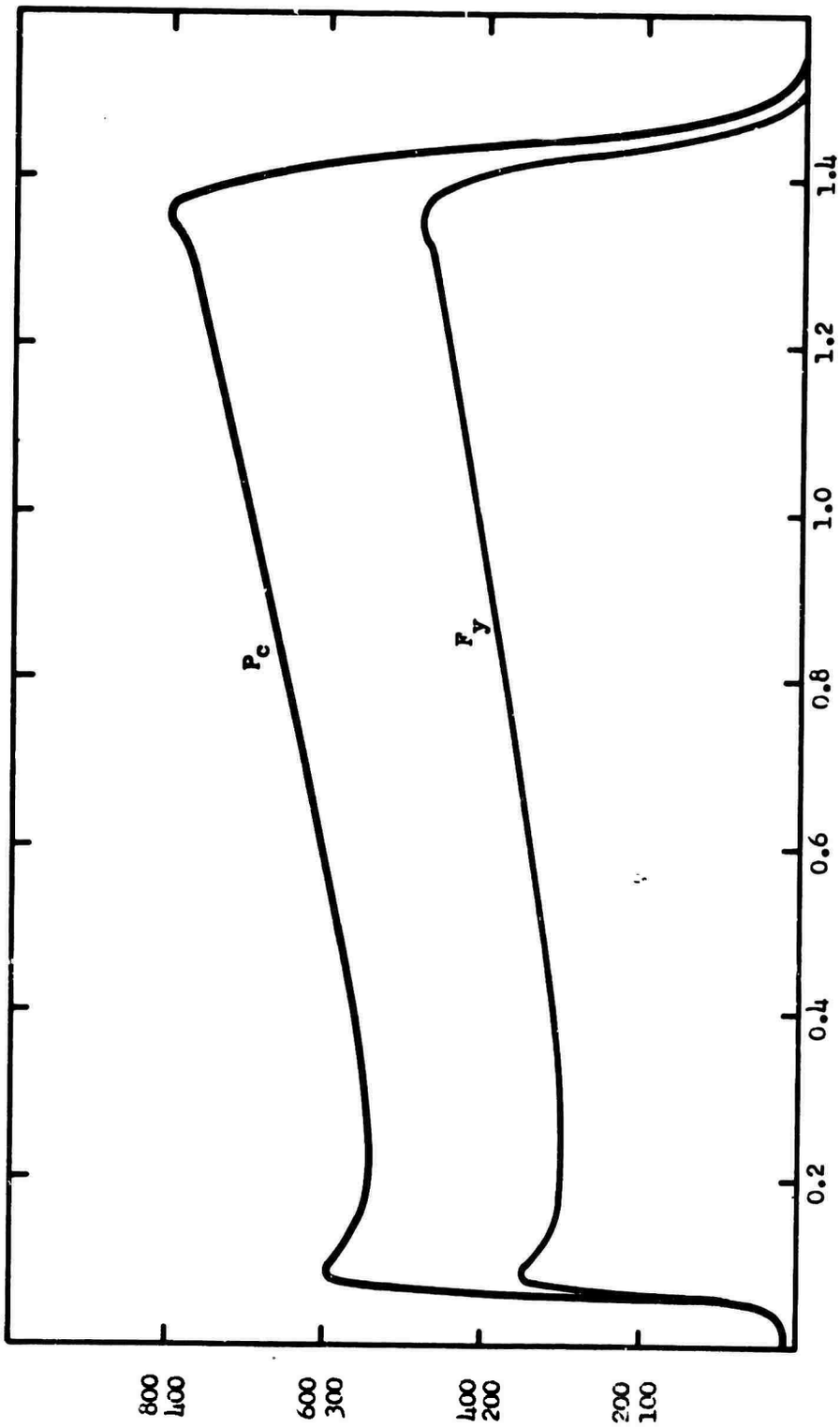

Motor Performance (Test Series FT-ZX-015-BH-1)

Figure 23

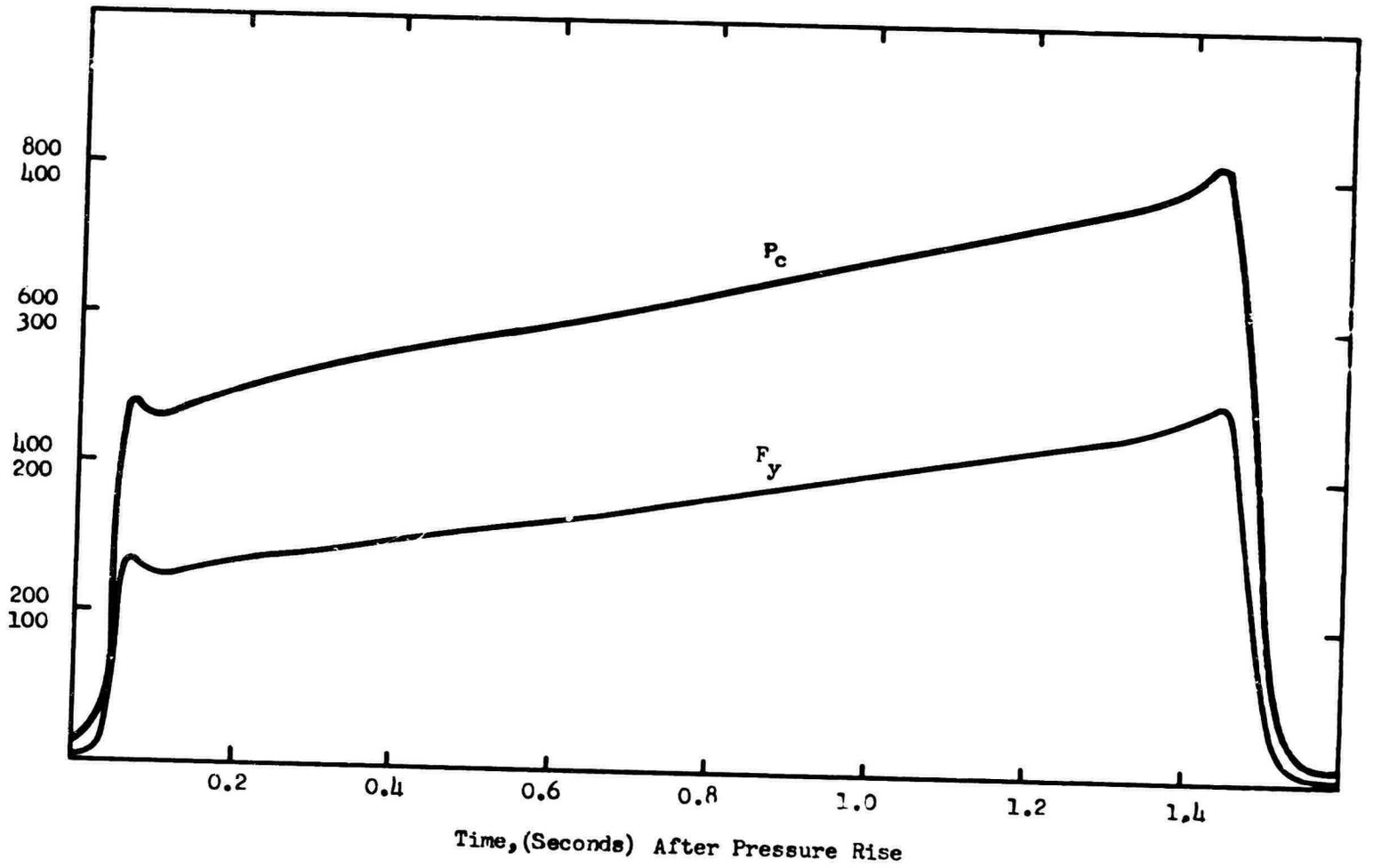

Figure 24

Motor Performance (Test Series FT-ZX-01S-BH-2)

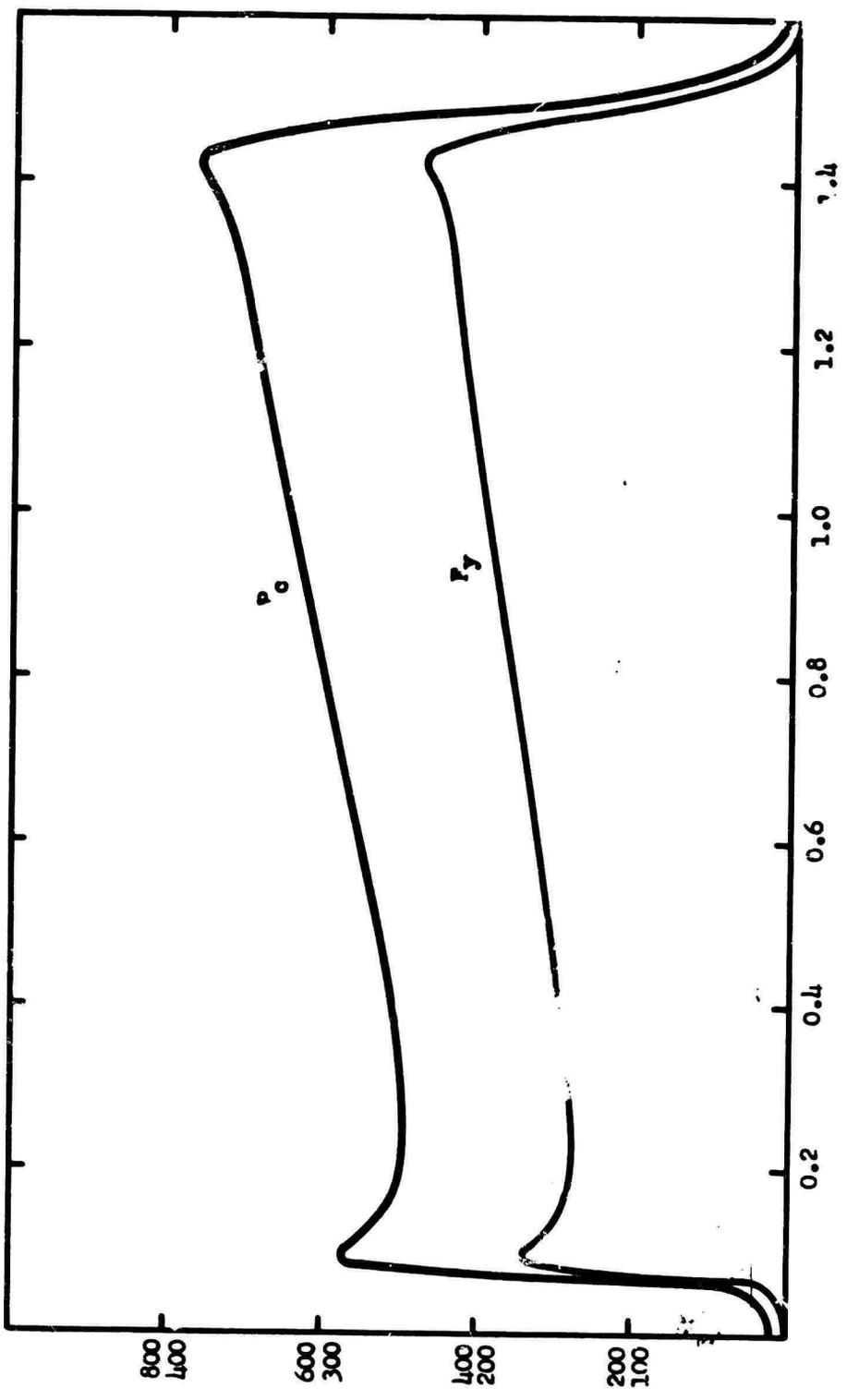

Motor Performance (Test Series FT-ZX-01S-BH-3)

Figure 25

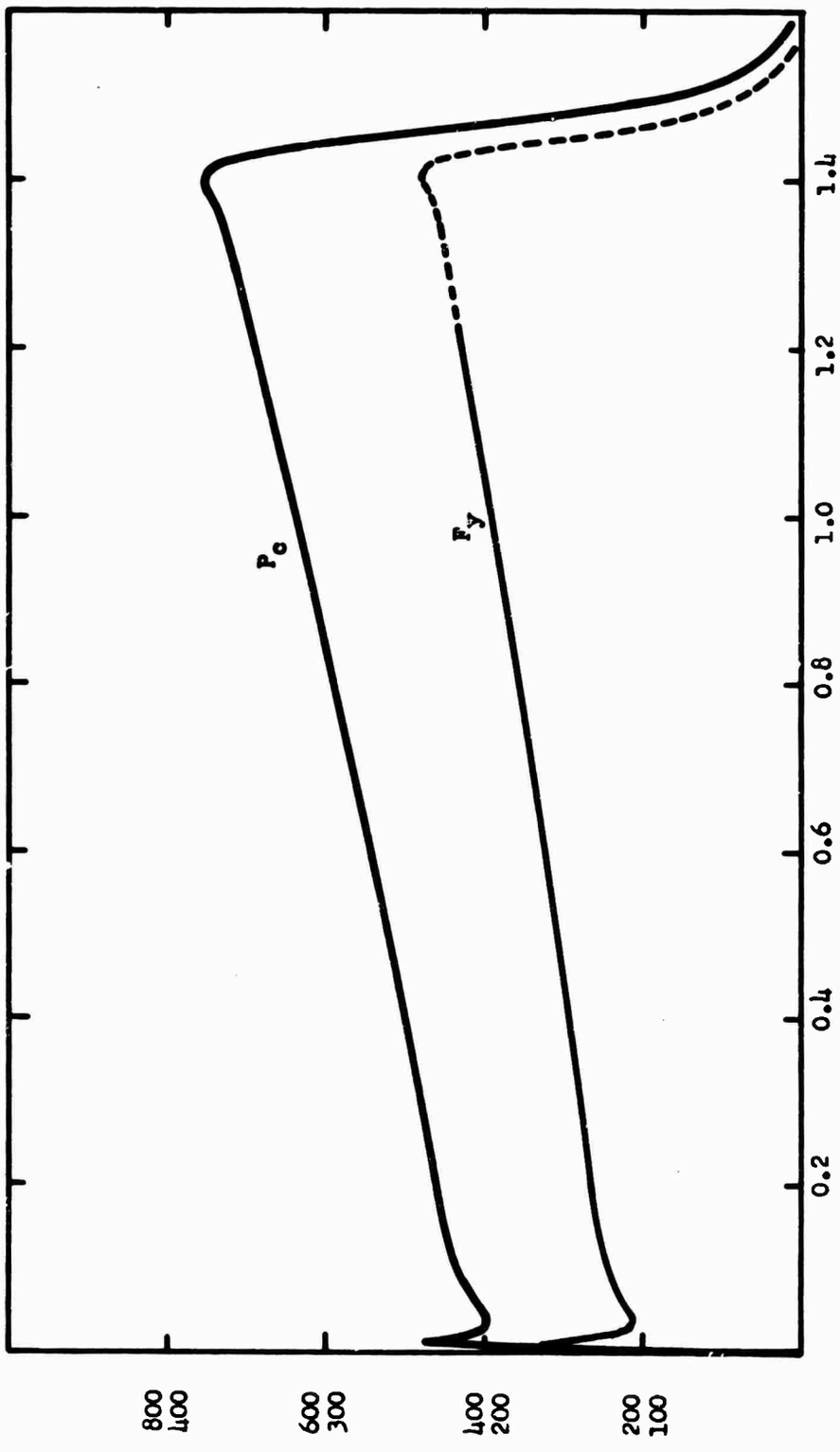

Motor Performance (Test Series FT-2X-01S-BH-5)

Figure 26

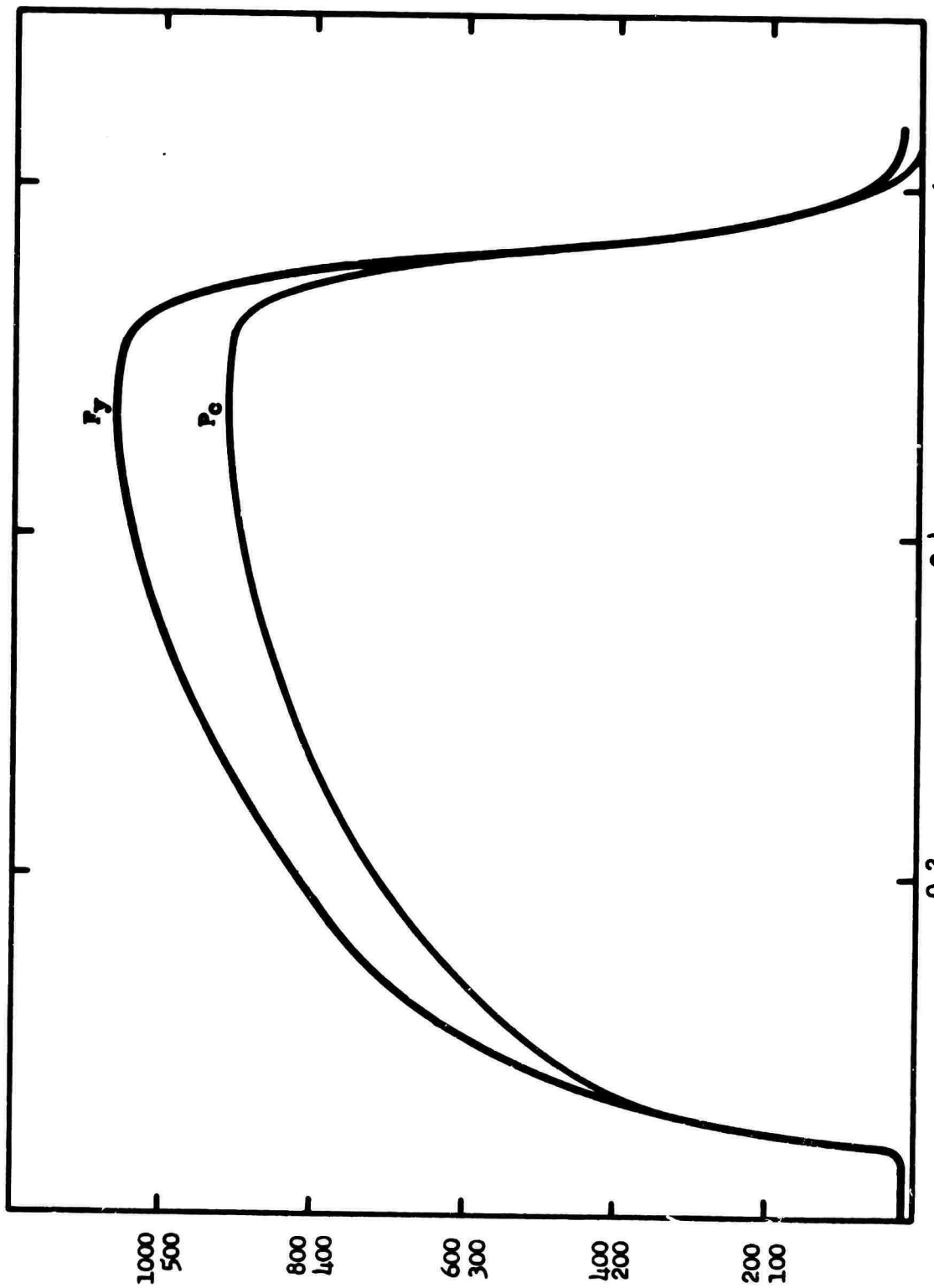

Motor Performance (Test Series FT-ZX-01S-BH-6)

Figure 27

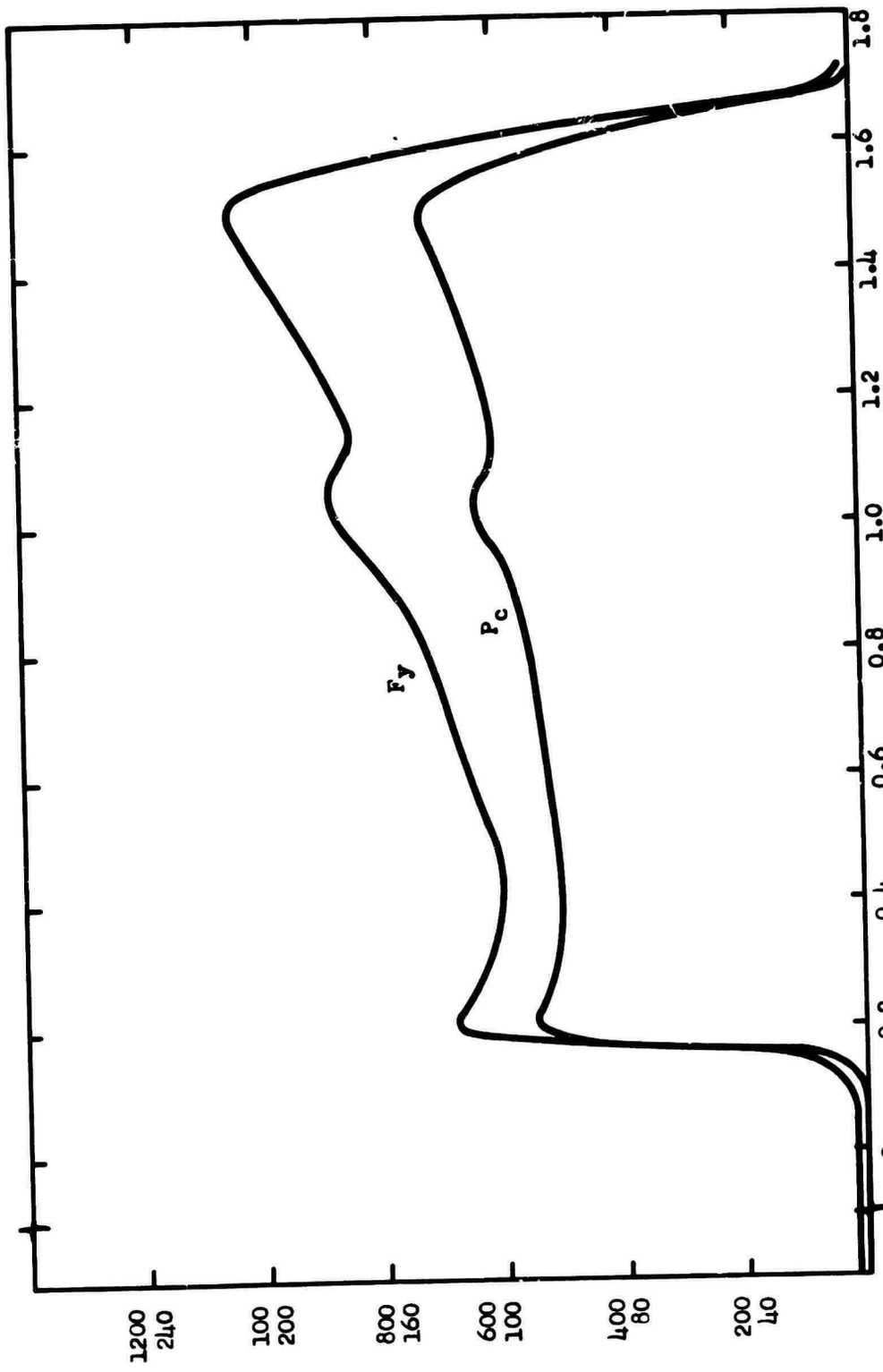

Motor Performance (Test Series FT-ZX-01S-BH-7)

Figure 28

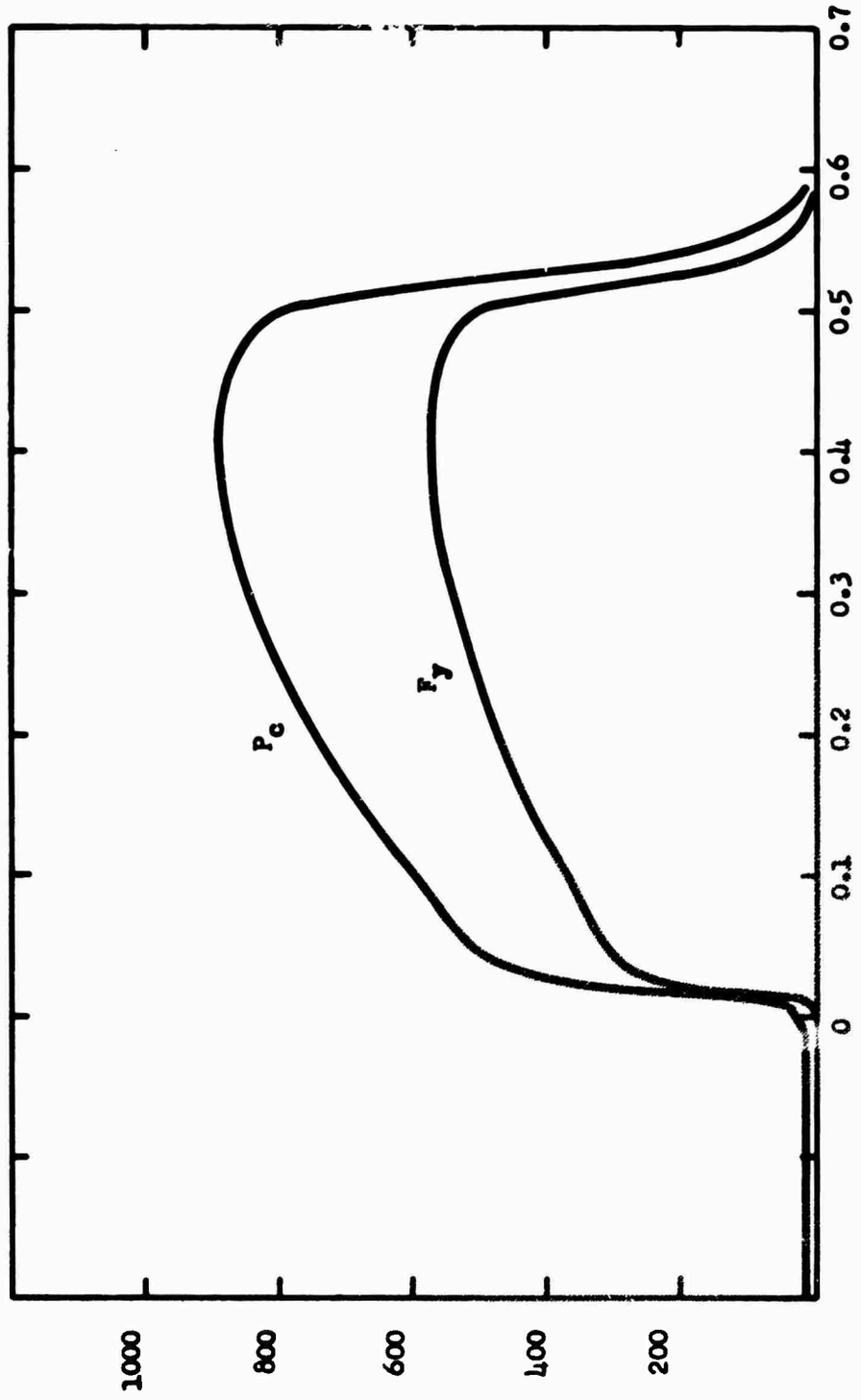

Motor Performance (Test Series FT-ZX-01S-BH-8)

Figure 29

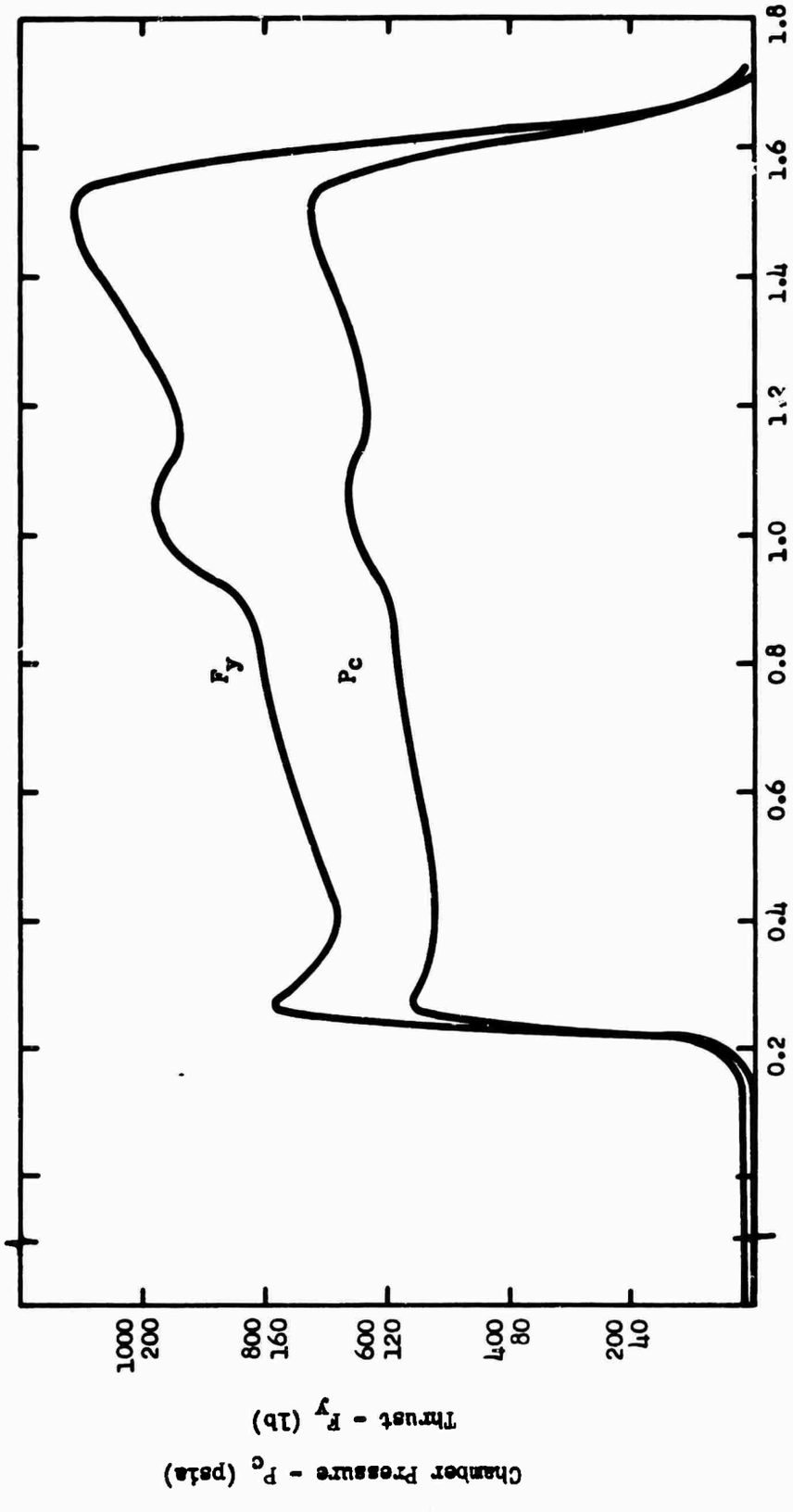

Motor Performance (Test Series FT-ZX-01S-BH-9)

Figure 30

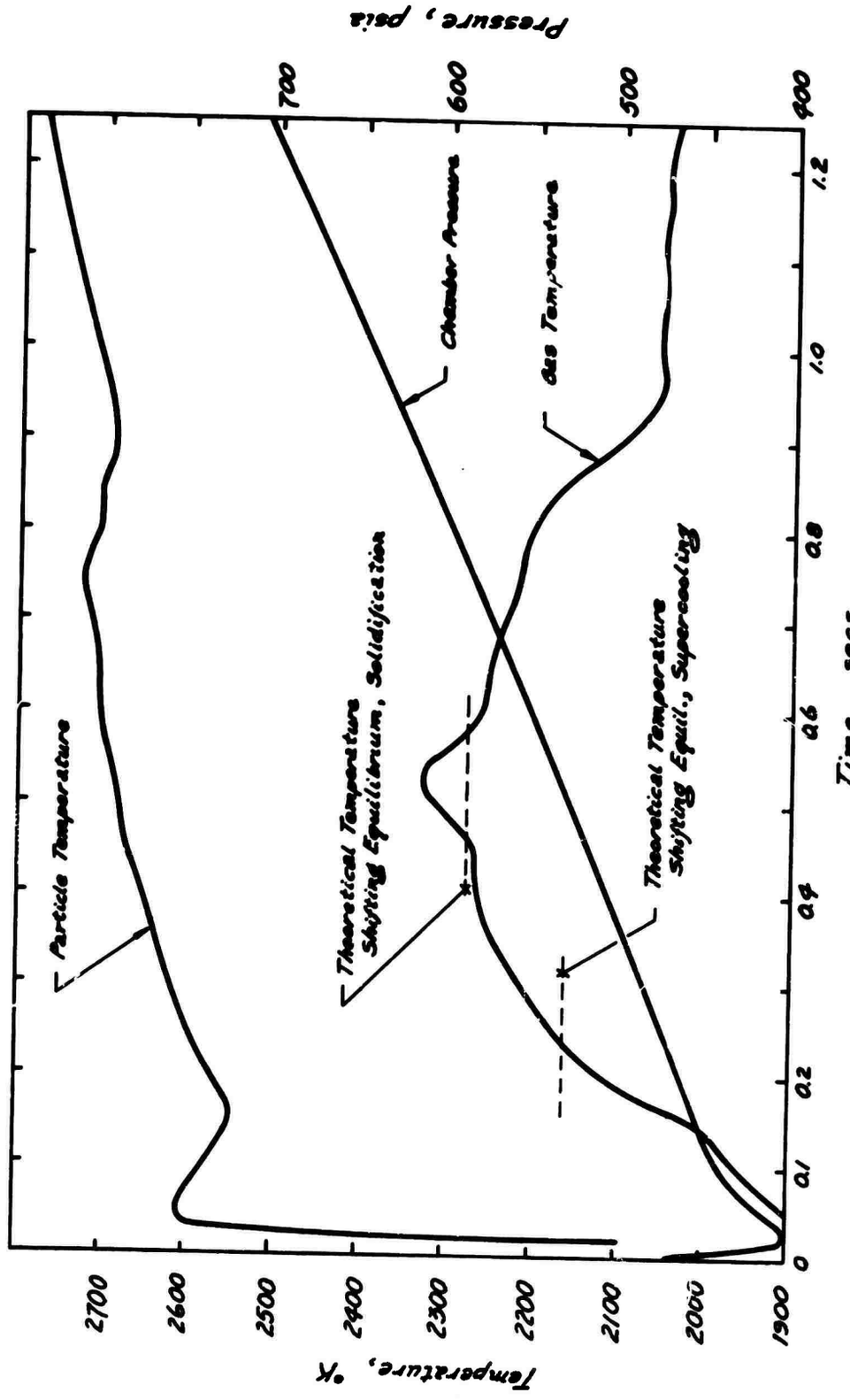

Measured Gas and Particle Temperatures, Exhaust Plume of 1KS-250 Motor, Aluminized Propellant

Figure 31

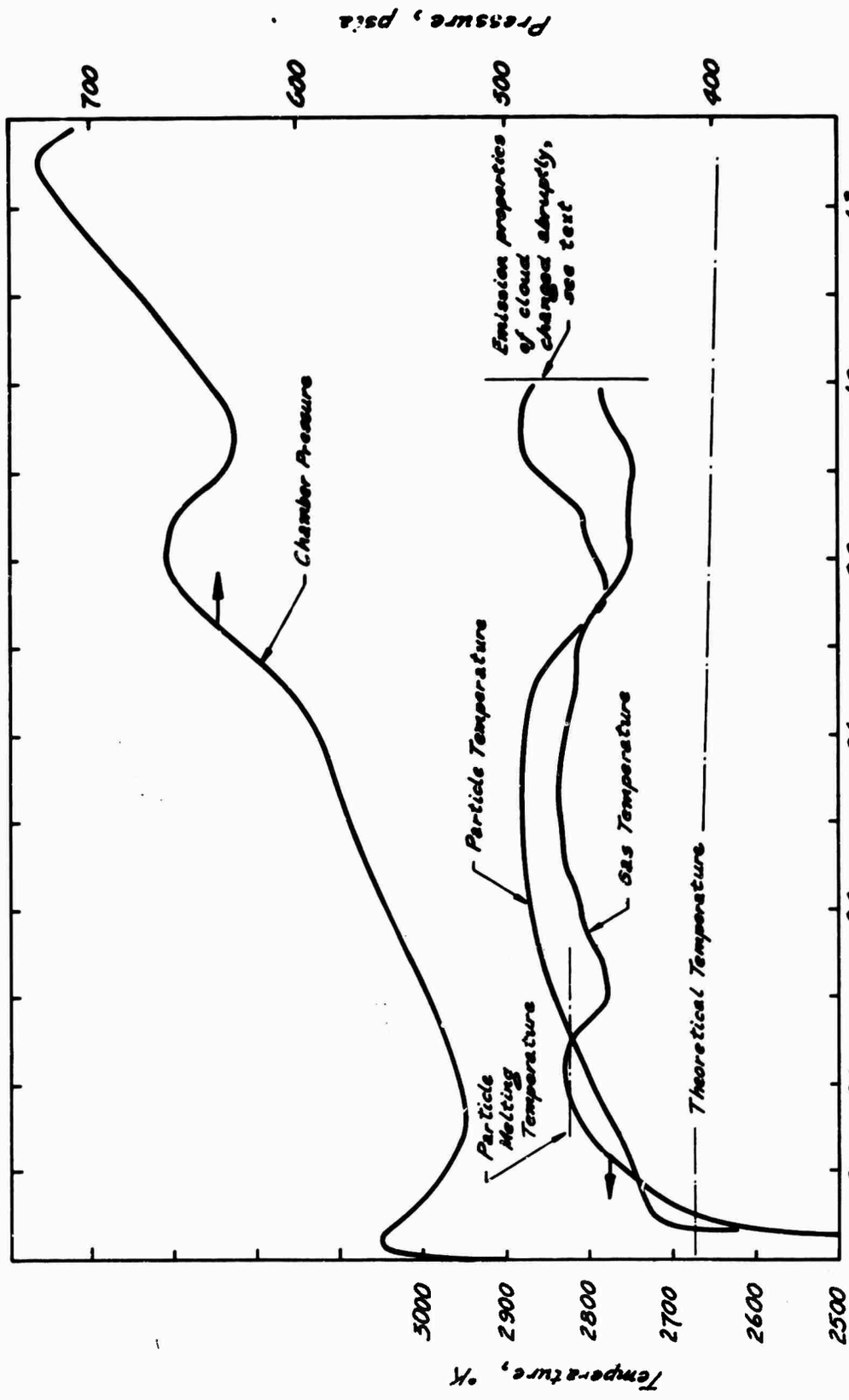

Measured Gas and Particle Temperatures, Exhaust Plume of 1 KS-250 Motor, LM-2 Propellant

Figure 32

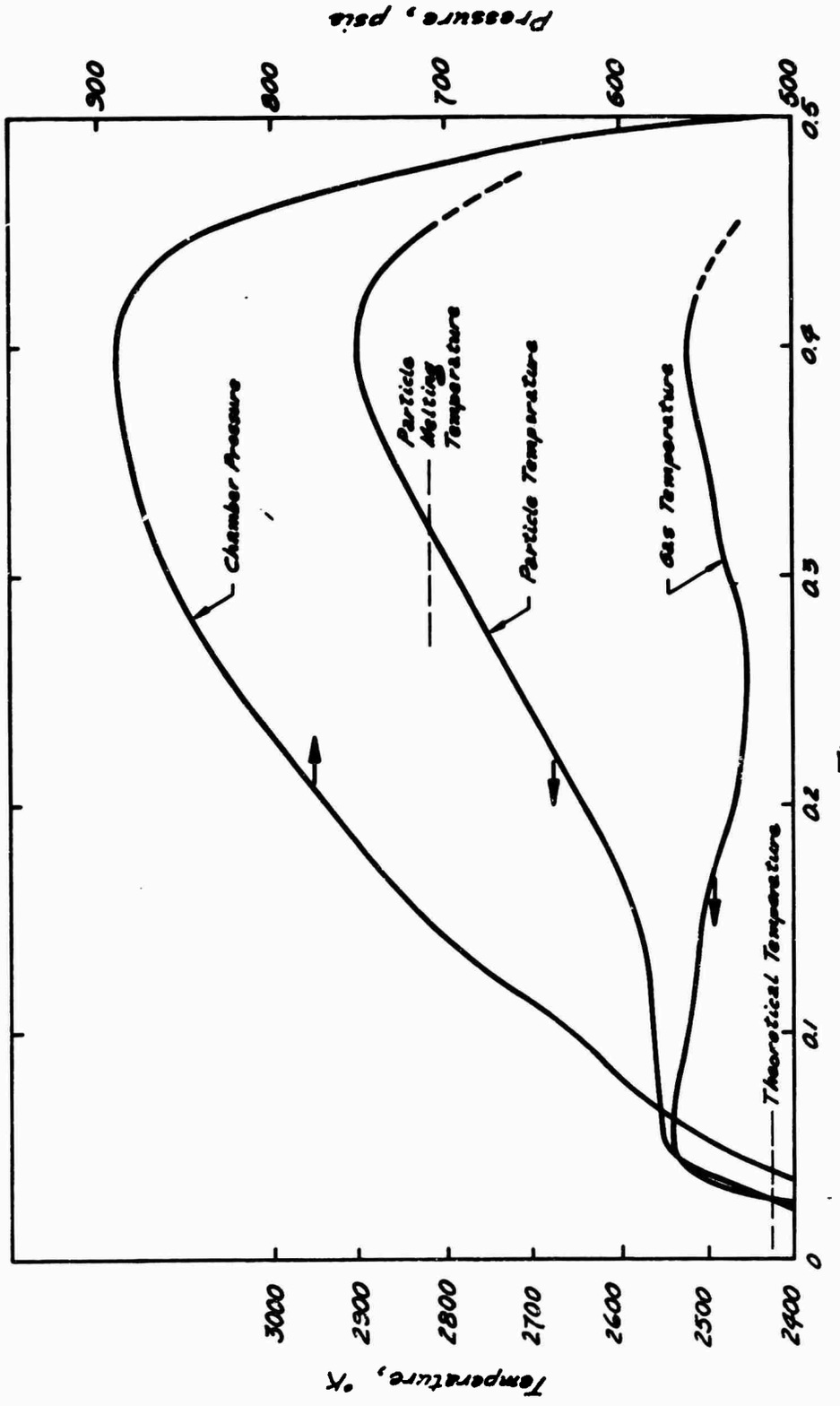

Measured Gas and Particle Temperatures, Exhaust Plume of 1KS-250 Motor, LMH-2 Propellant

Figure 33

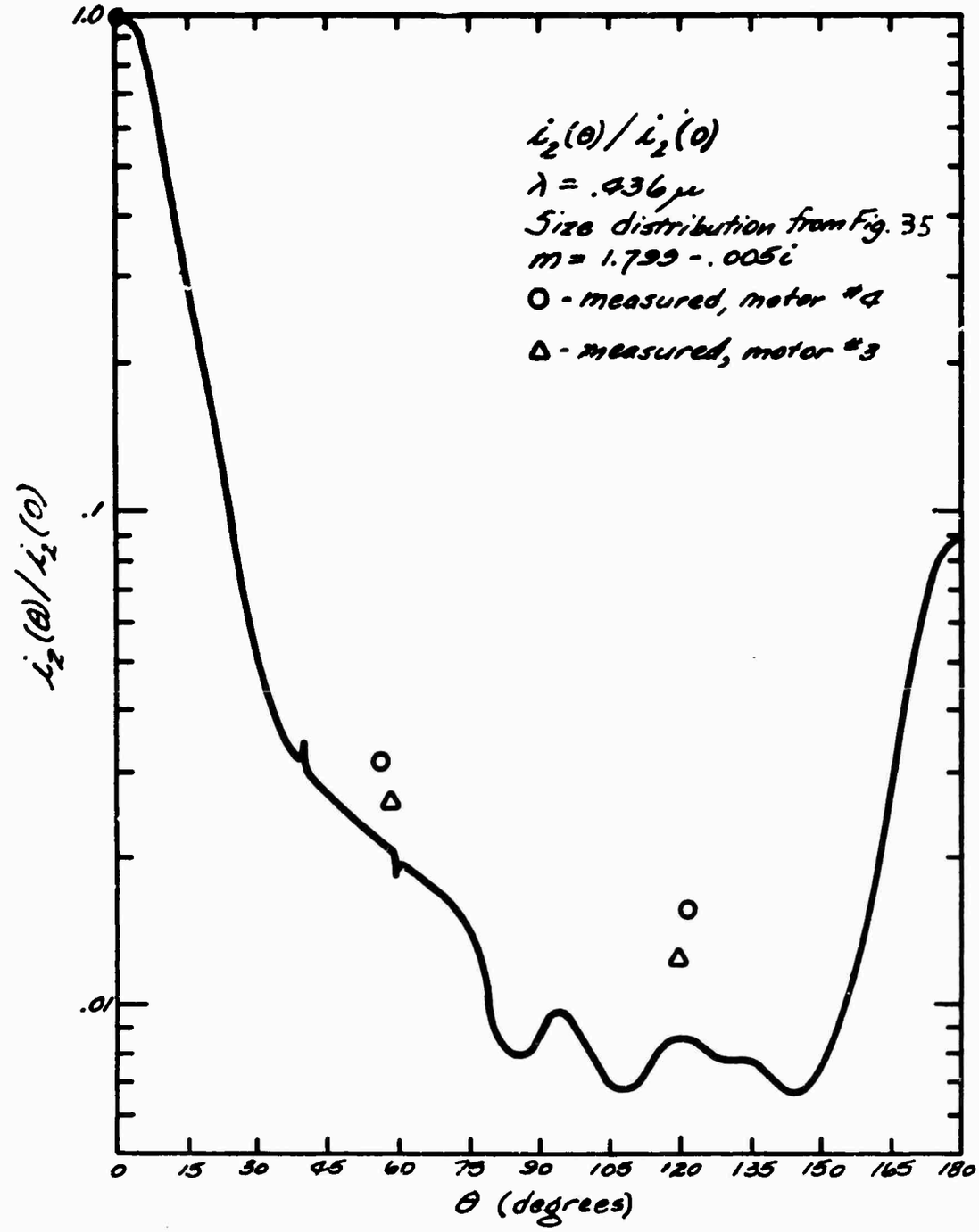

Light Scattering Diagram, i_2, Normalized to i_2 (0°), Motor Tests 3 and 4

Figure 34

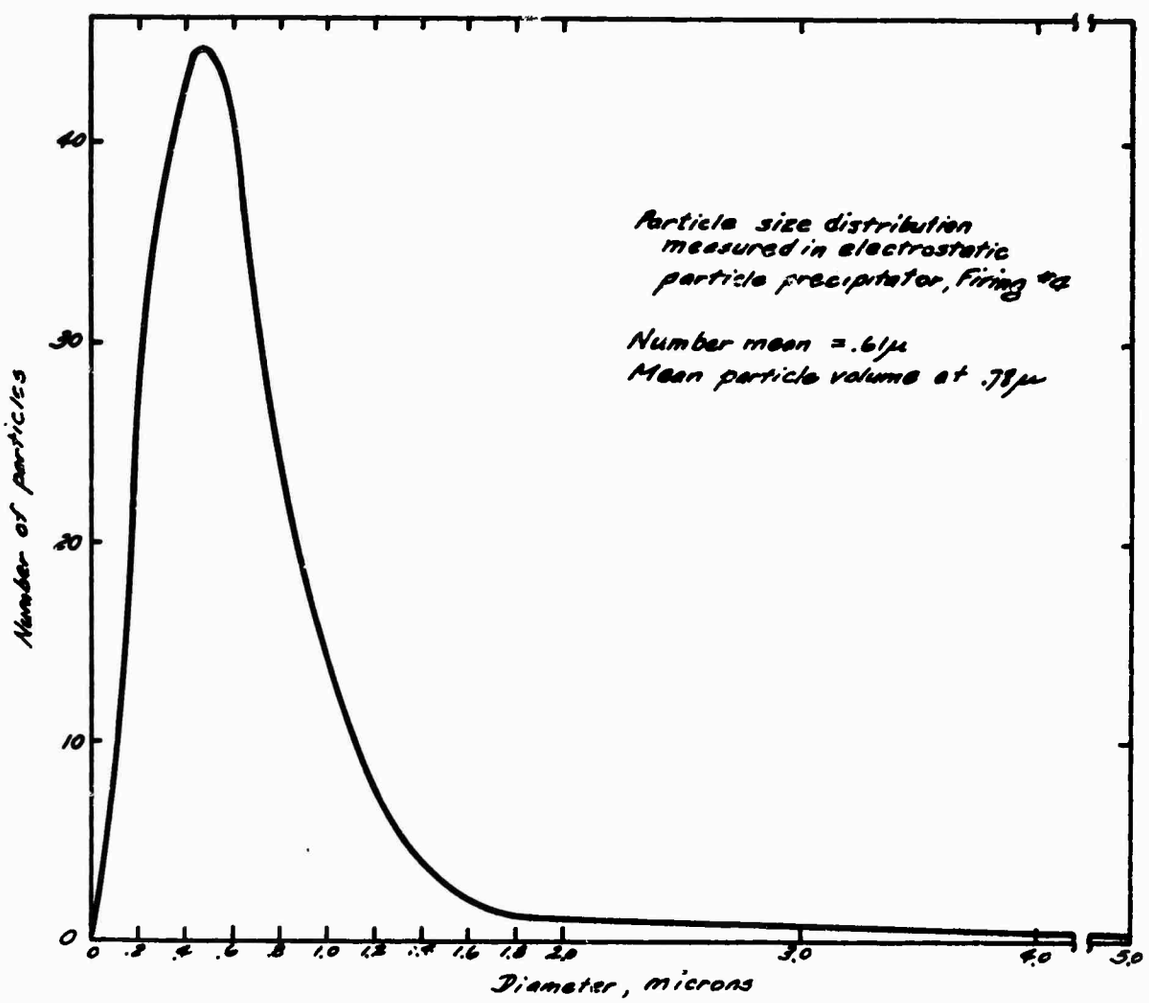

Particle Size Distribution Measured in Electrostatic
Particle Precipitation, Motor Test No. 4

Figure 35

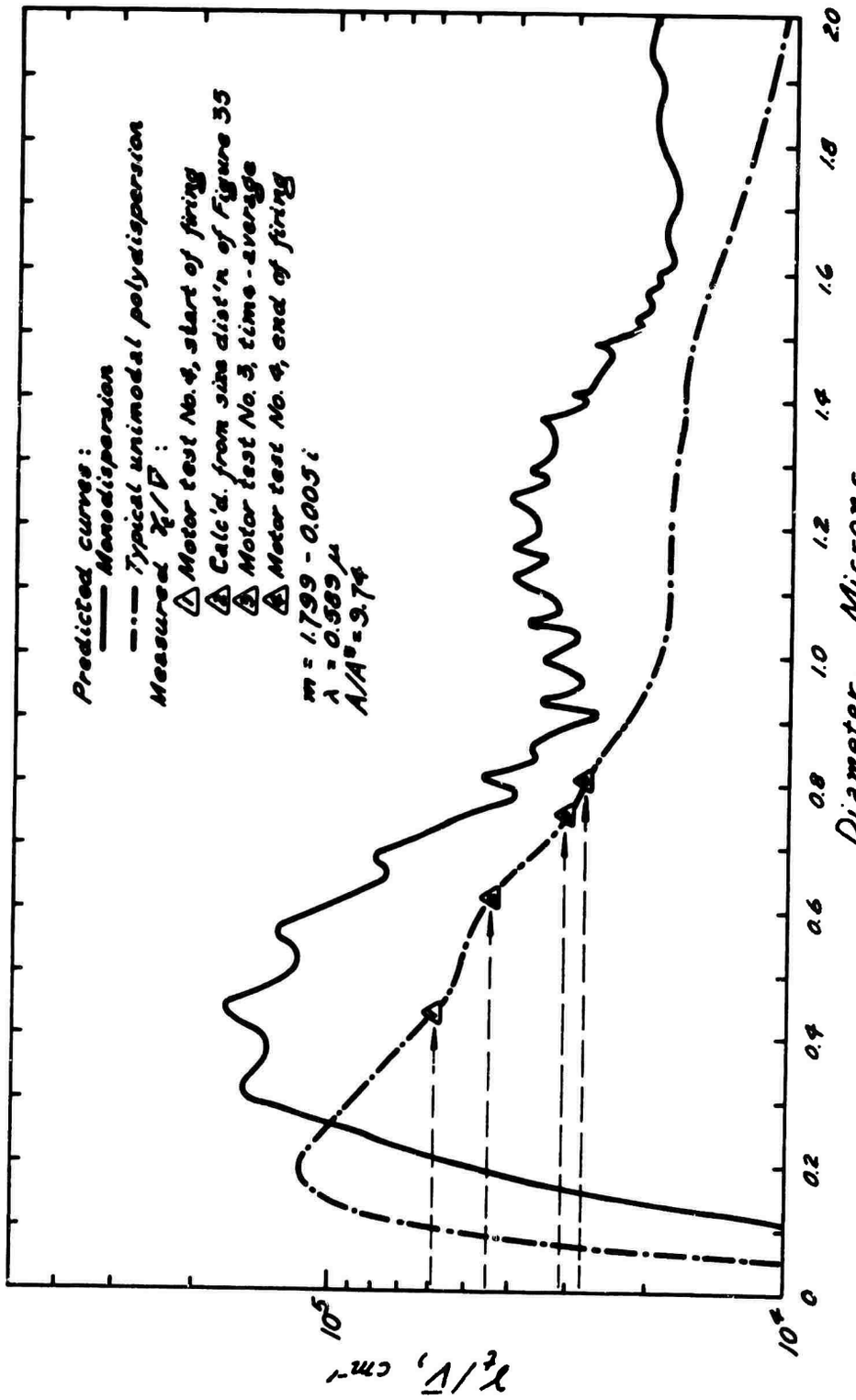

Extinction Parameter, Determined from Light Extinction Measurements in Exhaust Plume of 1KS-250 Motor (Tests 3 and 4) at $\lambda = 0.589\,\mu$

Figure 36

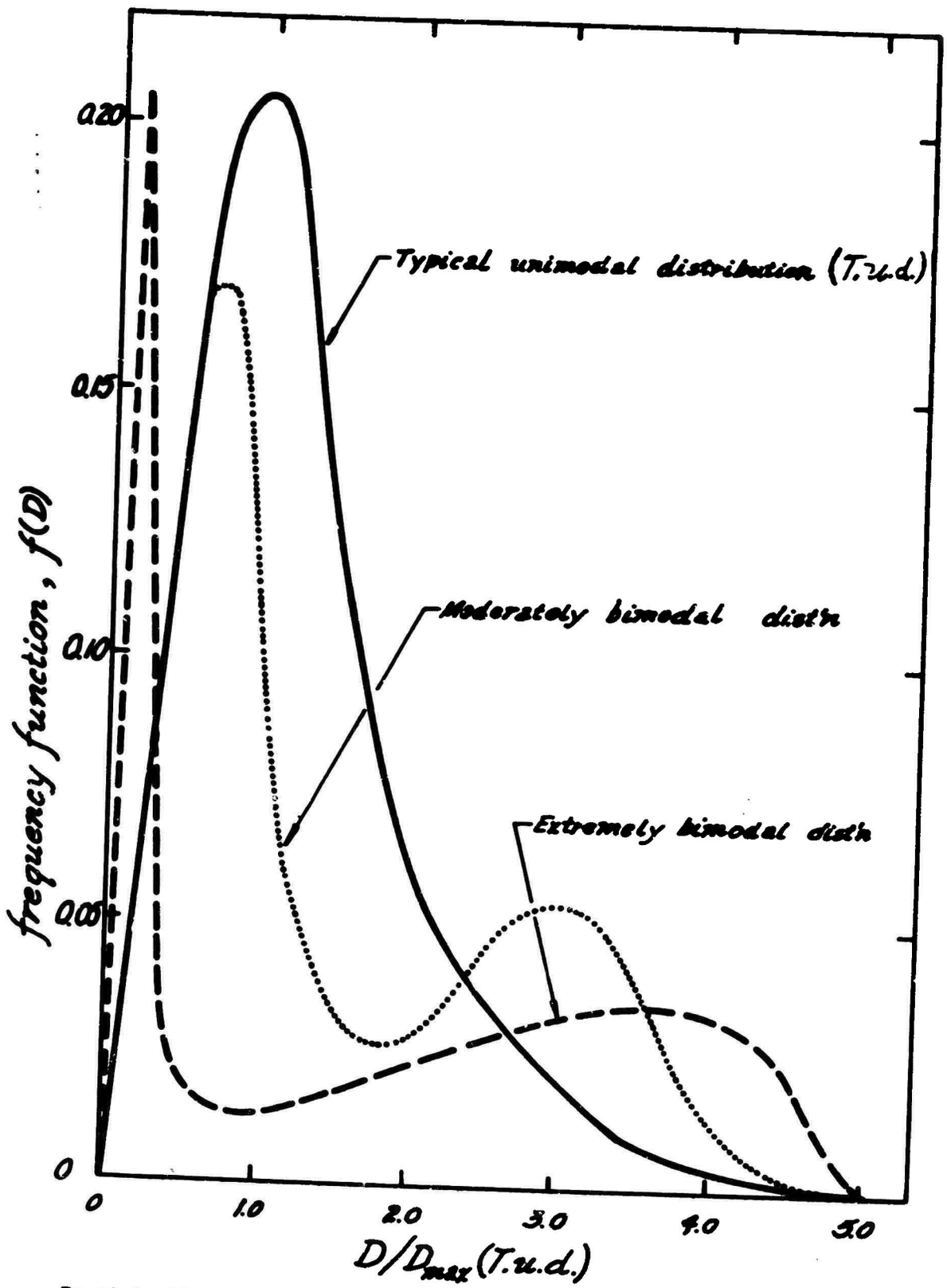

Particle Size Distributions Used in Generating Curves of Extinction Parameter vs Mean Particle Diameter

Figure 37

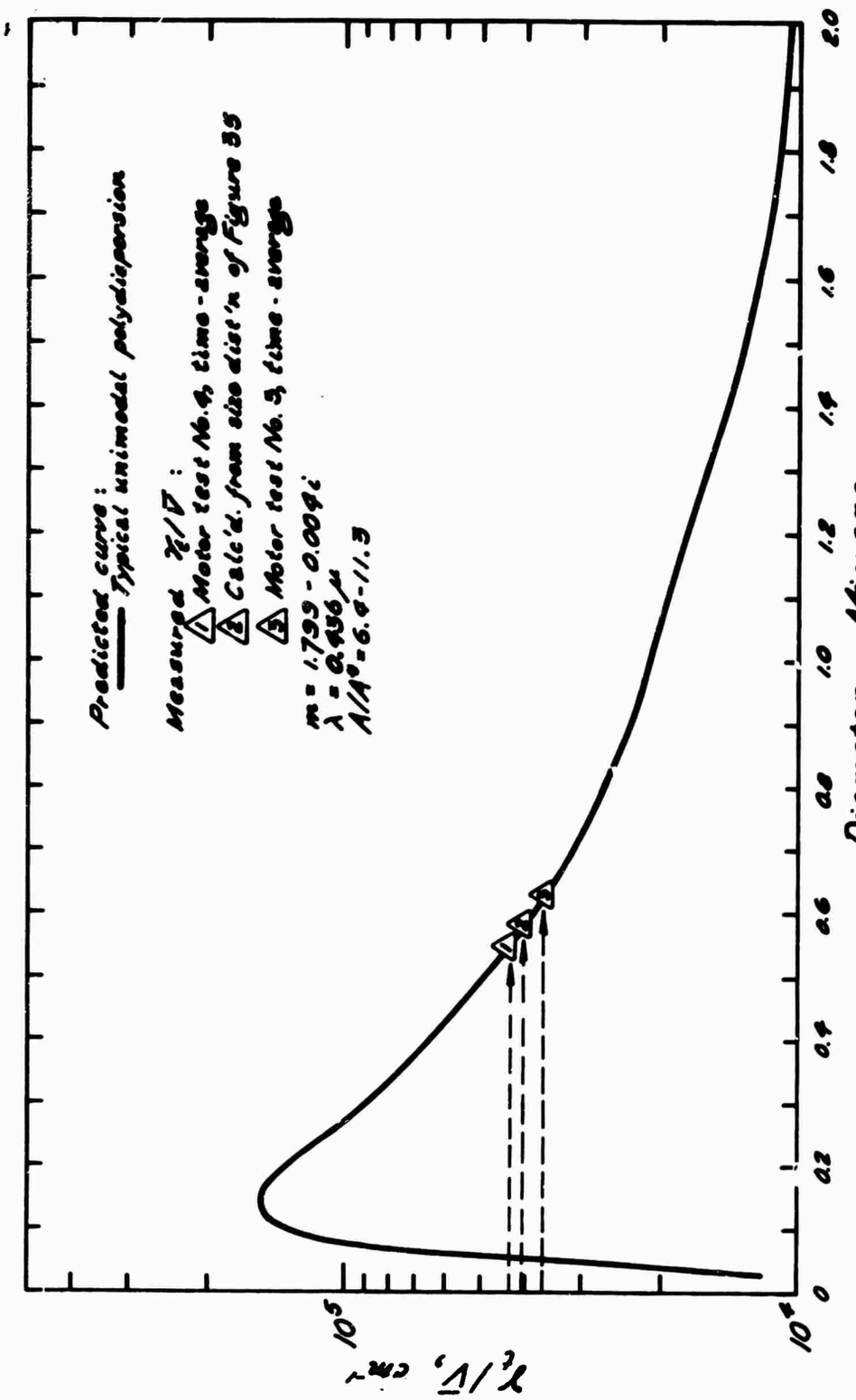

Extinction Parameter, Determined from Light Extinc [illegible] Measurements in Exhaust Plume of 1KS-250 Motor (Tests 3 and [illegible] λ = 0.436μ

Figure 38

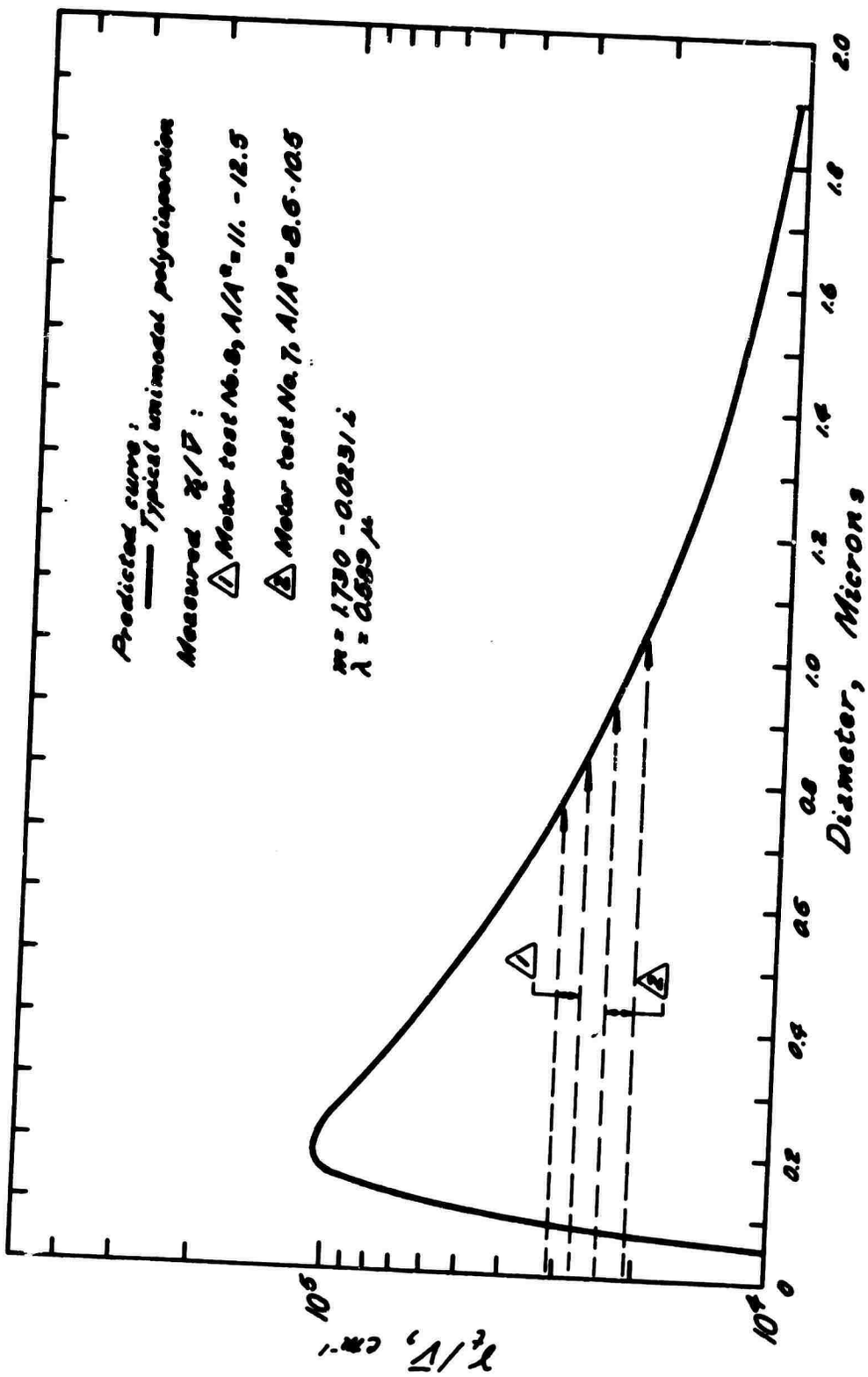

Extinction Parameter, Determined from Light Extinction Measurements in Exhaust Plume of 1KS-250 Motor (Tests 7 and 8) at $\lambda = 0.589\,\mu$

Figure 39

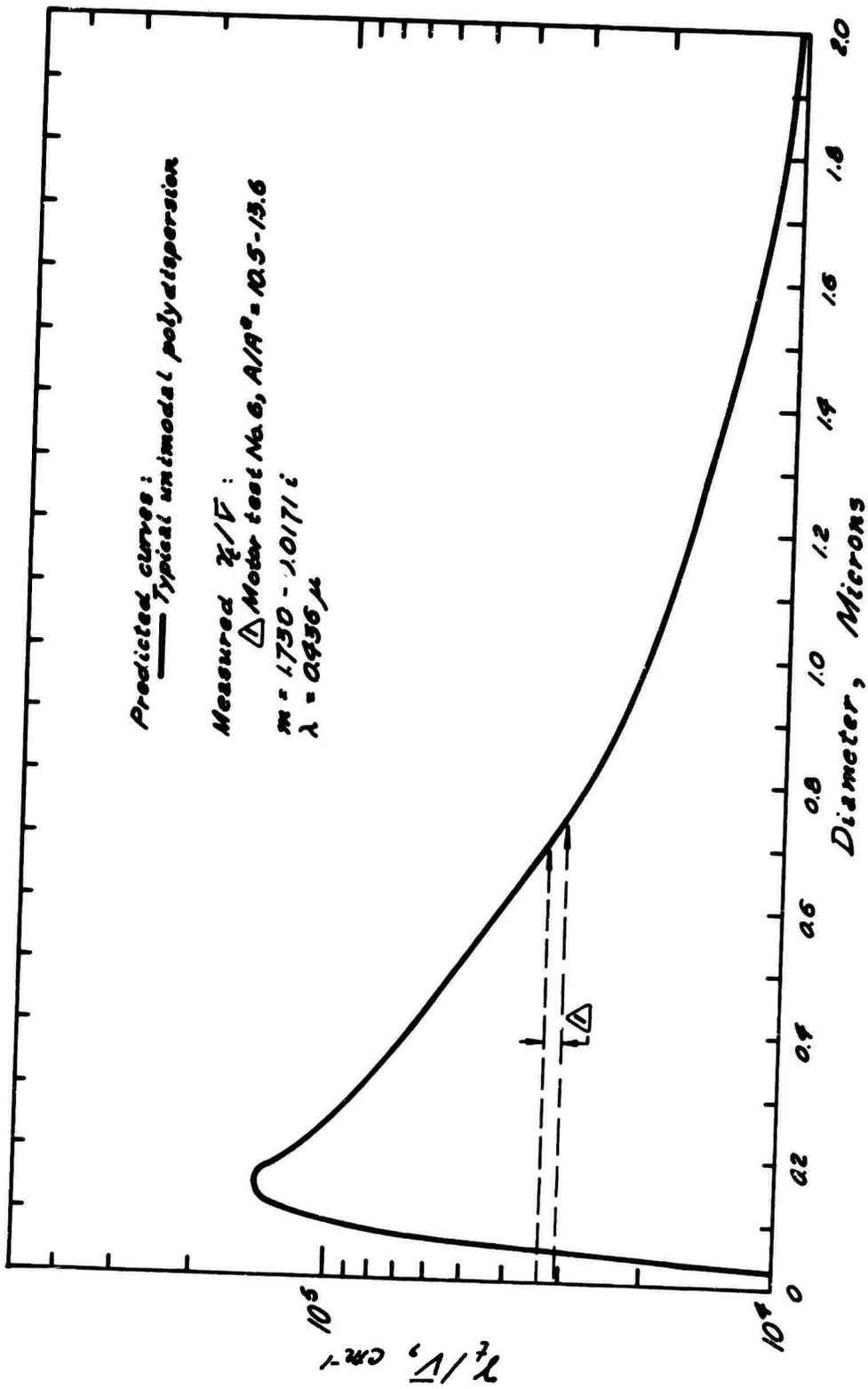

Extinction Parameter, Determined from Light Extinction Measurements in Exhaust Plume of 1KS-250 Motor (Test 6) at λ = 0.436 μ

Figure 40

APPENDIX A

GAS-PARTICLE SPECTROSCOPY OF SCATTERING MEDIA

To determine temperatures of both the gas and the condensed phase in a spectrally absorbing-emitting two-phase medium, it is necessary to determine the emissivity and radiance associated with the continuum emission of the condensed-phase cloud and the spectrum line emission of the gas. The emissivity is determined by measurement of the extinction of a beam of light from a reference light source (e.g., a tungsten ribbon lamp of known brightness temperature). This extinction occurs due to both absorption and scattering, but each contribution can be isolated through the use of the Mie scattering theory[1] with a knowledge of the complex refractive index of the dielectric which is present. From this treatment, the absorptivity of the particle cloud can readily be determined in the optically thin case. For a system in thermal equilibrium,[2] the emissivity of the cloud is equated to the absorptivity from Kirchoff's Law.

Figure A1 presents the normal and hemispherical emissivity as a function of optical depth, $\hat{N}(\gamma_a + \gamma_s)t$, with γ_a/γ_t as a parameter. This curve, reproduced here by permission of C. D. Bartky (1) is the result of work by Bartky (2) and by Romanova (3) on special solutions of the radiative transfer equation (4);

$$-\mu \frac{dI_\nu}{dx} = \hat{N}\gamma_t I_\nu - \frac{\hat{N}\gamma_s}{4\pi}\int_{4\pi} I_\nu\, i(\phi, \phi', \psi, \psi')\, d\omega'$$

$$- \hat{N}\gamma_a R^{\circ}_{i\nu}(T)$$

where ϕ, ψ are the transverse and azimuth angles to I_ν, respectively. An "optically thin" cloud of scatterers and absorbers corresponds to that region to the left of Figure A1 where the lines are straight; values of δ corresponding to the "knee" of the curves are associated with "optically thick" clouds. Finally when the emissivity reaches its maximum value, a condition of "infinite optical depth" is said to exist.

---

1 The details of the Mie scattering theory are given in Appendix B.

2 Although the reference light source and the cloud are, in general, not in thermal equilibrium with each other, no appreciable heating of the cloud occurs during the absorption of the reference light source beam, and Kirchoff's Law is applicable.

I. ANALYSIS FOR OPTICALLY THIN CLOUDS

Measurements of plume radiance and transmissivity are made within a region defined by the acceptor optics. This region takes the form of two colinear thin cones having a common apex at the centerline of the plume. (Figure A2). It is the scattering and absorption of the reference light source beam and the emission of the gas and particles within this region which are considered. The depth and particle concentration along the cone centerline defines the optical depth. For the case of exhaust plumes of IRS motors, the optical depth is approaching the "optically thick" case, but the "optically thin" analysis can be used with an error in temperatures of less than 1%.

Light collected by the acceptor optics is passed to the spectrometer where it is spectrally dispersed across the exit slit, caused an emf to be generated by the detector. In the following equations, E_{ij} represents a resulting galvanometer deflection at λ_i and T_j, and K_{ij} is a system multiplication constant which includes the response characteristics of the optical system, spectrometer, phototube and galvanometer. The galvanometer deflection is related to the radiance incident upon the phototube through the equation

$$E_{ij}\, K_{ij} = R\,(\lambda_i, T_j), \text{ the radiance}$$

Prior to making measurements on a flame, with only the reference source on, measurements of galvanometer deflection are made at various source temperatures. The deflection is related to the continuum emission from the source at λ_1 by equation (1), which also accounts for the transmissivity, τ, of both lenses or windows on either side of the flame:

$$E_{10}\, K_{10} = \frac{\epsilon_s\,(\lambda_1, T_s)\,\tau_{w1}^2}{\lambda_1^5\left[\exp\left(\frac{C_2}{\lambda_1 T_s}\right) - 1\right]} \qquad (1)$$

In the presence of the flame, the measured galvanometer deflection at λ_1 of the continuum is related to the radiance emitted by the particles with equation (2);

$$E_{12}\, K_{12} = \tau_w\ \epsilon_p\,(\lambda_1, T_p)\, R_i^o\,(\lambda_1, T_p) \qquad (2)$$

I, Analysis for Optically Thin Clouds (cont.)

where the particle cloud emissivity, $\epsilon_p(\lambda_i, T_p)$ is given by

$$\epsilon_p(\lambda_i, T_p) = 1 - e^{-\bar{N} \gamma_a t} \qquad (3)$$

To better explain the relationship shown in Figure A1, equation (3) can be rewritten as

$$\epsilon_p(\lambda_i, T_p) \cong \bar{N} \gamma_a t \quad \text{where} \quad \bar{N} \gamma_a t < 0.1$$

$$= \bar{N} (\gamma_a + \gamma_s) t (\gamma_a/\gamma_t) = \delta \cdot (\gamma_a/\gamma_t)$$

which would give a straight line relationship between ln ϵ_p and ln($\bar{N}$ ($\gamma_a + \gamma_s$) t), as is shown at the left of Figure A1. For a hypothetical cloud which has dimensions almost the same as those of the receptor "cones", radiation emitted from the far side of the region would be scattered and absorbed as it passed through the region toward the receptor. Thus the detector would see a lesser contribution from the more distant regions due to a net scattering loss. This condition, which probably could not arise in motor exhaust plumes, is termed the thin-transverse case and was analyzed by Adams Ref. (5). The other extreme case, called the thick-transverse case, where the transverse and longitudinal dimensions are roughly equal, results in no net loss due to scattering of light emitted from far regions, because scattering into the volume in a direction toward the receptor is equal to that light lost by scattering in this direction. Thus, the radiation collected by the receptor does not depend on the scattering cross section of the particles, and equations (2) and (3) result.

This is not characteristic of the reference light source beam as it traverses the plume, however. Because the source beam is anisotropic and because there is not thermal equilibrium between the plume and the source, light scattered out of the receptor cones is not scattered back entirely, but some absorption occurs outside of this volume. It will, for the present, be assumed that all the radiation from the reference source beam which is scattered out of a control volume is permanently lost. Actually, of course some of this radiation is recovered.

Equations (1) through (7), relating the gas and particle temperature to the measurements of radiance, cover the case just discussed and have been incorporated into an existing computer program which is used to reduce the exhaust plume measurements.

I, Analysis for Optically Thin Clouds (cont.)

With the reference source on, the measured signal at λ_1 is the sum of the transmitted source intensity and that coming from the particle emission, and is given by equation (4):

$$E_{11} K_{11} = \tau_{w_1} [1. - \exp(-\bar{N} \gamma_{a1} t)] R_1^o (\lambda_1, T_p) + \tau_{w_1}^2 [\exp(-\bar{N} (\gamma_{a1} + \gamma_{s1}) t)] R_i^o (\lambda_i, T_s) \varepsilon_s (\lambda_1, T_s) \quad (4)$$

At λ_2, a spectrum line is generated by the trace element and emission from both the particles and the gas occurs. This radiance is determined from equation (5):

$$E_{22} K_{22} = \frac{\tau_{w2} \gamma_g}{\bar{N} \gamma_{a2} + \gamma_g} [1 - \exp(-\bar{N} \gamma_{a2} + \gamma_g) t] R_i^o (\lambda_2, T_g) + \frac{\tau_{w2} \bar{N} \gamma_{a2}}{\bar{N} \gamma_{a2} + \gamma_g} [1 - \exp(-\bar{N} \gamma_{a2} + \gamma_g) t] R_i^o (\lambda_2, T_p) \quad (5)$$

With the reference source on, the resulting radiance at λ_2 is the sum of that from the continuum emission by the particles, the spectrum line emission by the gas (trace element) and that transmitted through the flame from the reference source beam. This sum is related to the resulting galvanometer deflection by equation (6):

$$E_{21} K_{21} = E_{22} K_{22} + \tau_{w2}^2 [\exp(-\bar{N} (\gamma_{a2} + \gamma_{s2}) + \gamma_g) t] R_1^o (\lambda_2, T_s) \varepsilon_s (\lambda_2, T_s) \quad (6)$$

where

$$R_i^o (\lambda_i, T_j) = \frac{1}{\lambda_i^5 (\exp(\frac{C_2}{\lambda_i T_j}) - 1)} \quad (7)$$

II. ANALYSIS FOR OPTICALLY THICK CLOUDS

A. OPTICAL DEPTH

The number density of particles or droplets in a combustion chamber or plume can be calculated from the relation

$$N = \frac{\rho_g \chi}{(1-\chi)\,\rho_L \bar{V} L_u} \tag{8}$$

where L_u, the velocity lag = u_p/u_g

$$\bar{V} = \text{mean particle volume} = \int_0^\infty f(D)\,\frac{\pi D^3}{6}\,dD \tag{9}$$

$$\int_0^\infty f(D)dD = 1 \tag{10}$$

χ is the mass fraction of particles

ρ_L, ρ_g are the condensed phase and gas densities, respectively.

The optical depth, δ, is then given by

$$\delta = \frac{\rho_g \chi}{(1-\chi)\,\rho_L L_u} \left(\frac{\gamma_a + \gamma_s}{\bar{V}}\right) t \tag{11}$$

properties of propellant and system $\equiv \xi$	properties of particle size and refractive index	actual thickness of plume

which we will write as

$$\delta = \xi\,(\gamma_t/\bar{V})\,t.$$

The ratio of transmitted light intensity, I, to incident intensity, I_o, is given by

$$\frac{I}{I_o} = e^{-\delta} \tag{12}$$

Therefore, we can determine the extinction parameter, $\gamma_t/\bar{V}$ from a transmission measurement by rewriting equation (12):

$$\frac{\gamma_t}{\bar{V}} = \frac{1}{\xi t} \ln \left(\frac{I_o}{I}\right). \tag{13}$$

II, Analysis for Optically Thick Clouds (cont.)

B. EXTINCTION PARAMETER

Since $\gamma_t/\bar{V} = f_1(\bar{D}, \sigma)$

where $\bar{D}$ is the mean diameter
σ is a size distribution function,

and since $\gamma_a/\gamma_t = f_2(\bar{D}, \sigma)$
we can write

$$\gamma_a/\gamma_t = f_3(\gamma_t/\bar{V})$$

which dependence is presented in Figures A3 through A5. The refractive index for the LM oxide was determined from measurements of Kendall (6) and Bauer (7). The dependence of the imaginery part of the refractive index on temperature was determined by equating it to that already determined for alumina, including the region above the melting point.

C. PARTICLE CLOUD EMISSIVITY

Having the relationship expressed by Figures A3 through A5, the emissivity of a cloud can be determined from Figure A1, since

$$\epsilon_p = \epsilon(\gamma_a/\gamma_t, \delta)$$

and hence

$$\epsilon_p = (\gamma_a/\gamma_t, \gamma_t/\bar{V}, \xi, t)$$

where ξ is determined from the propellant and system properties. The resulting relationship for a typical propellant system is shown in Figure A6. This figure was determined for conditions of motor No. 6, from which particle emissivity was determined. It is interesting to note the following features of Figure A6:

1. The emissivity of any particle cloud goes through a minimum. This means that, even if no reference light source is used to measure the extinction parameter, limits on emissivity definitely exist, thereby fixing limits on the temperature determined from the observed radiance. This fact was used to good advantage in motor test number six, since from Figure A6,

$$0.51 < \epsilon_p < 1.0$$

which fact, together with the measured radiance, fixed the particle temperature between the limits

$$2880°K < T_p < 3035°K$$

II, C, Particle Cloud Emissivity (cont.)

2. The emissivity curve is practically independent of the particle size distribution used. This conclusion is established by observing the differences in Figure A5, γ_a/γ_t versus $\gamma_t/\bar{V}$, calculated for three size distributions.[1] The actual mean particle diameter is of no importance to the determination of cloud emissivity.

3. The use of an extremely intense light source, such as a Q-switched laser, allows narrow limits on emissivity to be established, even if no transmitted light from the beam is detected. As is shown in Figure A6, if for the conditions within the motor chamber (test number six again) the value of $\gamma_t/\bar{V}$ is less than $1.5 \times 10^4 cm^{-1}$, the transmitted beam will be detected[2]. If the transmitted beam is detected, a value of $\gamma_t/\bar{V}$ can be determined[3] and the limits on emissivity are fixed by the two possible values of γ_a/γ_t (corresponding to two possible particle sizes. By an extinction measurement at another wavelength, the emissivity is fixed). If on the other hand, no transmitted radiation from the laser pulse is observed, the limits on emissivity are

$$\epsilon(\gamma_t/\bar{V})_{max}) < \epsilon_p < \epsilon_{max}((\gamma_t/\bar{V})_{min})$$

Figure A6 shows the maximum value of $\gamma_t/\bar{V}$ corresponding to the level which could be detected from a 200 megawatt pulsed laser with a beam diameter of 25 mm.[4]

Figure A7 shows the sequence involved in determining the particle and gas temperature from the measurements made on the cloud.

D. GAS EMISSIVITY

For optically thick clouds, the gas emissivity presents a slightly different but no less difficult problem than that which has just been discussed. Since line emission is the characteristic of the gas, the measurement technique presented in the preceding paragraphs could be used only if another laser is used, emitting at a wavelength corresponding to the center of the spectrum line of interest. Such a device is not practicable at present and may be theoretically impossible. Instead a knowledge of the gas emissivity in the optically thick region is determined from measurements conducted on the same gas in an optically thin region downstream.

---

1. The three size distributions are shown in Figure 37 of the main body of this report.

2. The lower limit on detectable transmitted radiance is ~0.1 of the emitted radiance from the cloud.

3. See Flagnote 2, Figure A6, as an example.

4. Flagnote 1, Figure A6.

II, D, Gas Emissivity (cont.)

The gas emissivity in the chamber and resulting temperature were calculated for motor test number six from measurement of sodium line emissivity in the exhaust plume of motor number eight. The two motors were of identical type and contained propellant from the same batch. The assumption necessary to the calculation is that the mass concentration of the emitting species be the same for both the optically thick region and that region where the measurement is made. The determination of gas spectral emission coefficient, given by

$$\gamma_g = \frac{1}{t} \ln(1-\epsilon_g)$$

(for optically thin regions) is extrapolated to the optically thick zone through the method shown by Buchele (8). Having γ_g, the gas emissivity can be determined from the parameters[1]

$$\frac{\gamma_g}{\tilde{N}(\gamma_a + \gamma_s) + \gamma_g} \quad \text{and} \quad [\tilde{N}(\gamma_a + \gamma_s) + \gamma_g]\, t$$

by a computational technique which is similar to that used in the determination of particle cloud emissivity. Such a computation was carried out for motor test number six which resulted in the stated gas temperatures. As in the preceding case, limits resulted because of the interdependence of particle and gas emissivity at the spectrum line in the optically thick case.

E. EMBODIED ASSUMPTIONS

Because of the complexity of the foregoing presentation, it becomes incumbent on the author to present the assumptions embodied in the treatment in a concise manner. They are the following:

1. The radiative transfer equation is extremely difficult to solve in the general case. The determination of emissivity given in Figure A1 is based on the assumption that the normal albedo of the scattering medium is 0.13 (3). That is, the fraction of the radiation scattered through angles from 90° to 180° to an incident light beam is 0.13 of the incident radiation from that beam. This is the so-called "back-scattered" radiation; the value of 0.13 is adjudged to be sufficiently accurate for the cases under study here (cf. Figure 34 of the report).

1. Note the similarity to the parameters used in a determination of particle cloud emissivity.

II, E, Embodied Assumptions (cont.)

2. Temperature, density, or particle concentration gradients are assumed not to exist in the region under study here. This assumption is not necessary to the solution of the problem, but its elimination adds an unwarranted complexity in view of other uncertainties.

3. The mass fraction of particulate matter is calculated from the propellant properties with the assumption that the system is at thermodynamic equilibrium, i.e. all reactions have gone to completion.

4. It is assumed that there is no radiation from the reference light source which, once lost from the acceptor covers, is scattered back into the acceptor.

F. MEASUREMENT PRECISION

With the use of a -switched laser, the particle cloud emissivity is seen to have a range of uncertainty which depends upon whether any transmitted radiance from the laser is detected across the plume or cloud. This characteristic is further seen to be a function of particle size. If the mean particle diameter within the observed region is greater than 1.00 or less than 0.05 [1], the beam from a 200 MW light source will penetrate the plume and be detected. The greatest uncertainty in temperature will be the result of the unknown particle size. Further uncertainty results because of uncertainties in gas and solid density, particle mass fraction, and particle refractive index. The best estimate of the 95% confidence interval about particle temperature is given in Table I, where all these factors are considered. The estimate of variance for temperature was determined from the relation

$$\sigma^2_{T_p} = \left(\frac{\partial T_p}{\partial \bar{D}}\right)^2 \sigma^2_{\bar{D}} + \left(\frac{\partial T_p}{\partial m}\right)^2 \sigma^2_m + \left(\frac{\partial T_p}{\partial \rho_g}\right)^2 \sigma^2_{\rho_g} + \left(\frac{\partial T_p}{\partial \rho_L}\right)^2 \sigma^2_{\rho_L} + \left(\frac{\partial T_p}{\partial \chi}\right)^2 \sigma^2_\chi$$

which results in

$$\sigma^2_{T_p} = \left(\frac{dT_p}{d\epsilon}\right)^2 \left[\left(\frac{\partial \epsilon}{\partial \bar{D}}\right)^2 \sigma^2_{\bar{D}} + \left(\frac{\partial \epsilon}{\partial m}\right)^2 \sigma^2_m + \cdots\right]$$

where

$$T_p = \frac{C_2}{\lambda_1^5 \left[\text{Constant} + \ln \epsilon\right]},$$

1. The conditions shown by flagnote 1 of Figure A6.

II, F, Measurement Precision (cont.)

TABLE I

95% Confidence interval about T_p = 2500°K

± 75 °K	Laser beam penetrates.
± 97 °K	Laser beam does not penetrate.
± 175 °K	Laser not used.

A similar uncertainty in gas temperature will result because of the dependence of gas emissivity on particle emissivity at high optical depth.

APPENDIX A REFERENCES

1. Bartky, C. D., Personal Communication with J. M. Adams, June 7, 1966.

2. Bartky, C. D. and E. Bauer, "Predicting the Emittance of a Homogeneous Plume Containing Alumina Particles," Aeronutronic Publ. No. U-3232 Contract NOnr 3907(00), Aug, 1965.

3. Romanova, L. M., Opt. and Spectry, 14, 135 (1963).

4. Chandrasekhar, S., Radiative Transfer, Dover, 1960.

5. Adams, J. M. and L. Cann. "The Spectrophotoelectric Measurement of Gas and Particle Temperature", Aerojet-General Corp. TP-139, June 1964.

6. Kendall, E. G. and J. D. McClelland, "Materials and Structures," Aerospace Rept. No. TDR-930(2240-66) TR-1, March 1962.

7. Carlson, D. J., "Radiation from Rocket Exhaust Plumes," Aeronutronic Report. To be presented at Joint Specialists Conferences, Colorado Springs, Colorado, June 1966.

8. Buckele, D., "A Self-Balancing Line Reversal Pyrometer," NACA TN 3656, August 1956.

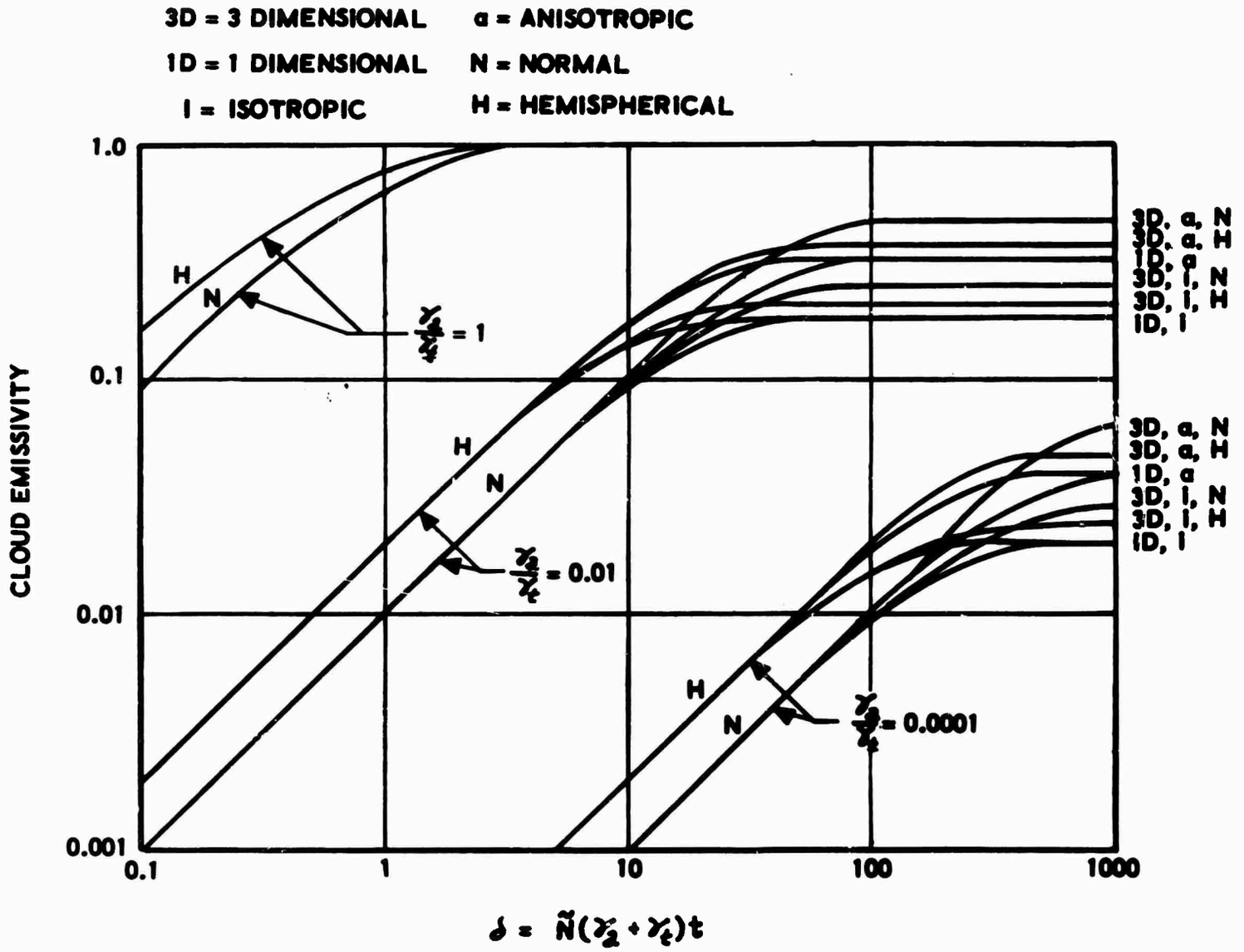

Figure A1

(Reproduced by permission of C.D. Bartky of Aeronutronic, Corp.)

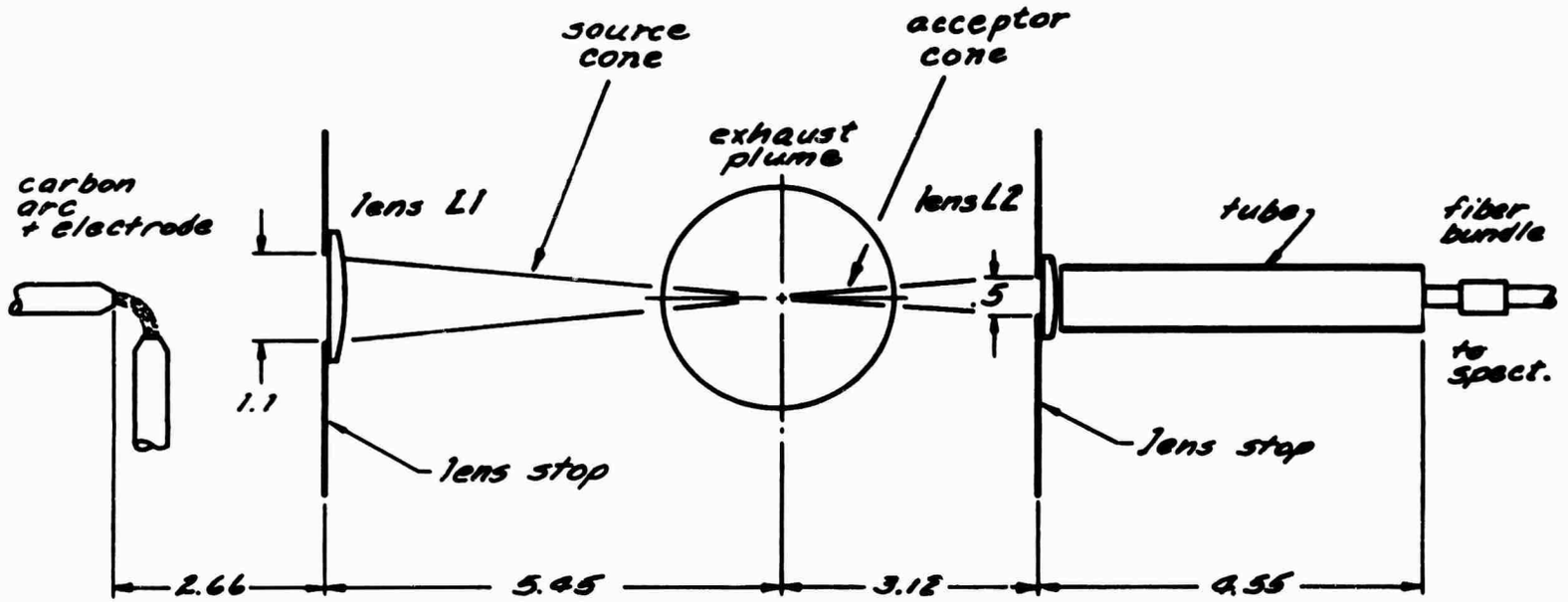

Figure A2

lens L1, L2 FL:-50 mm DIA - 22.5 mm

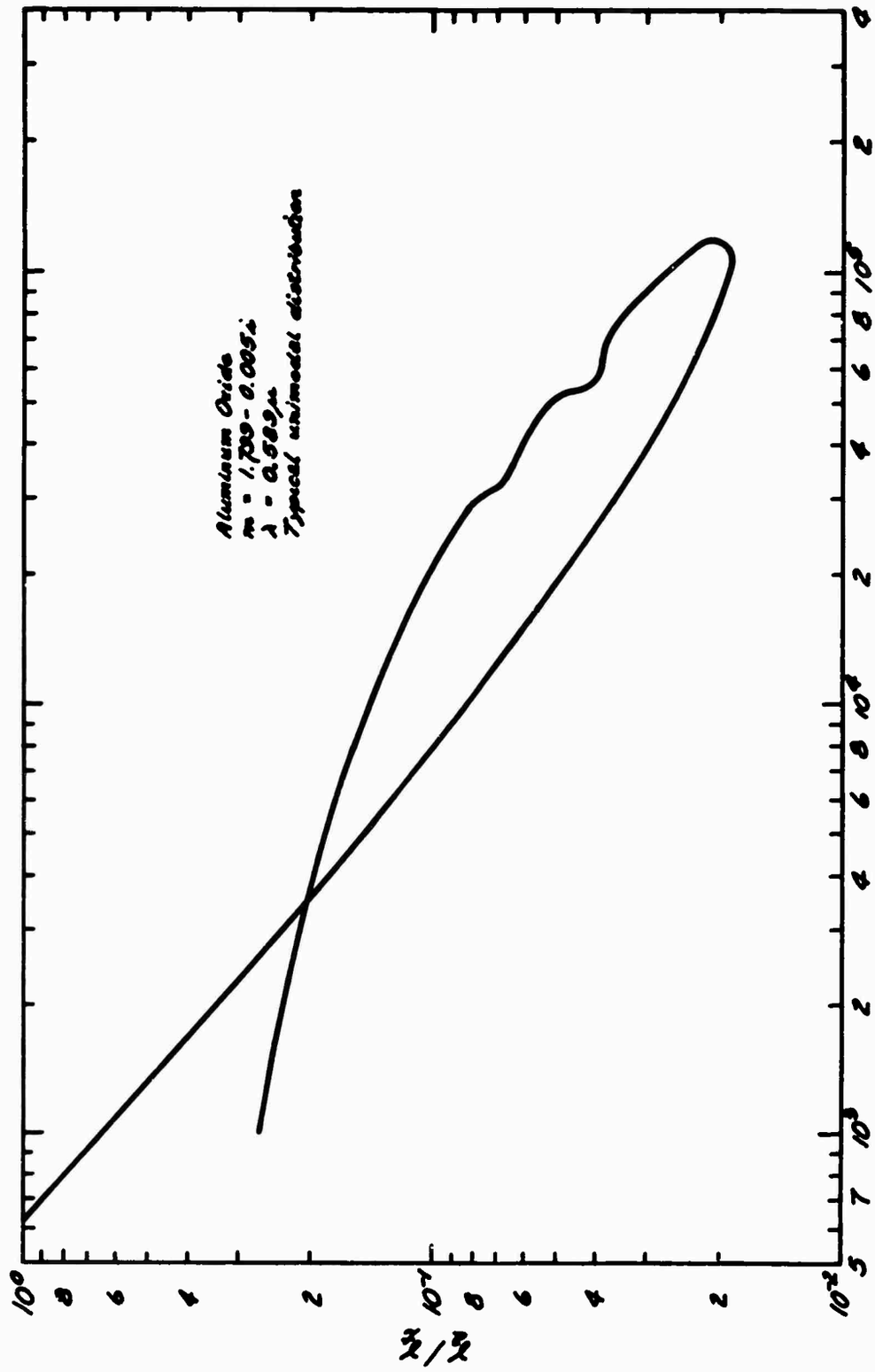

Absorption/Total Cross Section vs Extinction Parameter for Aluminum Oxide Spherical Particles (Particle Size Distribution from Figure 37 of Report)

Figure A3

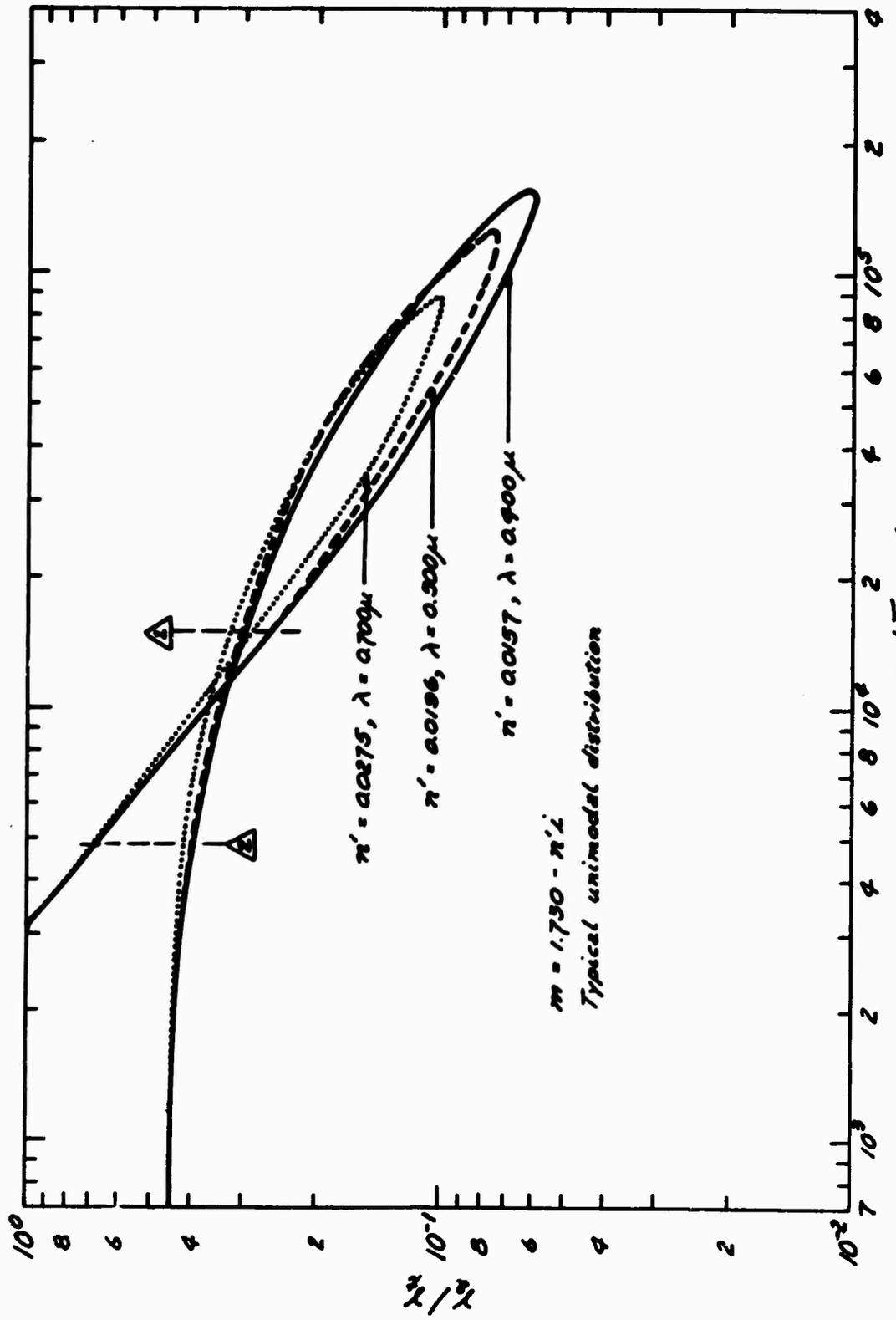

Absorption/Total Cross Section vs Extinction Parameter for LM Oxide Spherical Particles: Dependence on η' (Particle Size Distribution from Figure 37 of Report)

Figure A4

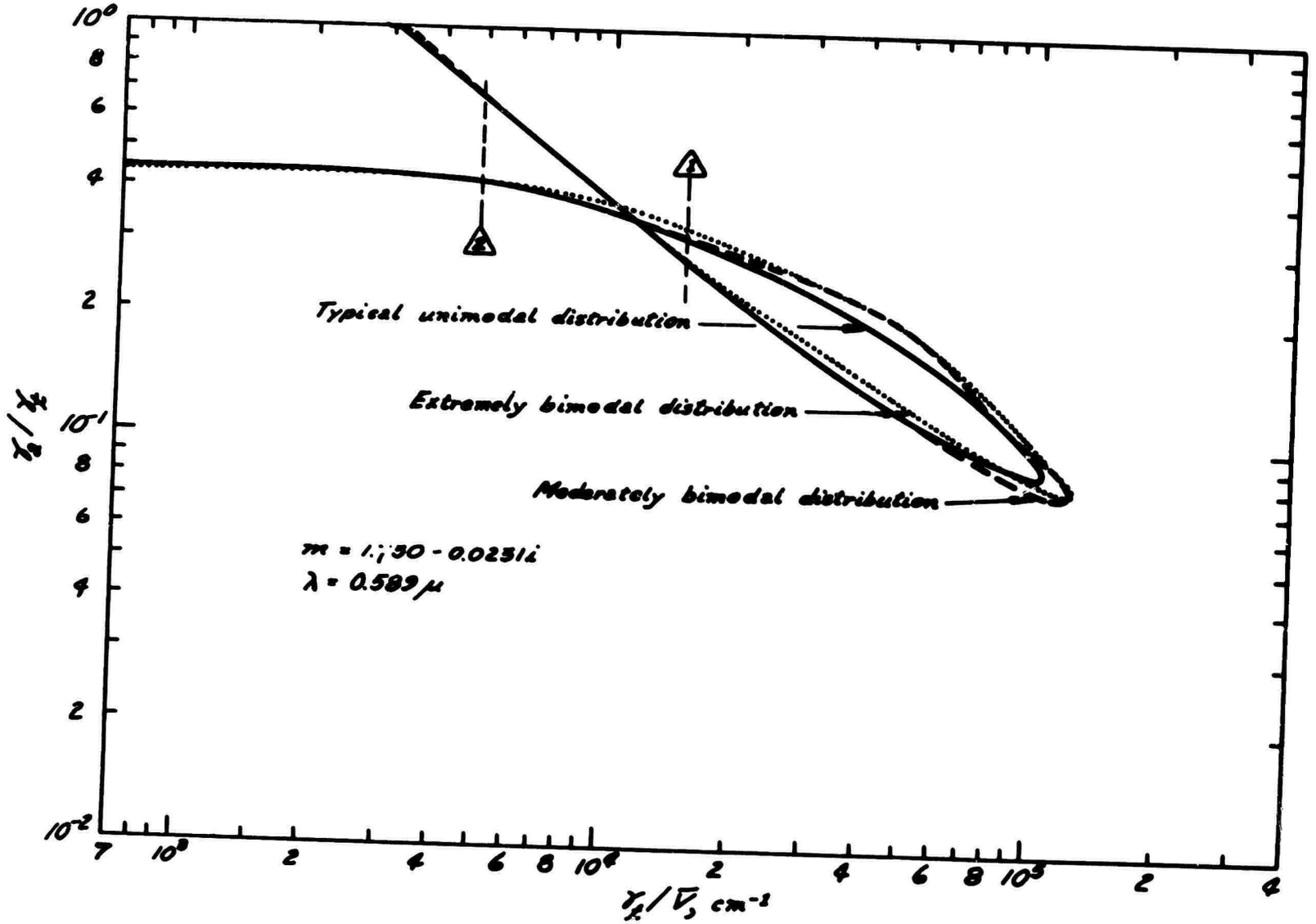

Figure A5

Absorption/Total Cross Section vs Extinction Parameter for LM Oxide Spherical Particles: Dependence on Size Distribution, $f(D)$ vs D (Particle Size Distributions from Figure 37 of Report)

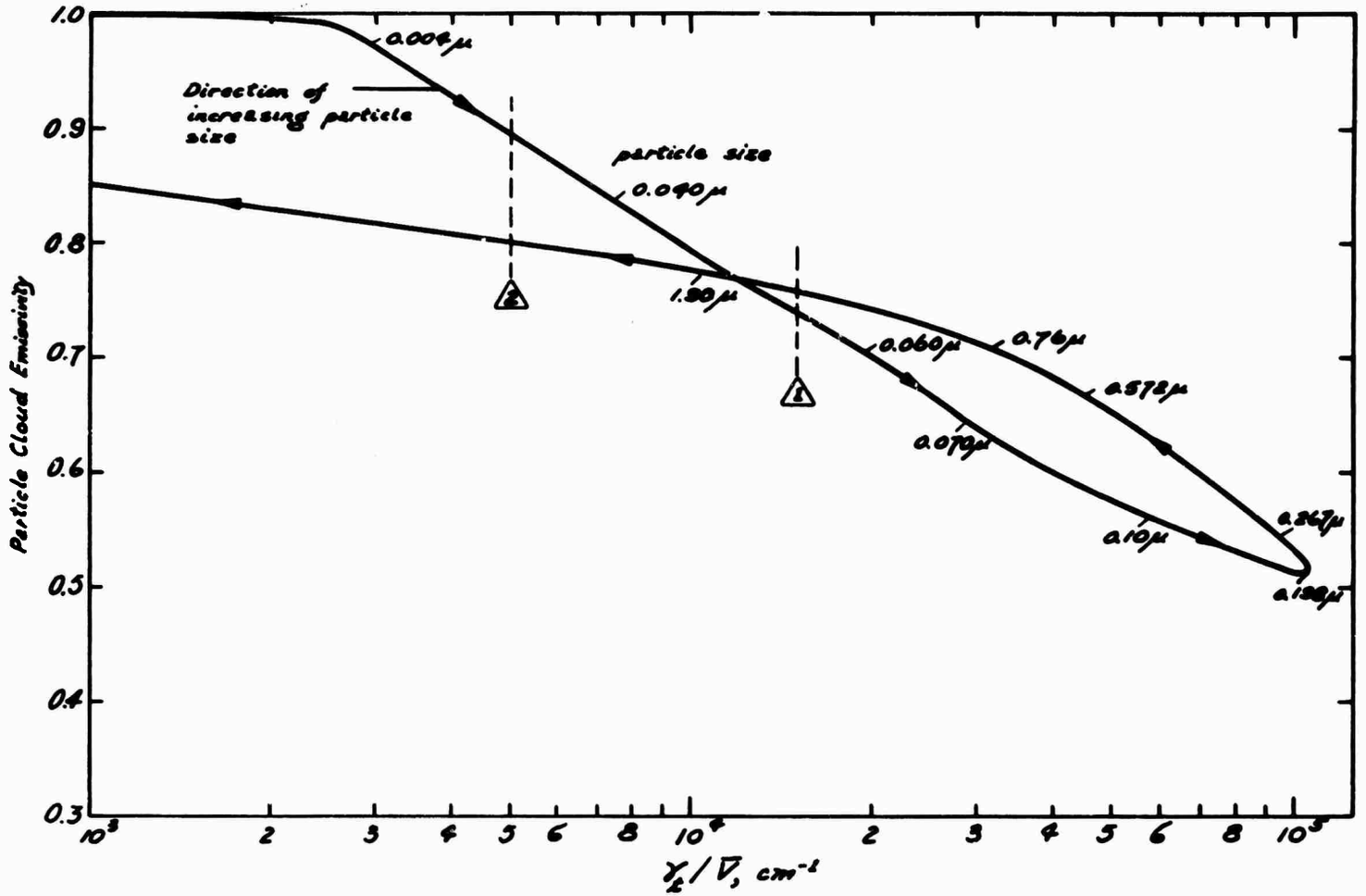

Figure A6

Particle Cloud Emissivity vs Extinction Parameter for LM Oxide Spherical Particles-Determined for Chamber Conditions in 1KS-250 Motor, LM-2 Propellant. Laser Beam Penetration Levels are Indicated

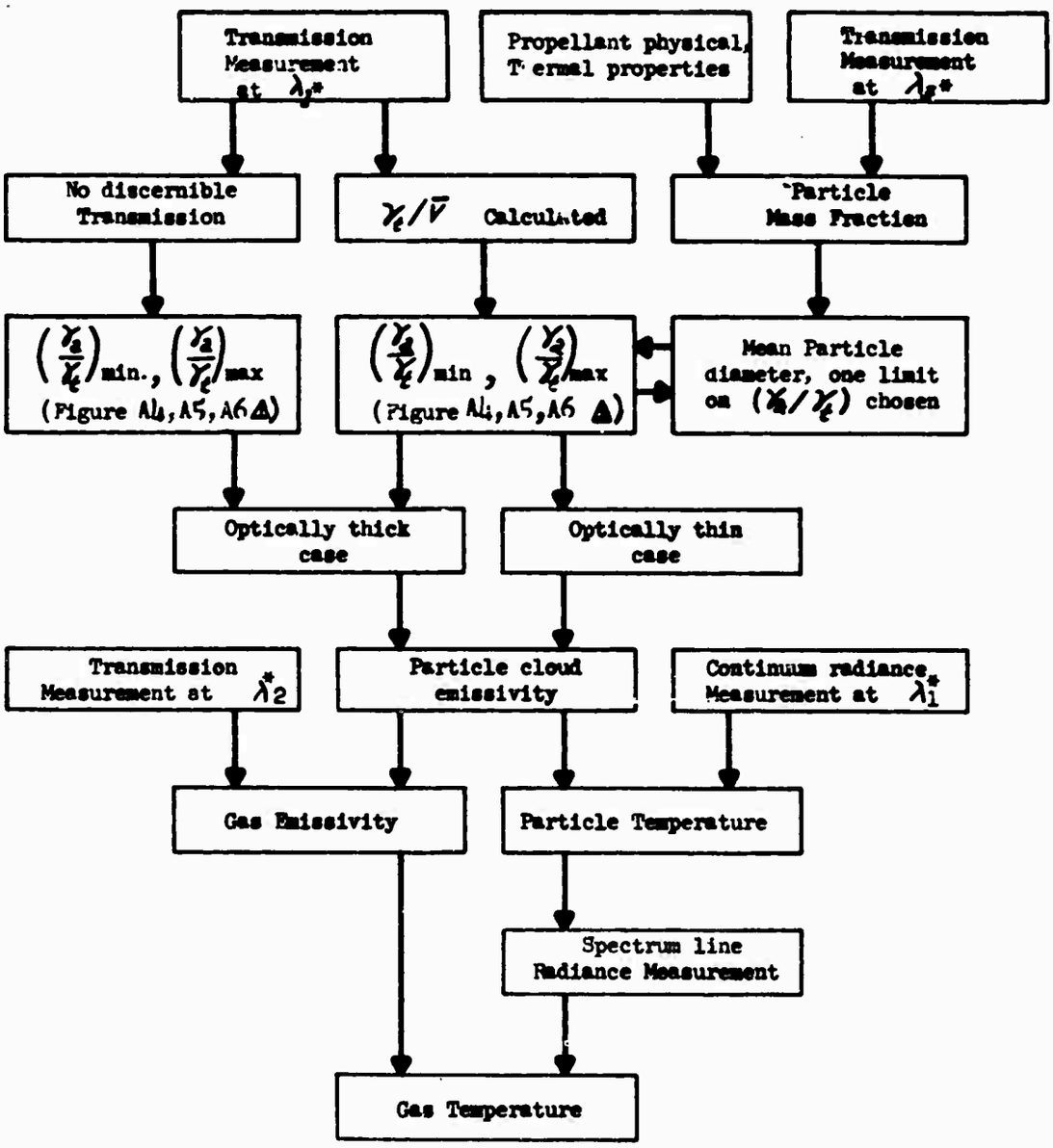

* λ_1 - Wavelength in spectral region removed from spectrum line

λ_2 - Wavelength corresponding to spectrum line

λ_3 - Wavelength in spectral region far removed from λ_1, and removed from spectrum line

Sequence of Computations/ Measurements Necessary to Determine Gas and Particle Temperature from Extinction and Radiance Measurements

Figure A7

APPENDIX B

MIE SCATTERING THEORY FOR SPHERICAL PARTICLES

The following treatment presents the basic results of the Mie theory for spherical scatterers. From this theory an IBM 7094 computer program has been written which will permit rapid generation of scattering diagrams and cross sections. The computer program is presented at the end of this treatment.

The scattered light intensity at an angle θ to the incident light beam for the two-plane polarized components and the resultant are given by the following (see Figure 1) (Reference 1).

Light intensity in plane of observation:

$$I_1 \propto a_1^2 *$$

$$I_1 = \frac{i_1(\alpha, m, \theta)}{k^2 r^2} I_{o,1} \qquad \text{(Eq 1)}$$

Light intensity perpendicular to plane of observation:

$$I_2 \propto a_2^2$$

$$I_2 = \frac{i_2(\alpha, m, \theta)}{k^2 r^2} I_{o,2} \qquad \text{(Eq 2)}$$

Resultant (total intensity)

$$I = \frac{i_1 + i_2}{2 k^2 r^2} I_o \qquad \text{(Eq 3)}$$

*See Nomenclature for definition of symbols.

$$i_1(\alpha, m, \theta) = \left[\sum_{n=1}^{\infty} \frac{2n+1}{n(n+1)} \left\{ a_n \pi_n(\cos\theta) + b_n \tau_n(\cos\theta) \right\} \right]^2 \quad \text{(Eq 4)}$$

$$i_2(\alpha, m, \theta) = \left[\sum_{n=1}^{\infty} \frac{2n+1}{n(n+1)} \left\{ b_n \pi_n(\cos\theta) + a_n \tau_n(\cos\theta) \right\} \right]^2 \quad \text{(Eq 5)}$$

a_n, b_n are <u>scattering coefficients</u>, defined by

$$a_n = \frac{S_n'(m\alpha) S_n(\alpha) - m S_n'(\alpha) S_n(m\alpha)}{m S_n'(m\alpha) \phi_n(\alpha) - \phi_n'(\alpha) S_n(m\alpha)} \quad \text{(Eq 6)}$$

$$b_n = \frac{m S_n'(m\alpha) S_n(\alpha) - S_n'(\alpha) S_n(m\alpha)}{m S_n'(m\alpha) \phi_n(\alpha) - \phi_n'(\alpha) S_n(m\alpha)} \quad \text{(Eq 7)}$$

$$\phi_n(Z) = S_n(Z) + i C_n(Z)$$

$$C_n(Z) = (-1)^n \sqrt{\pi Z/2}\, J_{-(n+\frac{1}{2})}(Z)$$

$$S_n(Z) = \sqrt{\pi Z/2}\, J_{n+\frac{1}{2}}(Z)$$

$$\pi_n(\cos\theta) = \frac{1}{\sin\theta} P_n^1(\cos\theta)$$

$$\tau_n(\cos\theta) = \frac{d}{d\theta} P_n^1(\cos\theta)$$

$P_n^1(\cos\theta)$ is an associated Legendre polynominal. In the general case, m, the ratio of the index of refraction of the scattering medium to that of the surrounding medium, is complex, i.e.,

$$m = n + in' \qquad \text{(Eq 8)}$$

The above set of equations can then be solved for i_1, i_2 for the given values of α, m at each value of θ.

The scattering and absorption cross section are related to the spectral reflectivity and spectral absorptivity as shown in Appendix A. They are related to the scattering coefficients through the following equations

$$\gamma_s(\alpha) = \frac{\lambda^2}{2\pi} \sum_{n=1}^{\infty} (2n+1)\left(|a_n|^2 + |b_n|^2\right) \qquad \text{(Eq 9)}$$

$$\gamma_a(\alpha) = \frac{\lambda^2}{2\pi} \sum_{n=1}^{\infty} (2n+1)\left[\mathcal{R}(a_n + b_n) - |a_n|^2 - |b_n|^2\right] \qquad \text{(Eq 10)}$$

For a distribution of particle sizes, the frequency function $f(\alpha)$ is used, which represents the normalized frequency at which a particular α occurs in a sample. The following equations might prove helpful in defining the frequency function

$$\int_0^{\infty} f(\alpha)\, d\alpha = 1 \qquad \text{(Eq 11)}$$

$$\bar{\alpha} = \frac{\int_0^{\infty} \alpha f(\alpha)\, d\alpha}{\int_0^{\infty} f(\alpha)\, d\alpha} \quad \text{the mean } \alpha \qquad \text{(Eq 12)}$$

The effective cross sections, then, are given by

$$\overline{\gamma_s(\alpha)} = \int_0^\infty \gamma_s(\alpha)\, f(\alpha)\, d\alpha = \gamma_{p,s} \qquad \text{(Eq 13)}$$

$$\overline{\gamma_a(\alpha)} = \int_0^\infty \gamma_a(\alpha)\, f(\alpha)\, d\alpha = \gamma_{p,a} \qquad \text{(Eq 14)}$$

Further, the effective i_1 for a distribution of particle sizes are given by

$$\overline{(i_1(\theta)} = \int_0^\infty i_1(\alpha,\theta)\, f(\alpha)\, d\alpha \qquad \text{(Eq 15)}$$

$$\overline{i_2(\theta)} = \int_0^\infty i_2(\alpha,\theta)\, f(\alpha)\, d\alpha \qquad \text{(Eq 16)}$$

The above integrals are evaluated by using Simpsons rule:

$$\int_0^y f(x)\, dx = \frac{h}{3}\Big[f(o) + 4\ f(x_1) + f(x_3) + \ldots f(x_{n-2}) + 2\ f(x_2) + f(x_4) + \ldots f(x_{n-1}) + f(x_n)\Big] \qquad \text{(Eq 17)}$$

$$y = x_n$$

where n is odd, and

$$h = x_n - x_{n-1}$$

The computer programs which have been written around these equations are included here as Table I, (Reference 2).

NOMENCLATURE

a_n	-	scattering coefficient, see p. 2
b_n	-	scattering coefficient, see p. 2
$f(\alpha)$	-	frequency function
h	-	incremental distance
I_o	-	incident light intensity
I_1	-	plane-polarized component of light intensity in plane of observation
I_2	-	plane-polarized component of light intensity perpendicular to plane of observation
$J_{n+\frac{1}{2}}$	-	Bessel Function of first kind, half order
k	-	wave number, $2\pi/\lambda$
m	-	index of refraction
P_n^1	-	Associated Legendre polynomial of the first kind
r	-	distant from scattering volume to detector

Greek

α	-	$\pi D/\lambda$, particle size parameter
γ_s	-	absorption cross section, spectral absorption coefficient
γ_a	-	scattering cross section, spectral scattering coefficient
λ	-	wavelength
θ	-	angle from line of observation to line of incident radiation

REFERENCES

1. Erickson, W. D. "Light Scattering: A Technique for Studying Scat in Flame" Ph.D. Thesis in Chemical Engineering, M. I. T., December 1961.

2. Dalzell, W. H., Personal Communication, January 1965.

TABLE I

COMPUTER PROGRAM FOR CALCULATING MIE SCATTERING INTENSITIES

```
C  PROGRAM 53006  MIE SCATTERING INTENSITIES WITH DISTRIBUTION          53006  1
C  FOR J. M. ADAMS  DEPT. 4635  BLDG 2019  EXT 5-7641                  53006  2
C     PROGRAM FOR CALCULATING MIE SCATTERING INTENSITIES,ADA 650409     53006  3
   10 FORMAT(F10.9)                                                    53006  4
   20 FORMAT(2F10.4,I10)                                               53006  5
   30 FORMAT( 20H1   AVERAGE ALPHA =     F7.4,15H   STD. DEV. =  F7.5/ 53006  6
     126H0   INDEX OF REFRACTION = F9.7 ,  3H - F12.9, 3H I )          53006  7
   40 FORMAT( 51H0    ALPHA     DENSITY     CROSS SECTIONS - SQ. CM,/  53006  8
     1 55H                FUNCTION    ABSORPTION     SCATTERING   /1H0 ) 53006  9
   50 FORMAT ( 47H0                              INTENSITY FUNCTIONS /   53006 10
     172H0   ANGLE          PERPENDICULAR            PARALLEL          53006 11
     2 TOTAL    )                                                      53006 12
   60 FORMAT(4X,F7.4,5X,F6.4,4X,E12.5,3X,E12.5 )                       53006 13
   70 FORMAT(1H0F8.1,3E21.5)                                           53006 14
   80 FORMAT(F8.1,3E21.5)                                              53006 15
   90 FORMAT(17H0   WAVELENGTH = F7.5,  9H MICRONS / 31H0   ABSORPTION C53006 16
     1ROSS SECTION = E12.5,12H SQUARE CM      / 31H0   SCATTERING CROSS 53006 17
     2SECTION = E12.5, 12H SQUARE CM      )                            53006 18
      COMMON PI,TAU,C,S                                                53006 19
      DIMENSION  PI(200),TAU(200),C(200),S(200),P(200),Z(200),L(200),  53006 20
     1AREAL(200),AIMAG(200),BREAL(200),BIMAG(200),GREAL(200),GIMAG(200),53006 21
     2ANGLE(370),TCOS(370),DPI(200),DENS(10),X(10),PRI(10,370),        53006 22
     3PLI(10,370),YPRI(10,370),YPLI(10,370),GAMS(10),GAMA(10),YGAMA(10),53006 23
     4PHIA(370),PLIA(370),TLIA(370),YGAMS(10)                         53006 24
C     DEFINE ALL ANGLES                                                53006 25
      ANGLE(1)=0.0                                                     53006 27
      DO 100 M=1,360                                                   53006 28
      K=M+1                                                            53006 29
  100 ANGLE(K)=ANGLE(K-1)+0.5                                          53006 30
      MFDGR=(3.14159265979324)/360.0                                   53006 31
      READ INPUT TAPE 5,10,CONV                                        53006 32
  110 READ INPUT TAPE 5,20,U,V,IND                                     53006 33
      READ INPUT TAPE 5,20,XLAMDA                                      53006 34
      J=0                                                              53006 35
  120 READ INPUT TAPE 5,20,ALPHA,FREQ                                  53006 36
      IF(ALPHA)250,250,130                                             53006 37
  130 J=J+1                                                            53006 38
      X(J)=ALPHA                                                       53006 39
      DENS(J)=FREQ                                                     53006 40
      M=0                                                              53006 41
  140 DCONS=U**2+V**2                                                  53006 42
      DREAL=U/DCONS                                                    53006 43
      DIMAG=V/DCONS                                                    53006 44
      SINH=(EXPF(2.*ALPHA*V)-EXPF(-2.*ALPHA*V))/2.                     53006 45
      COSH=(EXPF(2.*ALPHA*V)+EXPF(-2.*ALPHA*V))/2.                     53006 46
      GCONS=COSH-COSF(2.*ALPHA*U)                                      53006 47
      GREAL(1)=SINF(2.*ALPHA*U)/GCONS                                  53006 48
      GIMAG(1)=SINH/GCONS                                              53006 49
C     CALCULATE BESSEL FUNCTIONS                                       53006 50
      S(1)=SINF(ALPHA)                                                 53006 51
      C(1)=COSF(ALPHA)                                                 53006 52
      S(2)=S(1)/ALPHA-C(1)                                             53006 53
      C(2)=C(1)/ALPHA+S(1)                                             53006 54
      N=2                                                              53006 55
      ITEST=1                                                          53006 56
      GO TO 160                                                        53006 57
C     CALCULATE NEW BESSEL FUNCTION                                    53006 58
  150 ITEST=2                                                          53006 59
      NM1=N-1                                                          53006 60
      NM2=N-2                                                          53006 61
      TNN=NM1                                                          53006 62
      TN=TNN                                                           53006 63
```

TABLE I (cont.)

```
      S(N)=(2.0*TN-1.0)*S(NM1)/ALPHA-S(NM2)                    53006 64
      C(N)=(2.0*TN-1.0)*C(NM1)/ALPHA-C(NM2)                    53006 65
C     CALCULATE A AND B                                        53006 66
  160 P(N)=N-1                                                 53006 67
      L(N)=N-1                                                 53006 68
      EREAL=(2.*P(N)-1.)*DREAL/ALPHA-BREAL(N-1)                53006 69
      EIMAG=(2.*P(N)-1.)*DIMAG/ALPHA-BIMAG(N-1)                53006 70
      BCONS=EREAL**2+EIMAG**2                                  53006 71
      BREAL(N)=EREAL/BCONS                                     53006 72
      BIMAG(N)=-EIMAG/BCONS                                    53006 73
      WREAL=U*BREAL(N)+V*BIMAG(N)                              53006 74
      WIMAG=U*BIMAG(N)-V*BREAL(N)                              53006 75
      QREAL=WREAL*C(N)-C(N-1)                                  53006 76
      QIMAG=WIMAG*C(N)                                         53006 77
      RREAL=WREAL*S(N)-S(N-1)                                  53006 78
      RIMAG=WIMAG*S(N)                                         53006 79
      SCONS=RREAL**2+RIMAG**2                                  53006 80
      SREAL=(QREAL*RREAL+DIMAG*RIMAG)/SCONS                    53006 81
      SIMAG=(QIMAG*RREAL-DREAL*RIMAG)/SCONS                    53006 82
      BCONS=(1.-SIMAG)**2+SREAL**2                             53006 83
      BREAL(N)=(1.-SIMAG)/BCONS                                53006 84
      BIMAG(N)=-SREAL/BCONS                                    53006 85
      TREAL=DREAL*BREAL(N)-DIMAG*BIMAG(N)                      53006 86
      TIMAG=DIMAG*BREAL(N)+DREAL*BIMAG(N)                      53006 87
      UREAL=P(N)*(1.-DREAL**2+DIMAG**2)/ALPHA                  53006 88
      UIMAG=-2.*P(N)*DREAL*DIMAG/ALPHA                         53006 89
      VREAL=TREAL*UREAL                                        53006 90
      VIMAG=TIMAG*UIMAG                                        53006 91
      WREAL=VREAL*C(N)-C(N-1)                                  53006 92
      WIMAG=VIMAG*C(N)                                         53006 93
      XREAL=VREAL*S(N)-S(N-1)                                  53006 94
      XIMAG=VIMAG*S(N)                                         53006 95
      YCONS=XREAL**2+XIMAG**2                                  53006 96
      YREAL=(WREAL*XREAL+WIMAG*XIMAG)/YCONS                    53006 97
      YIMAG=(WIMAG*XREAL-WREAL*XIMAG)/YCONS                    53006 98
      ACONS=(1.-YIMAG)**2+YREAL**2                             53006 99
      AREAL(N)=(1.-YIMAG)/ACONS                                53006100
      AIMAG(N)=-YREAL/ACONS                                    53006101
      NCAL=N                                                   53006102
      GO TO (170,180),ITEST                                    53006103
C     DEFINE NEW ANGLE                                         53006104
  170 M=M+1                                                    53006105
      T=M-1                                                    53006106
      TCOS(M)=CCSF(T*HFDGR)                                    53006107
C     CALCULATE PI AND TAU                                     53006108
      PI(1)=0.0                                                53006109
      PI(2)=1.0                                                53006110
      DPI(1)=0.0                                               53006111
      DPI(2)=0.0                                               53006112
      TAU(2)=TCOS(M)                                           53006113
      N=2                                                      53006114
      SARP=0.0                                                 53006115
      SART=0.0                                                 53006116
      SBRP=0.0                                                 53006117
      SBRT=0.0                                                 53006118
      SAIP=0.0                                                 53006119
      SAIT=0.0                                                 53006120
      SBIP=0.0                                                 53006121
      SBIT=0.0                                                 53006122
      GO TO 190                                                53006123
  180 NM1=N-1                                                  53006124
      NM2=N-2                                                  53006125
```

TABLE I (cont.)

```
      TNN=NM1                                                                  93006126
      TN=TNN                                                                   93006127
      PI(N)=TCOS(N)*(2.0*TN-1.0)*PI(NM1)/(TN-1.0)-TN*PI(NM2)/(TN-1.0)          93006128
      DPI(N)=(2.0*TN-1.0)*PI(NM1)*DPI(NM2)                                     93006129
      TAU(N)=TCOS(N)*PI(N)-(1.0-TCOS(N)**2)*DPI(N)                             93006130
C     CALCULATE SERIES FOR I1 AND I2                                           93006131
  190 P(N)=N-1                                                                 93006132
      Z(N)=(2.*P(N)+1.)/(P(N)*(P(N)+1.))                                       93006133
      ARP=AREAL(N)*Z(N)*PI(N)                                                  93006134
      SARP=SARP+ARP                                                            93006135
      ART=AREAL(N)*Z(N)*TAU(N)                                                 93006136
      SART=SART+ART                                                            93006137
      BRP=BREAL(N)*Z(N)*PI(N)                                                  93006138
      SBRP=SRRP+BRP                                                            93006139
      BRT=BREAL(N)*Z(N)*TAU(N)                                                 93006140
      SBRT=SRRT+BRT                                                            93006141
      AIP=AIMAG(N)*Z(N)*PI(N)                                                  93006142
      SAIP=SAIP+AIP                                                            93006143
      AIT=AIMAG(N)*Z(N)*TAU(N)                                                 93006144
      SAIT=SAIT+AIT                                                            93006145
      BIP=BIMAG(N)*Z(N)*PI(N)                                                  93006146
      SBIP=SRIP+BIP                                                            93006147
      BIT=BIMAG(N)*Z(N)*TAU(N)                                                 93006148
      SBIT=SRIT+BIT                                                            93006149
      PRI(J,M)= (SARP+SBRT)**2+(SAIP+SBIT)**2                                  93006150
      PLI(J,M)= (SART+SBRP)**2+(SAIT+SBIP)**2                                  93006151
      DPRI=(ARP+BRT)**2+(AIP+BIT)**2                                           93006152
      DPLI=(ART+BRP)**2+(AIT+BIP)**2                                           93006153
C     CONVERGENCE TEST                                                         93006154
      R1=DPRI/PRI(J,M)                                                         93006155
      R2=DPLI/PLI(J,M)                                                         93006156
      IF(R1-CONV)200,200,210                                                   93006157
  200 IF(R2-CONV)220,220,210                                                   93006158
C     SERIES NOT YET CONVERGED                                                 93006159
  210 N=N+1                                                                    93006160
      IF(NCAL-N)150,180,180                                                    93006161
C     CONVERGED-GO TO NEXT ANGLE                                               93006162
  220 IF(P-361)170,230,230                                                     93006163
  230 YAN=0.0                                                                  93006164
      YSN=0.0                                                                  93006165
      DO 240 N=2,NCAL                                                          93006166
      CC=2*(N-1)+1                                                             93006167
      YAN=YAN+CC*(AREAL(N)*BREAL(N)-AREAL(N)**2-AIMAG(N)**2-BREAL(N)**2        93006168
     1-BIMAG(N)**2)                                                            93006169
  240 YSN=YSN+CC*(AREAL(N)**2+AIMAG(N)**2+BREAL(N)**2+BIMAG(N)**2)             93006170
      YLAMDA=XLAMDA/10000.                                                     93006171
      GAMS(J)=YLAMDA**2*YSN/(2.*HFDGR*360.)                                    93006172
      GAMA(J)=YLAMDA**2*YAN/(2.*HFDGR*360.)                                    93006173
      GO TO 120                                                                93006174
  250 JFINAL=J                                                                 93006175
      T=JFINAL-1                                                               93006176
      H=(X(JFINAL)-X(1))/T                                                     93006177
      DO 260 M=1,361                                                           93006178
      SEPRI=0.0                                                                93006179
      SOPRI=0.0                                                                93006180
      SEPLI=0.0                                                                93006181
      SOPLI=0.0                                                                93006182
      DO 260 J=1,JFINAL                                                        93006183
      YPRI(J,M)=PRI(J,M)*DENS(J)                                               93006184
  260 YPLI(J,M)=PLI(J,M)*DENS(J)                                               93006185
      II=JFINAL+1                                                              93006186
      YPRI(II,M)=0.0                                                           93006187
```

TABLE I (cont.)

```
      YPLI(II,M)=0.0                                                    53006188
      DO 270 J=1,JFINAL,2                                               53006189
      SEPRI=SEPRI+YPRI(J+1,M)                                           53006190
      SOPRI=SOPRI+YPRI(J,M)                                             53006191
      SEPLI=SEPLI+YPLI(J+1,M)                                           53006192
  270 SOPLI=SOPLI+YPLI(J,M)                                             53006193
      PRIA(M)=(M/3.0)*(4.*SOPRI+2.*SEPRI)                               53006194
      PLIA(M)=(M/3.0)*(4.*SOPLI+2.*SEPLI)                               53006195
  280 TLIA(M)=(PRIA(M)+PLIA(M))/2.                                      53006196
      XMEAN= 0.0                                                        53006197
      DO 290 J=1,JFINAL                                                 53006198
  290 XMEAN=XMEAN+X(J)*DENS(J)*H                                        53006199
      SIG2=0.0                                                          53006200
      DO 300 J=1,JFINAL                                                 53006201
  300 SIG2=SIG2+(X(J)-XMEAN)**2*DENS(J)*H                               53006202
      SIGMA=SQRTF(SIG2)                                                 53006203
      SEGAMA=0.0                                                        53006204
      SOGAMA=0.0                                                        53006205
      SEGAMS=0.0                                                        53006206
      SOGAMS=0.0                                                        53006207
      DO 310 J=1,JFINAL                                                 53006208
      YGAMA(J)=GAMA(J)*DENS(J)                                          53006209
  310 YGAMS(J)=GAMS(J)*DENS(J)                                          53006210
      YGAMA(II)=0.0                                                     53006211
      YGAMS(II)=0.0                                                     53006212
      DO 320 J=1,JFINAL,2                                               53006213
      SEGAMA=SEGAMA+YGAMA(J+1)                                          53006214
      SOGAMA=SOGAMA+YGAMA(J)                                            53006215
      SEGAMS=SEGAMS+YGAMS(J+1)                                          53006216
  320 SOGAMS=SOGAMS+YGAMS(J)                                            53006217
      GA=(H/3.)*(4.*SOGAMA+2.*SEGAMA)                                   53006218
      GS=(H/3.)*(4.*SOGAMS+2.*SEGAMS)                                   53006219
      WRITE OUTPUT TAPE 6,30,XMEAN,SIGMA,U,V                            53006220
      WRITE OUTPUT TAPE 6,90,XLAMDA,GA,GS                               53006221
      WRITE OUTPUT TAPE 6,40                                            53006222
      WRITE OUTPUT TAPE 6,60,(X(J),DENS(J),GAMA(J),GAMS(J),J=1,JFINAL ) 53006223
      WRITE OUTPUT TAPE 6,50                                            53006224
      WRITE OUTPUT TAPE 6,70,(ANGLE(M),PRIA(M),PLIA(M),TLIA(M),M=1,361) 53006225
      CALL LPLOT (ANGLE,PLIA,PRIA)                                      53006226
      GO TO (110,330),IND                                               53006227
  330 WRITE OUTPUT TAPE 8,80,(ANGLE(M),PRIA(M),PLIA(M),TLIA(M),M=1,361) 53006228
  340 GO TO 110                                                         53006229
      END                                                               53006230
      SUBROUTINE LPLOT (ANGLE,PL,PR)
C     ---------- ----- -------------
C
      DIMENSION ANGLE(370),PL(370),PR(370),PLP(361),PRP(361),
     1          AXES(4),TITLE(6)
      AXES(1)=(+6H      )
      AXES(2)=(+6HANGLE )
      AXES(3)=(+6HLG PL=)
      AXES(4)=(+6H1,PR=2)
      TITLE(1)=(+6H      )
      TITLE(2)=(+6H      )
      TITLE(3)=(+6HPROGRA)
      TITLE(4)=(+6HM 5300)
      TITLE(5)=(+6H6     )
      TITLE(6)=(+6H      )
C
C        FIND MAX, MIN VALUES
C
      FMAX=-10000.
```

TABLE I (cont.)

```
      FMIN=-FMAX
      DO 200 I=1,361
      PLP(I)=.434294482*LOGF(PL(I))
      PRP(I)=.434294482*LOGF(PR(I))
      IF (PLP(I)-FMIN) 100,110,110
  100 FMIN=PLP(I)
  110 IF (PRP(I)-FMIN) 120,130,130
  120 FMIN=PRP(I)
  130 IF (FMAX-PLP(I)) 140,150,150
  140 FMAX=PLP(I)
  150 IF (FMAX-PRP(I)) 160,200,200
  160 FMAX=PRP(I)
  200 CONTINUE
C
C        CALL PLOT ROUTINES - 2 CURVES
C
      CALL FRAME (ANGLE,ANGLE(361),FMIN,FMAX,AXES,AXES(3),TITLE,1,-1)
      CALL CURVE (ANGLE,PLP,361,-1)
      CALL CURVE (ANGLE,PRP,361,-1)
      RETURN
      END
      DATA
```

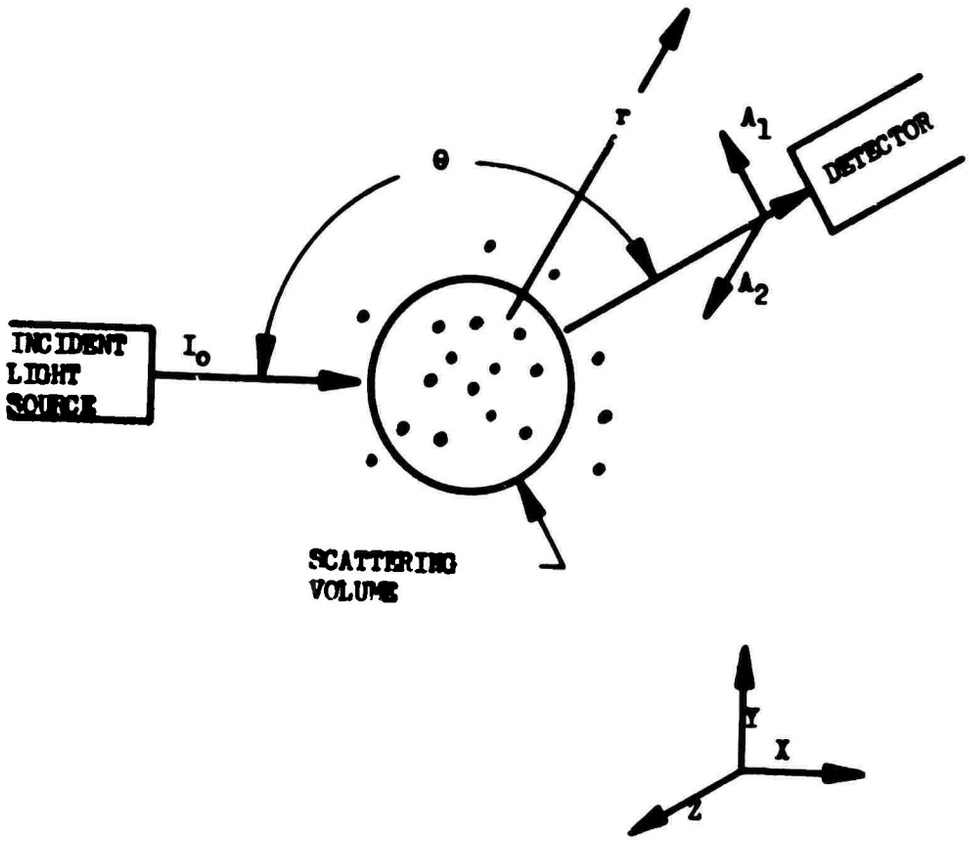

XY PLANE - PLANE OF OBSERVATION

A_1, A_2 - COMPONENTS OF VECTOR WHICH DEFINE DIRECTION AND AMPLITUDE OF THE PERIODIC MOTION OF THE OSCILLATING CHARGE

Diagram of Scattered Light Intensity

Figure B1

APPENDIX C

PROPERTIES OF PROPELLANTS

PROPERTIES OF PROPELLANTS (u)

	ANP-2969	ANP-2991 MOD IA	ANP-3130
Composition, wt%			
Ammonium Perchlorate	55.0	60.0	46 0
Aluminum	20.0	-	-
Beryllium	-	14.0	-
Beryllium Hydride	-	-	21.5
Binder	25.0	26.0	32.5
Theoretical Properties (1000/14.7 psia, opt exp., 0° half angle)			
Specific Impulse, lb_f-sec/lbm	263.1	280.5	315.8
Chamber Temp, °F	6010	5767	5706
Exhaust Temp, °F	3710	3925	3972
Mass Flow Coefficient, lbm/lb_f-sec	0.00621	0.00594	0.00534
Specific Heat Ratio (γ)	1.20	-	1.0849
Measured Ballistic Properties (1000/14.7 psia, opt exp., 15° half angle)			
Specific Impulse, lb_f-sec/lbm			
1KS-250 size motor (1-lb grain)	-	240	259
3KS-500 size motor (5-lb grain)	-	-	264
3KS-500 size motor (6-lb grain)	-	250	-
3KS-1000 size motor (15-lb grain)	-	253	-
10KS-2500 size motor (100-lb grain)	243.5	256.3	-
Burning Rate Law, in./sec	$0.0351\ p_c^{0.30}$	-	$0.02242\ p_c^{0.534}$
Density, $lb/in.^3$	0.0644	0.0602	0 0460
Pressure Exponent	-	0.36 (KE)(1) 0.43 (HG)(2)	-

(1) KE oxidizer blend is 65% + 48 mesh NH_4ClO_4, 35% unground

(2) HG oxidizer blend is 80% unground NH_4ClO_4, 20% high-speed Mikro Pulverizer ground

APPENDIX D

DESCRIPTION OF ROCKET MOTOR TEST HARDWARE

I. ANCILLARY EQUIPMENT

Following is a description of the complete instrumentation support package and layout of ancillary equipment which allows simultaneous measurements to be made in the chamber and at two positions in the exhaust plume, during live motor firings. This system is shown schematically in Figure D-1.

Since the firing duration of the test motors was about 1 sec, automated techniques for high-speed spectral measurement of three locations and one reference position was provided for the first two tests. The temperature measurement technique was similar to that described for the laboratory experiments, but high-speed optical switching between the three selected measurement locations was included.

A. SYSTEM FOR MOTOR FIRING STUDIES

The experiments consisted of 10 millisec, 20 Angstrom scans, in the applicable wave band. The data was recorded on a CEC-type oscillograph for manual data reduction. Each data scan was preceded and followed by a calibration scan with the radiance of the carbon arc at known brightness temperature used as a standard. Three measurement positions, one in the combustion chamber and two in the exhaust plume, were selected.

The three measurement positions and one reference position are represented in Figure D-1. The carbon arc was mechanically positioned so that its radiance was directed to each of the three measurement locations over identical optical paths by the rotation of the optical sampling scanner (Figure D-2). The two optical sampling scanners were driven by the same motor connected by flexible shafts to provide for their synchronization. The fourth optical path, running past the forward end of motor B, in Figure D-1, provided unattenuated system calibration.

To avoid interference caused by acoustic or mechanical vibration from the test motor, fiber-optic light guides consisting of bundles of individual optical fibers, 0.003 in. in diameter, were used for transmission of light from the test motor to the optical sampling scanner. Each fiber has a core of 1.62 index glass and is coated with 1.52 index glass to serve as optical insulation and thus protect the reflected surface of the core. This combination of indices provides a numerical aperture (N.A.) of 0.55. The general arrangement of the special test equipment in the test stand is illustrated in Figure D-3.

Each measurement location was scanned twice, the first scan with the carbon arc radiation imposed on the gas and the second scan without any comparison light source. The scan synchronization was as shown in Figure D-4.

B. DATA RECORDING

Data which were recorded during each firing included the information from the phototube, the scanning arm position indicator signal ($\Delta\lambda$), the thrust, and the chamber pressure.

I, B, Data Recording (cont.)

To provide highly accurate temperature analysis over the broad range of potential temperatures, the data were recorded simultaneously on seven oscillograph channels with gains of 2 to 100, two of which were biased to allow high resolution of peaks in signal. To avoid saturation of overranged channels, the input to the individual record amplifier was equipped with Xener diode circuits, ranged to effectively short the amplifier input after full-scale signals were reached. The composite temperature data contained an equivalent electrical spectrum ranging from dc to 5 kc.

II. DESCRIPTION OF TEST MOTORS

A. DESIGN CALCULATIONS FOR 1KS-250 MOTOR

1KS-250 motors fired for an interval of about 1 sec have been successfully used to economically assess specific impulse for new propellant formulations. Therefore, this motor design with suitable modifications to permit chamber temperature measurements, was chosen for this program. The motor burning time was set at approximately 1 sec, and the average chamber pressure was set at 600 psia. This was done to avoid the low specific impulse efficiencies associated with low chamber pressures, especially with the LM-2 and LMH-2 propellants.

In the interest of simplicity a cylindrical grain design was chosen which yields a progressive pressure-time curve. The range of pressures and calculated durations for the three propellants chosen are shown in Table D-I. The nozzle throat diameter was calculated from the continuity equation based on mid-web conditions for burning surface area

$$\dot{w} = C_w p_c A_t = A_b \kappa \dot{r} \qquad \text{(Eq 7)}$$

where

$$\dot{r} = a p_c^n ,$$

and C_w, κ and a, are constants for the specific propellant used.

Therefore:

$$A_t = \frac{\kappa a}{C_w} \frac{A_b}{p_c^{1-n}} \qquad \text{(Eq 8)}$$

TABLE D-1

MOTOR DESIGN PARAMETERS

		Propellant Type		
		ANP-2969 (Al.)	ANP-2991 Mod IA (Be)	ANP-3130 (BeH_2)
A.	Grain Dimensions			
	OD, in.	2.25	2.25	2.25
	ID, in.	1.50	1.50	1.30
	Length, in.	8.00	8.00	8.00
	Web, in.	0.38	0.38	0.48
B.	Motor Parameters			
	P_c range, psia	363 to 650	440 to 780	320 to 1000
	P_c average (mid web), psia	500	610	600
	Duration, sec	1.69	1.74	0.71
C.	Nozzle Dimensions			
	D_t, in.	0.500	0.500	0.750
	D_e, in.	1.35	1.35	2.00
	Expansion ratio	7.3	7.3	7.14
	Entrance half angle	45	45	45
	Exit half angle	15	15	15
	Throat radius of curvature index	0.50	0.50	0.75
	Exit pressure range, psia			
	(min)	6.9	10.8	8.1
	(max)	9.5	19.1	25.2

II, A, Design Calculations for 1KS-250 Motor (cont.)

Where throat diameter is based on mid-web conditions, such that $A_b = \bar{A}_b$, and $P_c = \bar{P}_c$

$$A_t = \frac{\bar{A}_b \left(\frac{\kappa a}{C_w}\right)}{\left(\frac{}{\bar{P}_c}\right)^{(1-n)}} \qquad \text{(Eq 9)}$$

The maximum and minimum pressures occur, therefore, at maximum and minimum values of the burning surface area.

$$P_c = \left(\frac{\pi d_g L \kappa a}{A_t C_w}\right)^{(1/1-n)} = B_1 \left(\frac{d_g}{A_t}\right)^{(1/1-n)}$$

where

$$B_1 = \left(\frac{\pi L \kappa a}{C_w}\right)^{(1/1-n)}$$

In view of the simplicity of the grain (cylindrical, internal burning), the motor burning time (t_b) was estimated from

$$t_b = \frac{web}{\dot{r}} . \qquad \text{(Eq 10)}$$

Based on the one-dimensional compressible flow tables, the exit area was calculated for the mid-web condition or average chamber pressure ($\bar{p}_c$) assuming 14.7-psi exit pressure (p_e), and the corresponding value of specific heat ratio (γ) for each propellant. Using this value of exit area, the exit pressure at the start of firing and at the end of firing was calculated and the minimum exit pressure checked to ensure that nozzle flow would not separate.

These results are summarized in Table D-I where it can be seen that the identical nozzle and propellant grain design are used for both the aluminum- and beryllium-propellants. This nozzle was first designed for the beryllium propellant in accordance with the aforementioned technique, then checked for the aluminum propellant, ANP-2969. This then allowed both the aluminum- and beryllium-propellant test series to use identical hardware. The beryllium hydride propellant

II, A, Design Calculations for 1KS-250 Motor (cont.)

to be used, ANP-3130, required separate designs for the nozzle and propellant grain. A thicker grain web (smaller ID) was required to obtain a duration of 0.71 sec because of the high burning rate, and a larger throat diameter was required to obtain a reasonable pressure range using a grain midpoint pressure of approximately 600 psia.

B. DESCRIPTION OF TEST EQUIPMENT

The test motors chosen for use in this program were modified 1KS-250 motors, containing about 1 lb of solid propellant. The motor modifications were made to the aft closure region, downstream of the internal burning grain, to accommodate transparent viewports which were used in the chamber temperature measurements. These are shown in the cutaway drawing of Figure D-5.

Nozzles were fabricated from ATJ graphite. The ends were contained by V-44 rubber spacers both to allow for linear thermal expansion and to seal against gas leakage along the graphite external diameter. These were enclosed by a two-piece steel aft closure.

A plenum chamber was provided between the end of the propellant grain and the nozzle approach which contained adjustable viewports, 180° apart, for particle and gas temperature measurements. For some of the tests, the chamber modifications also included a second pair of windows for light scattering measurements, located approximately 63° from the aforementioned viewports. All of these transparent windows or viewports were adjustable inward from the chamber inside diameter to approximately a 1-in.-dia circle.

The viewports contained a transparent quartz window, focusing lens, miscellaneous positioning devices, and the fiber optic bundles or light guides. These viewports were used to carry light to the chamber from the carbon-arc light source[1] and to carry either reflected or refracted light from the chamber to the spectrometer. It was necessary to incorporate a focusing lens between the quartz window and the fiber bundles to focus the entering light and to minimize the entrance light losses. The completed design is shown in Figure D-5.

C. LOCATION OF EXHAUST MEASUREMENT STATIONS

Definition of the exhaust-plume temperature-measurement stations for this program required consideration of three basic factors. The first is that to obtain reasonably representative values of vacuum specific impulse from these motors, the nozzles should have expansion ratios sufficient to allow full expansion of the exhaust from chamber to ambient pressure. The second consideration is to obtain a true measurement of specific impulse, flow disturbances created by the fiber optic bundles or light pickups must not be felt within the nozzle exhaust. Third, the pickup must be located so as to obtain measurements in a region in which temperature equilibrium exists.

---

[1] Only for the first two motor tests.

II, C, Location of Exhaust Measurement Stations (cont.)

To satisfy these considerations, it was necessary to locate the pickups at positions downstream from the exit plane and outside of the exhaust plume to avoid influencing the nozzle pressure. Further, since complete temperature equilibrium will not exist at or immediately downstream of a shock wave, the pickups should be located at stations upstream of the initial normal shock or Mach disk existing in the exhaust plume.

To select the specific measurement stations, then, it was necessary to determine the jet plume flow, including the location of the Mach disk, for each of the motors to be tested. The minimum distance from the nozzle exit plane to the Mach disk for the lowest pressure case was initially estimated to be 1.5 exit diameters or approximately 4 throat diameters through preliminary calculations. These were verified by additional calculations using the method-of-characteristics solution of the potential-flow equations to accurately describe the exhaust plume flow-field, for the various motor designs. These calculations provided complete pressure and Mach number distribution, as well as the Mach disk location in the exhaust plume. Table II presents the predicted location of the Mach disk for each of the three propellants at the nominal chamber pressures. Since the temperature measurements in the exhaust plumes were made within 0.5 in. downstream of the nozzle exit, it is evident that no interference of the normal shock wave on the gas and particle temperature measurements existed.

Table D-II

MACH DISK LOCATION AS A FUNCTION OF CHAMBER PRESSURE

Propellant	Chamber Pressure Range, psia	Disk Location (inches aft of nozzle exit)
ANP-2969	363 to 650	1.73 to 2.32
ANP 2991, Mod 1A	440 to 780	1.80 to 2.38
ANP-3130	320 to 1000	2.24 to 3.95

The calculated plume flow characteristics were used to obtain theoretical temperatures at the measurement stations with which measured temperatures were compared (see body of report).

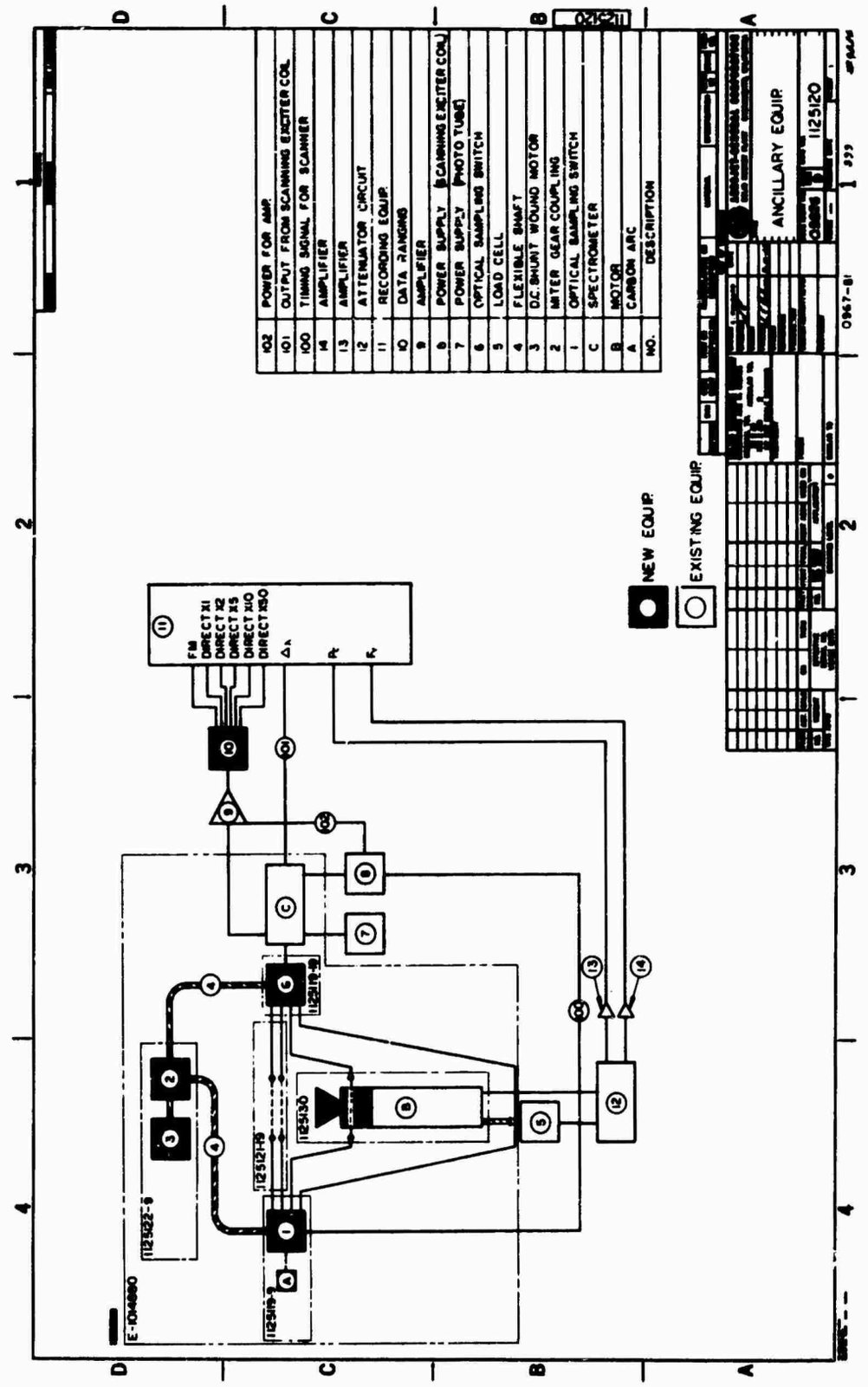

Schematic of Ancillary Equipment, SCP

Figure D1

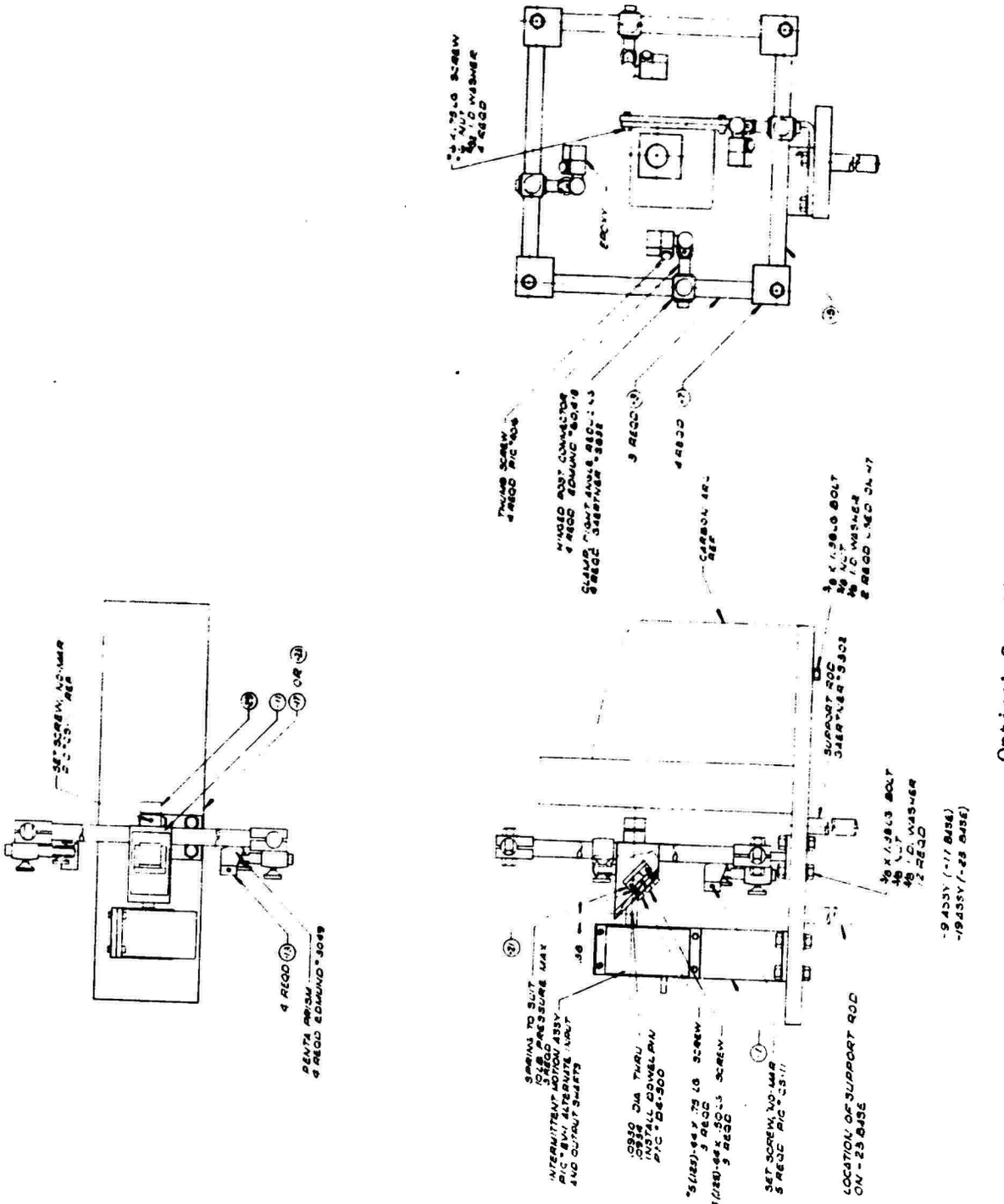

Optical Sampling Scanner

Figure D2

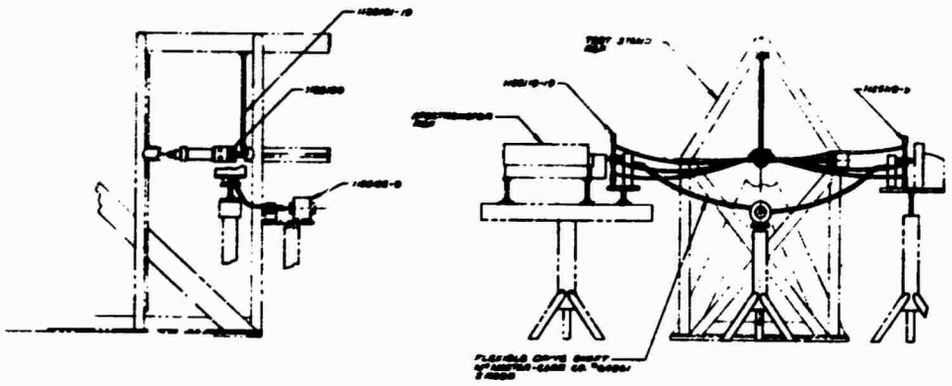

Special Test Equipment for Motor Tests

Figure D3

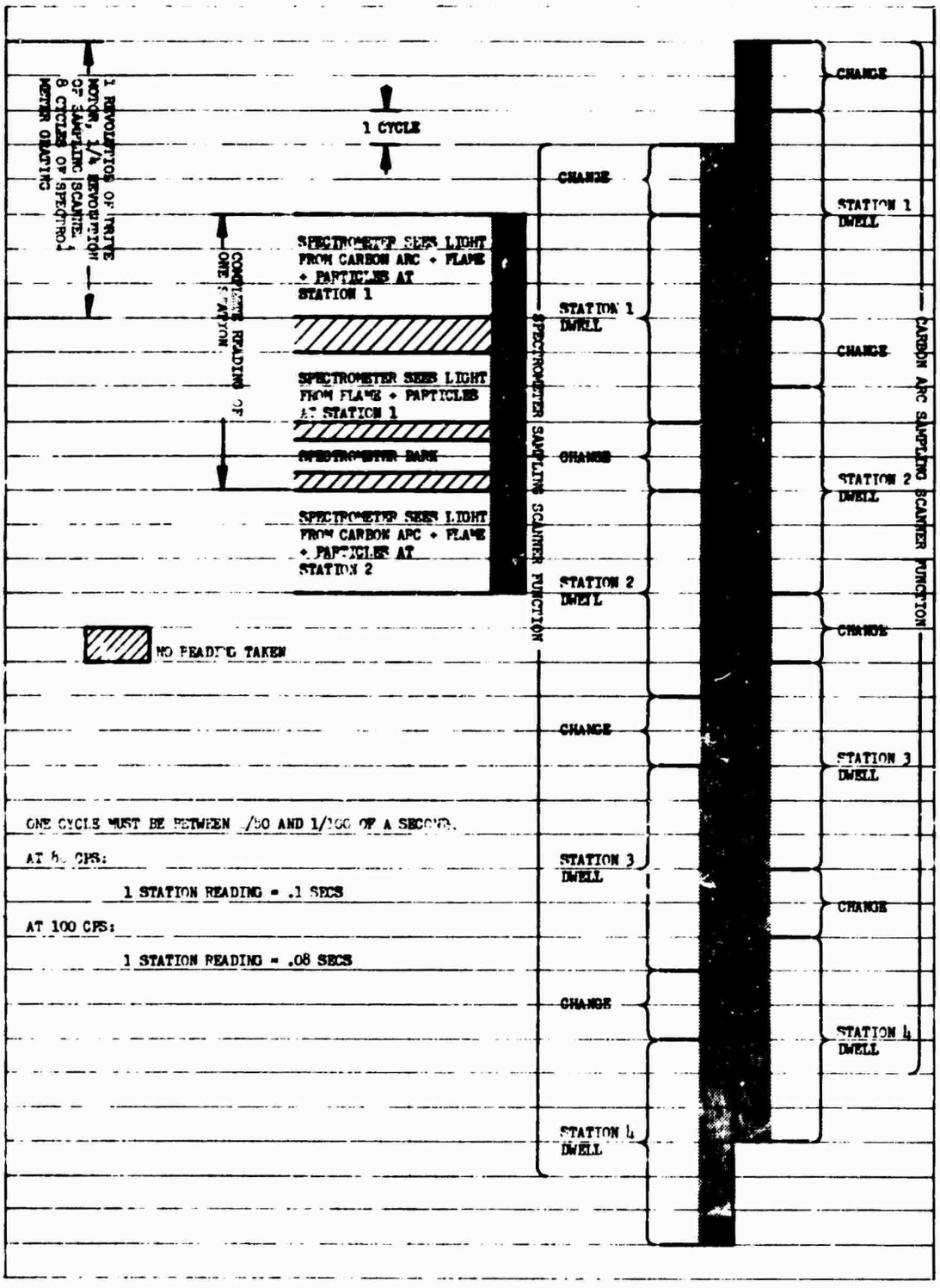

Pictorial Synchronization of Optical Sampling Scanners and Spectral Scanner

Figure D4

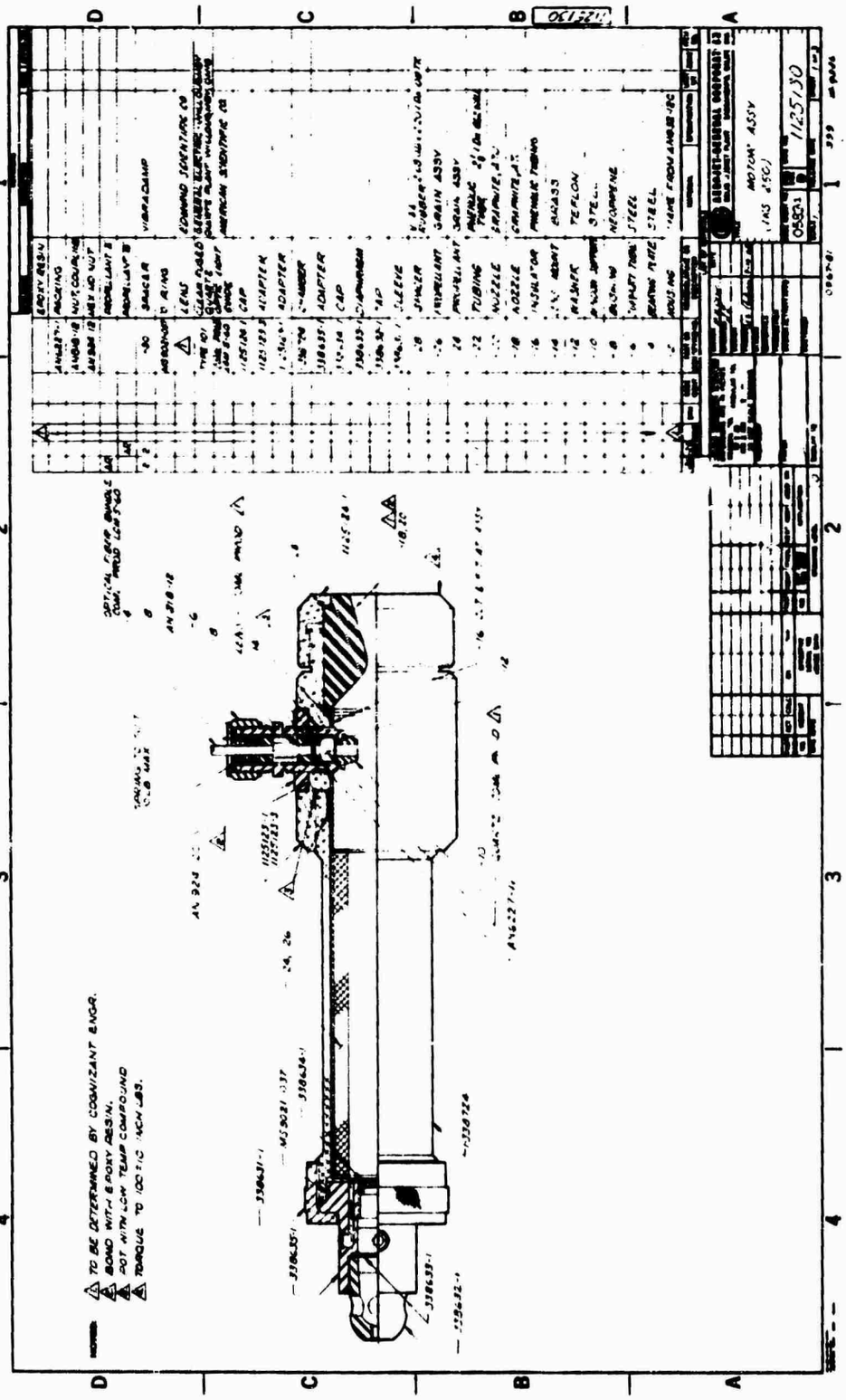

Test Motor Assembly

Report AFRPL-TR-66-203

Attachment
to
DD Form 1473
DOCUMENT CONTROL DATA - R&D

UNCLASSIFIED ABSTRACT

The spectral comparison method has been developed for the measurement of temperatures of both the gas and condensed phase in a flame. This method utilizes measurements of spectrum line emission from the gas and continuum emission from the particle cloud to allow determination of the temperature of both phases. The method accounts for the effect of scattering by the particle cloud through measurements of effective particle size and number density used in conjunction with the Mie theory.

The measurement precision for this method for a clean gas was determined from measurements on a H_2/O_2 flame; the resulting standard deviation in gas temperature was 16°K. With particles of alumina introduced into the flame, the standard deviation in gas temperature was increased to 40.8°K. For the particle temperature the standard deviation was 140°K, a relatively high value because of the uncertainty in the refractive index of molten alumina.

The first spectral line of the sodium doublet (0.589) was assessed to be a good indicator of the gas temperature in flames. This was determined by a comparison to the lithium line at 0.6708 which is associated with an electron transition of longer radiative lifetime.

Measurements of particle cloud emittance in small flames were obtained under controlled conditions from which the imaginary part of the refractive index for molten alumina could be determined. These measurements and emittance data of other investigators were used to determine an approximate average value of 0.005 for the imaginary part for alumina above its melting temperature. Light scattering measurements were also performed using small flames with entrained alumina particles. Particle number density determined from the scattering measurements gave striking agreement with the quantity derived from a material balance.

Measurements were taken of light extinction and emission in the plumes of small rocket motors having propellants which contained aluminum, LM-2, or LMH-2. These measurements indicated a mean particle diameter in the plume of 0.6 to 1.0 and thermal lag as high as 700°K. Gas and particle temperatures were measured and in the chamber of an LM-2-type motor, which indicated that significant combustion is occurring downstream of the propellant grain. The measurements definitely help to clarify the combustion-expansion phenomena and demonstrate the valuable utility of the measurement technique in this type of investigation.

Report AFRPL-TR-66-20?

Unclassified

Security Classification

DOCUMENT CONTROL DATA - R&D

(Security classification of title, body of abstract and indexing annotation must be entered when the overall report is classified)

1 ORIGINATING ACTIVITY (Corporate author) Aerojet-General Corporation Sacramento, California 9580?	2a REPORT SECURITY CLASSIFICATION Confidential 2b GROUP N/A

3 REPORT TITLE

Flame Temperature Measurement of Metallized Propellant

4 DESCRIPTIVE NOTES (Type of report and inclusive dates)

Final Report, 19 May 1965 - 19 June 1966

5 AUTHOR(S) (Last name, first name, initial)

Colucci, Steve E.
Adams, Jim M.

6 REPORT DATE September 1966	7a TOTAL NO OF PAGES 157	7b NO OF REFS 33
8a CONTRACT OR GRANT NO. AF 04(611)10545 b PROJECT NO. PBSN 314803 Program Structure No. 750G	9a ORIGINATOR'S REPORT NUMBER(S) AFRPL-TR-66956 9b OTHER REPORT NO(S) (Any other numbers that may be assigned this report) None	

10 AVAILABILITY/LIMITATION NOTICES

Foreign announcement and dissemination of this rep.
DDC is not authorized.

11 SUPPLEMENTARY NOTES None	12 SPONSORING MILITARY ACTIVITY Air Force Rocket Propulsion Lab(RPCL) Edwards AFB, Calif. 93523

13 ABSTRACT

See attached sheet.

DD FORM 1 JAN 64 1473

Security Classification

Unclassified

Security Classification

14. KEY WORDS	LINK A		LINK B		LINK C	
	ROLE	WT	ROLE	WT	ROLE	WT
1. Spectral Comparison Pyrometer						
2. Refractive Index for Alumina						
3. Flame Temperature Measurement						
4. Light Scattering Studies						
5. Condensed Specie (particle) Temperature						
6. Spectroscopic Measurements						
7. Mie Scattering Theory						
8. Particle Cloud Emission						

INSTRUCTIONS

1. **ORIGINATING ACTIVITY:** Enter the name and address of the contractor, subcontractor, grantee, Department of Defense activity or other organization (*corporate author*) issuing the report.

2a. **REPORT SECURITY CLASSIFICATION:** Enter the overall security classification of the report. Indicate whether "Restricted Data" is included. Marking is to be in accordance with appropriate security regulations.

2b. **GROUP:** Automatic downgrading is specified in DoD Directive 5200.10 and Armed Forces Industrial Manual. Enter the group number. Also, when applicable, show that optional markings have been used for Group 3 and Group 4 as authorized.

3. **REPORT TITLE:** Enter the complete report title in all capital letters. Titles in all cases should be unclassified. If a meaningful title cannot be selected without classification, show title classification in all capitals in parenthesis immediately following the title.

4. **DESCRIPTIVE NOTES:** If appropriate, enter the type of report, e.g., interim, progress, summary, annual, or final. Give the inclusive dates when a specific reporting period is covered.

5. **AUTHOR(S):** Enter the name(s) of author(s) as shown on or in the report. Enter last name, first name, middle initial. If military, show rank and branch of service. The name of the principal author is an absolute minimum requirement.

6. **REPORT DATE:** Enter the date of the report as day, month, year; or month, year. If more than one date appears on the report, use date of publication.

7a. **TOTAL NUMBER OF PAGES:** The total page count should follow normal pagination procedures, i.e., enter the number of pages containing information.

7b. **NUMBER OF REFERENCES:** Enter the total number of references cited in the report.

8a. **CONTRACT OR GRANT NUMBER:** If appropriate, enter the applicable number of the contract or grant under which the report was written.

8b, 8c, & 8d. **PROJECT NUMBER:** Enter the appropriate military department identification, such as project number, subproject number, system numbers, task number, etc.

9a. **ORIGINATOR'S REPORT NUMBER(S):** Enter the official report number by which the document will be identified and controlled by the originating activity. This number must be unique to this report.

9b. **OTHER REPORT NUMBER(S):** If the report has been assigned any other report numbers (*either by the originator or by the sponsor*), also enter this number(s).

10. **AVAILABILITY/LIMITATION NOTICES:** Enter any limitations on further dissemination of the report, other than those imposed by security classification, using standard statements such as:

(1) "Qualified requesters may obtain copies of this report from DDC."

(2) "Foreign announcement and dissemination of this report by DDC is not authorized."

(3) "U. S. Government agencies may obtain copies of this report directly from DDC. Other qualified DDC users shall request through _____."

(4) "U. S. military agencies may obtain copies of this report directly from DDC. Other qualified users shall request through _____."

(5) "All distribution of this report is controlled. Qualified DDC users shall request through _____."

If the report has been furnished to the Office of Technical Services, Department of Commerce, for sale to the public, indicate this fact and enter the price, if known.

11. **SUPPLEMENTARY NOTES:** Use for additional explanatory notes.

12. **SPONSORING MILITARY ACTIVITY:** Enter the name of the departmental project office or laboratory sponsoring (*paying for*) the research and development. Include address.

13. **ABSTRACT:** Enter an abstract giving a brief and factual summary of the document indicative of the report, even though it may also appear elsewhere in the body of the technical report. If additional space is required, a continuation sheet shall be attached.

It is highly desirable that the abstract of classified reports be unclassified. Each paragraph of the abstract shall end with an indication of the military security classification of the information in the paragraph, represented as (*TS*). (*S*). (*C*). or (*U*).

There is no limitation on the length of the abstract. However, the suggested length is from 150 to 225 words.

14. **KEY WORDS:** Key words are technically meaningful terms or short phrases that characterize a report and may be used as index entries for cataloging the report. Key words must be selected so that no security classification is required. Identifiers, such as equipment model designation, trade name, military project code name, geographic location, may be used as key words but will be followed by an indication of technical context. The assignment of links, rules, and weights is optional.

Unclassified

Security Classification